



**Politecnico  
di Torino**



**Politecnico di Torino**

**Belgian Nuclear higher Education Network**

**Master of Science in Energy and Nuclear Engineering  
a.a. 2022/2023**

**Sensitivity and uncertainty analysis for  
nuclear data of relevance in spent nuclear  
fuel characterization**

**Supervisors**

**Prof. Sandra DULLA**

**Prof. Pierre-Etienne LABEAU**

**Co-supervisors**

**Dr. Luca FIORITO**

**Dr. Pablo ROMOJARO**

**Candidate**

**Enrica BELFIORE**

**March 2023**



# Summary

For an adequate assessment of the spent nuclear fuel, it is necessary to consider all possible uncertainties that affect the design, performance and possible accidents in nuclear facilities environment. Nuclear data is a source of uncertainty that is involved in neutronics, fuel depletion and activation calculations. Methodologies for performing the uncertainty propagation calculations need to be implemented in order to analyze the impact of the nuclear data uncertainties on critical responses during operation and in the event of accident, such as decay heat or neutron multiplication factor. Nevertheless, it is necessary to understand the current status of nuclear data and their uncertainties, in order to be able to handle this type of data. For this purpose, the state-of-the-art of different nuclear data libraries was analyzed during the development of this thesis, focusing on two main kinds of data: radioactive decay and fission yield data. To process these data the SANDY code was used. In this nuclear data sampling code two methodologies were added to obtain perturbed decay data and fission yields. A revision of the state-of-the-art of fission yield data shows inconsistencies in uncertainty data. For this reason, the possibility to use the formulas of the Bayesian/Generalised Least Square (GLS) update technique was also inserted in SANDY. Another contribution in the development of SANDY is related to the sampling methodology. Indeed, the possibility to choose between different distributions to sample from was inserted. The three distributions analyzed are: Gaussian, lognormal and uniform. Then the Fission Pulse Decay Heat problem is tackled: first because of its importance during events after shutdown and because it is a clear exercise for showing the impact and importance of decay and fission yield data uncertainties, testing the implemented perturbation methodologies. In this frame, a sensitivity and uncertainty analysis was carried out to evaluate the final uncertainty of fission pulse decay heat due to the uncertainties on the mentioned input data, to study the individual contribution of each nuclide and to quantify the most relevant isotopes. Finally, the sampling methodology was used to test the new fission yield evaluations realised by CEA and to produce several sets of samples for each input distribution analysed.

# Acknowledgements

Words cannot express my gratitude to my professors Sandra Dulla and Pierre Etienne Labeau for their invaluable patience and feedback. Additionally, this endeavor would not have been possible without the support of my mentor Luca Fiorito and co-mentor Pablo Romojaro, who guided me in this nuclear research world. I also could not have undertaken this journey without all the workers of the NSP group at BR1 in SCK CEN, who generously provided knowledge and expertise.

I am also grateful to my BNEN classmates and cohort members, especially my office mates and all the guys in the Boeretang dormitory, for their editing help, late-night feedback sessions, and moral support. Thanks should also go to the librarians, research assistants, and study participants from the Politecnico di Torino, who affected and inspired me in these five years, especially Betta, Eleonora and Diana. In addition, I want to mention Federico, Anna, Federica, Thomas, Emil, Koray and all the members of the "Amster-gang". Your support made me feel at home, even 2500 km away.

Lastly, I would be remiss in not mentioning my family, especially my parents, my sister, Giuseppe and all my friends from Sicily. Their belief in me has kept my spirit and motivation high during this process.

*Thank you for all.*



# Table of Contents

<b>List of Tables</b>	VII
<b>List of Figures</b>	VIII
<b>Acronyms</b>	XII
<b>1 Introduction</b>	1
1.1 Thesis objectives and motivation . . . . .	1
1.2 Nuclear data . . . . .	2
1.3 Thesis structure . . . . .	4
<b>2 State-of-the-art of nuclear data libraries</b>	6
2.1 Nuclear data libraries . . . . .	6
2.2 ENDF-6 format . . . . .	8
2.3 Covariance matrix . . . . .	10
<b>3 Nuclear data uncertainty propagation</b>	12
3.1 Basic definitions . . . . .	12
3.1.1 Neutron interactions . . . . .	13
3.2 The transport equation . . . . .	14
3.3 The adjoint transport equation . . . . .	16
3.4 Perturbation theory . . . . .	20
3.4.1 SPT - Standard Perturbation Theory . . . . .	21
3.4.2 GPT- Generalized Perturbation Theory . . . . .	22
3.5 Perturbation Theory vs Total Monte Carlo . . . . .	24
3.6 Sensitivity and uncertainty analysis . . . . .	26
3.7 Global vs Local sensitivity analysis . . . . .	28
<b>4 Contributions to SANDY development</b>	30
4.1 Development of SANDY . . . . .	31
4.2 Working scheme . . . . .	32

4.3	Sampling procedure . . . . .	33
4.3.1	Truncation of negative values . . . . .	35
4.3.2	Change of the input parameter distributions . . . . .	37
4.4	Generalized Least Squares update technique . . . . .	39
<b>5</b>	<b>Perturbation methodology of decay data</b>	<b>42</b>
5.1	Algorithm to obtain perturbed decay data in SANDY . . . . .	43
5.2	Decay constant . . . . .	46
5.3	Branching ratio . . . . .	46
5.3.1	Generalized least squares update vs normalization procedure	47
5.4	Decay energy . . . . .	48
<b>6</b>	<b>Perturbation methodology of fission yields</b>	<b>51</b>
6.1	Algorithm to obtain perturbed fission yield in SANDY . . . . .	54
6.2	Generalized Least Squares update of independent fission yields co- variance matrix . . . . .	55
6.2.1	Uncertainty reduction . . . . .	58
6.3	Cumulative fission yields covariance matrix . . . . .	59
<b>7</b>	<b>Fission pulse decay heat</b>	<b>63</b>
7.1	Set-up of the model . . . . .	64
7.2	Results . . . . .	65
7.2.1	Perturbation of decay data . . . . .	66
7.2.2	Perturbation of fission yields . . . . .	73
<b>8</b>	<b>Fission yield evaluations performed by CEA</b>	<b>76</b>
8.1	Propagation through FPDH model . . . . .	77
8.2	Propagation through UAM Pincell and Turkey Point models . . . . .	78
8.2.1	Uncertainty evaluation on $keff$ . . . . .	80
8.2.2	Uncertainty evaluation on nuclide concentrations . . . . .	83
<b>9</b>	<b>Conclusions</b>	<b>86</b>
<b>A</b>	<b>Impact of PDFs when propagating fission yield uncertainties in burnup calculations</b>	<b>89</b>
<b>B</b>	<b>Generalized Least Squares formulas</b>	<b>92</b>
<b>C</b>	<b>Q matrix formula</b>	<b>94</b>
<b>D</b>	<b>Sandwich rule</b>	<b>96</b>
	<b>Bibliography</b>	<b>98</b>

# List of Tables

2.1	Some of the most relevant nuclear data libraries, their formats and country of origin . . . . .	7
3.1	Operator definitions useful to write the transport equation in a more concise way . . . . .	15
5.1	Number of isotopes without uncertainties in their decay energies for the analysed libraries . . . . .	49
5.2	Half life groups . . . . .	50
6.1	Summary of the reported equations for the constraints that can be used to create covariances with Generalized Least Squares method for independent fission yields. . . . .	56
7.1	Nuclides with higher contribution in half life uncertainty . . . . .	67
7.2	Average decay energy uncertainty per decay mode between the data taken from JEFF-3.3 library for the fission products of $^{235}\text{U}$ thermal fission . . . . .	69
7.3	Nuclides with higher contribution in decay energy uncertainty . . .	69
7.4	Nuclides with higher contribution in branching ratio uncertainty . .	72
7.5	List of the nuclides with higher contribution in the uncertainty of $^{235}\text{U}$ Fission Pulse Decay Heat . . . . .	74

# List of Figures

1.1	Activities associated with nuclear data [4] . . . . .	3
2.1	Structure of an ENDF-6 data tape [13] . . . . .	9
3.1	Flowchart of the uncertainty propagation from Total Monte Carlo and perturbation method [35] . . . . .	26
3.2	Scatterplots of Y versus $Z_1, Z_2, Z_3, Z_4$ [36] . . . . .	29
4.1	SANDY's workflow [35] . . . . .	31
4.2	SANDY's documentation on GitHub platform [43] . . . . .	32
4.3	Methods to handle negative samples with Normal PDF . . . . .	36
4.4	Standard deviation of the original PDF vs. standard deviation of the truncated PDFs . . . . .	36
4.5	Lognormal distribution [51] . . . . .	37
4.6	Irwin–Hall distribution [53] . . . . .	39
5.1	Nuclide chart [63] . . . . .	43
5.2	UML Class diagram with the main python classes, attributes and methods used for the implementation of the algorithm for the perturbation of radioactive decay data implemented in SANDY . . . . .	44
5.3	Algorithm to obtain perturbed decay data . . . . .	45
5.4	Branching ratios of $^{64}\text{Cu}$ [67] . . . . .	46
5.5	Correlation matrix of 50 samples branching ratios without correlations . . . . .	48
5.6	Comparison of correlation matrices of branching ratios obtained with GLS and Normalization method . . . . .	48
5.7	Number of isotopes with no uncertainty in their decay energy, classified in half life groups reported in Table 5.2 . . . . .	50
6.1	Independent fission yield distribution for a thermal fission of $^{235}\text{U}$ . Nuclear data is taken from the ENDF/B-VIII.0 library [68] . . . . .	52
6.2	Mass distribution of fission product yields for thermal neutron fission of $^{235}\text{U}$ , $^{229}\text{Th}$ and $^{239}\text{Pu}$ [68] . . . . .	53

6.3	UML Class diagram with the main python classes, attributes and methods used for the implementation of the algorithm for the perturbation of fission yields implemented in SANDY . . . . .	54
6.4	Comparison between correlation matrices of the two sensitivity matrices $D_c$ and $D_m$ . . . . .	57
6.5	Comparison between IFY updated covariance matrices . . . . .	57
6.6	Independent fission yield uncertainties reduction for some JEFF-3.3 $^{235}\text{U}$ thermal fission data. The reduction is caused by the GLS update of the covariance matrix. . . . .	59
6.7	Comparison between evaluated IFY with B matrix approach and IFY stored in the JEFF-3.3 library . . . . .	60
6.8	Cumulative fission yields covariance matrix . . . . .	62
7.1	Comparison of evaluated FPDH and data taken from the ANS5.1 and AESJ standard . . . . .	66
7.2	Uncertainty FPDH with various uncertainty contributions . . . . .	68
7.3	Comparison between the propagated uncertainty from the decay energies uncertainties available in the JEFF-3.3 library and adding the average uncertainty per decay when missing . . . . .	70
7.4	Comparison between the propagated uncertainty from correlated and non-correlated branching ratios . . . . .	70
7.5	Comparison between the original branching ratio uncertainty and the reduced one of some nuclides . . . . .	73
7.6	Uncertainty of $^{235}\text{U}$ FPDH evaluated from the uncertainty propagation of FYs with diagonal and GLS covariance matrices . . . . .	75
7.7	Comparison between the original fission yield uncertainty stored in JEFF-3.3 and the reduced one of some nuclides of interest in FPDH uncertainty after $10^3$ seconds of cooling time. The reduced uncertainties come from the GLS update technique. . . . .	75
8.1	Covariance matrix obtained from the correlation matrix released by CEA with C1 approach . . . . .	77
8.2	Uncertainty of FPDH evaluated from the uncertainty propagation of FYs with diagonal and CEA covariance matrices . . . . .	78
8.3	Geometry configurations of the analyzed models . . . . .	79
8.4	Comparison of the model results (C) against the reference results (E). . . . .	80
8.5	Comparison of CFYs evaluated by CEA and stored in JEFF-3.1.1 against the values in JEFF-3.3. The uncertainties are reported as error bars . . . . .	80

8.6	Discrepancies (in pcm) on $keff$ parameter uncertainty (also called C/C-1) obtained propagating the CEA IFY uncertainties with respect to ones obtained propagating the IFY uncertainties stored in JEFF-3.1.1 . . . . .	81
8.7	FY uncertainty propagation to $keff$ . . . . .	82
8.8	Contribution of different fissioning systems to the variance of $keff$ . . . . .	82
8.9	Nuclide vector deviations from JEFF-3.1.1 . . . . .	83
8.10	Uncertainty on nuclide vector . . . . .	84
8.11	Fraction of variance due to the different fissioning systems . . . . .	85
A.1	Nuclide vector uncertainty evaluated with different input distributions . . . . .	90
A.2	Input and output sample distributions . . . . .	91



# Acronyms

**AESJ**

Atomic Energy Society of Japan

**ALEPH**

Monte Carlo burn-up code

**ANS**

American National Standard

**BLUE**

Best Linear Unbiased Estimator

**CEA**

Atomic Energy Commission

**CI**

Continuous Integration

**CIELO**

Collaborative International Evaluation Library Organization

**CFY**

Cumulative Fission Yield

**ChFY**

Chain Fission Yield

**CLT**

Central Limit Theorem

**CSEWG**

Cross Section Evaluation Working Group

**DH**

Decay Heat

**ENDF**

Evaluated Nuclear Data File

**FPDH**

Fission Pulse Decay Heat

**FY**

Fission Yield

**GLS**

Generalized Least Squares

**GM**

Gauss-Markov theorem

**GNDS**

Generalized Nuclear Database Structure

**GPT**

Generalized Perturbation Theory

**IAEA**

International Atomic Energy Agency

**IFY**

Independent Fission Yield

**IT**

Isometric Transition

**JEFF**

Joint Evaluated Fission and Fusion

**JENDL**

Japanese Evaluated Nuclear Data Library

**MFY**

Mass Fission Yield

**MCNP**

Monte Carlo N-Particle transport code

**NDA**

Non-Destructive Analysis

**NEA**

Nuclear Energy Agency

**NJOY**

Nuclear data processing code

**NNDC**

National Nuclear Data Center

**ODE**

Ordinary Differential Equations

**OLS**

Ordinary Least Squares

**PENDF**

Pointwise Evaluated Nuclear Data File

**PFNS**

Prompt Fission Neutron Spectra

**SA**

Sensitivity Analysis

**SANDY**

Sampler of Nuclear Data uncertainty

**SCK CEN**

Belgian Nuclear Research Centre

**SNF**

Spent Nuclear Fuel

**SPT**

Standard Perturbation Theory

**TMC**

Total Monte Carlo

**UML**

Unified Modeling Language

**UQ**

Uncertainty Quantification

# Chapter 1

## Introduction

### 1.1 Thesis objectives and motivation

Concerning the design of new nuclear reactors and the nuclear energy production, the quantification of uncertainties plays an important role in almost all parts of the fuel cycle to reduce the risks, have a deeper knowledge of the safety and security margins and to minimize the production of nuclear waste. For the licensing, design, and safety analyses of spent nuclear fuel storage, transportation, and repository systems, the spent fuel decay heat is an important observable to take under consideration. Therefore, many efforts are done to understand the accuracy of such data and to assess the impact of uncertainties on it [1]. In particular with this thesis the nuclear data of relevance in Spent Nuclear Fuel (SNF) characterization are addressed. SNF contains a lot of nuclides, which are formed after neutron-induced reactions and radioactive decay occurring during neutron irradiation and cooling periods. For the presence of radionuclides, a SNF assembly needs to be fully characterized for its decay heat and  $\gamma$ -ray and neutron emission for a secure, safe, ecological and economical transport, intermediate storage or final disposal. Some of the observables under consideration in this type of characterization are decay heat and neutron and  $\gamma$ -ray emission rate. They can be evaluated with Non-Destructive Analysis (NDA) methods. Unfortunately, a measurement of the decay heat of an assembly can last one full day (or even more), which is too long for routine operations. In addition, decay heat measurements can be very expensive and it is impractical to cover the multitude of existing operating conditions, fuel designs, and specific applications. Consequently, computer simulations are used to fulfilled some of the gaps of knowledge. The used codes must be validated and uncertainties on are quantified. These simulations are coupled with theoretical calculations to determine the inventory of specific nuclides for criticality safety assessments and for verification of the fuel history. The calculations involve a neutron transport

code combined with a nuclide creation and fuel depletion code. The results of such calculations are strongly dependent on nuclear data, fuel fabrication data, reaction operation and irradiation conditions [2].

Uncertainties are necessary to make meaningful consistency checks and comparisons between varied attempted measurements and calculations and to make scientifically-sound decisions. Wrong estimates may lead to erroneous conclusions on the validity of physics models and theories [3].

The aim of this thesis is to develop a possible methodology to assess the impact of the uncertainties of decay and fission yield data in nuclear calculations. In addition, different nuclear data libraries are studied and lacks of data are investigated; whenever possible, modifications or solutions are analyzed to add physical constraints to some correlated nuclear states. The impact of these modifications is also studied and the differences are discussed.

## 1.2 Nuclear data

"*Nuclear data*" is considered as the values resulting directly from experimental measurements or nuclear model calculations. These data and their corresponding uncertainties are evaluated using experimental and theoretical knowledge, but it is not always possible to measure with a good level of accuracy some physical parameters required for nuclear data applications. To fill in these gaps, nuclear modeling has become quite sophisticated and capable of predicting the major characteristics of important nuclear data but remains deficient in several areas [4].

In order to obtain sufficient data, a huge number of experiments must be performed and then these data must be compared between different measurements and eventually adjusted. The tasks associated with nuclear data are reported in Figure 1.1 and commented below.

- **Nuclear data production:** the task of data production is well coordinated by international collaborations. Laboratories that can perform experimental measurements have guidelines, which can help them to plan their activities. As already mentioned, when experimental data are not available, nuclear model calculations are used to interpolate or extrapolate experimental data and to resolve discrepancies. There is then a need for a database which would include all the available experimental values measured in all the laboratories in the world. This database already exists and it is regularly compiled and updated by different Nuclear Data centers, such as *NNDC* for USA and Canada or *NEA DB* for West European Countries and Japan. Due to the large amount of information, the databases must be handled in a computerized way: for this reason, special formats exist that can accommodate all relevant information about experiments and analytical model calculations;

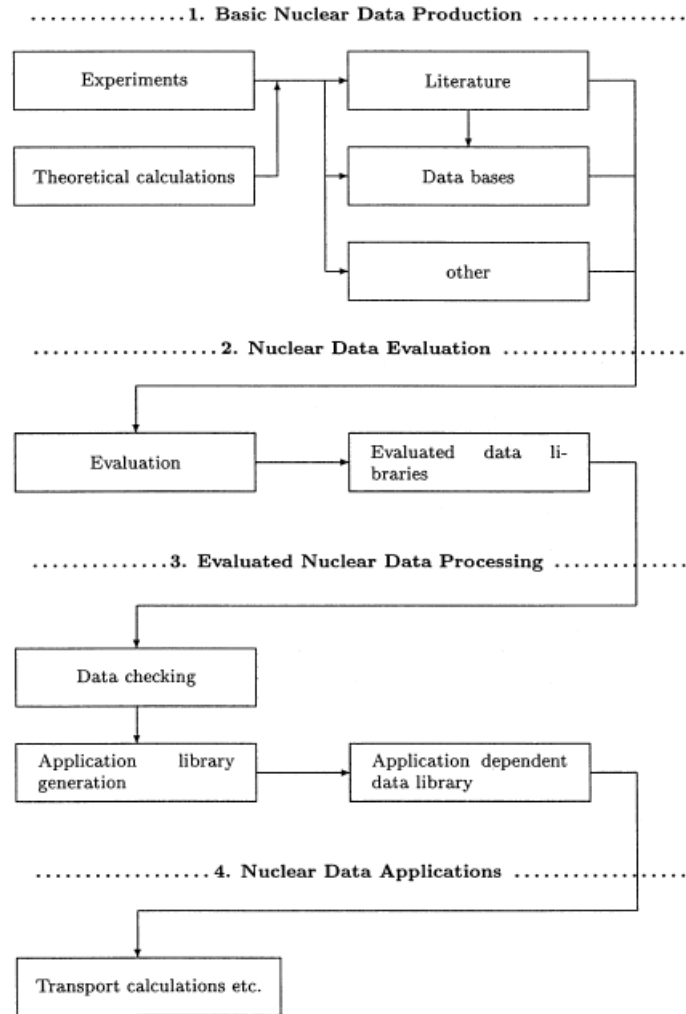


**Figure 1.1:** Activities associated with nuclear data [4]

- **Nuclear data evaluation:** the evaluators perform a critical review of all the available data and determine the *best estimate* values of the parameters. This is usually done using sophisticated numerical procedures. Evaluated data files are grouped by materials and data types. They are computer-readable and the most common used format is the ENDF-6 format;
- **Evaluated nuclear data processing:** the evaluated data files contain information that exceed the capacity of a computational tool for practical neutron transport applications. Deterministic methods solve the differential or the integral forms of the transport equation using one of the standard method,

dividing the energy interval in groups. Within a group, each energy-dependent parameter takes some average values. The accuracy of the calculation depends on the number of groups and the group averaging method. Before an evaluated data library can be used for practical applications, it must undergo a thorough *verification and validation* process. This is done to avoid processing code failure due to format rule violation and to ensure that the data on the file correspond to what the evaluator intend them to be and that they are consistent with integral experimental measurements, when they are available;

- **Nuclear data applications:** the processed nuclear data can be used in a very large variety of applications, such as: thermal power or fast reactors, small experimental thermal reactors, nuclear fusion applications, shielding problems, radiotherapy, radioactive isotope production, inventory estimation, transport, etc.

### 1.3 Thesis structure

This thesis can be divided in four different main parts.

- The first one is related to the state-of-the-art of nuclear data analyzed during the development of this work, considering the nuclear data libraries and the stored format adopted.
- The second part aims to explain the theoretical background behind the analysis performed in this thesis.
- The third part defines the contribution done for the SANDY development. It is a nuclear data sampling code compatible with nuclear data files in ENDF-6 format, explained in details in Chapter 4. The contributions to this development can be subdivided in four main groups:
  1. first of all, an improvement of the sampling procedure was introduced, adding the option to choose between different input parameter distributions, investigated in Section 4.3;
  2. the Generalized Least Squares (GLS) technique to perform an adjustment of an estimate or of the associated uncertainty, discussed in Section 4.4, was implemented;
  3. an algorithm to obtain perturbed decay data was added and it is explained in Chapter 5;
  4. finally, the methodology to perturb the fission yield data was inserted and it is reported in Chapter 6.

- The last part of this thesis is related to the set up of a Fission Pulse Decay Heat (FPDH) model: this was done to test the algorithms inserted in SANDY for the perturbation of decay and fission yields data. For this reason, an uncertainty analysis and then a sensitivity analysis were done and the results are reported in Chapter 7. Finally, the IFY sampling methodology was used to test the newly realised CEA independent fission yield covariance matrices and the obtained results are commented and compared in Chapter 8. The last part focuses on the conclusions obtained at the end of this work and the suggestion of further prospectives that can be analyzed.

## Chapter 2

# State-of-the-art of nuclear data libraries

This chapter presents the different nuclear data libraries and storing formats addressed during the development of this thesis.

The neutronics simulation of nuclear systems relies on the availability of nuclear data and their related uncertainties to provide accurate numerical representation of the underlying physical processes [5]. As already said in the Introduction 1, all this information is stored in a certain format in a proper nuclear data library, discussed in the following Sections.

### 2.1 Nuclear data libraries

The major general purpose nuclear data libraries investigated in this study are reported in Table 2.1.

In particular the ENDF/B and JEFF libraries were analyzed.

- The *Joint Evaluated Fission and Fusion* (JEFF) Nuclear Data Library: this project comes from a collaboration between Nuclear Energy Agency (NEA) <sup>1</sup> Data Bank participating countries. In particular the version of the JEFF-3.3 library, released in December 2017, was used in this contest [7]. The next version JEFF-4T1 was released as test version in February 2022. It includes two sets of data containing 562 and 2813 neutron cross section evaluations, respectively. The first set, as the previous versions of JEFF, includes the 562

---

<sup>1</sup>NEA is an intergovernmental agency that facilitates co-operation among countries with advanced nuclear technology infrastructures to seek excellence in nuclear safety, technology, science, environment and law [6].

**Table 2.1:** Some of the most relevant nuclear data libraries, their formats and country of origin

Country	Data File	Format	Comments
OECD/NEA	JEFF-3.3	ENDF-6	Latest realised version of European files
OECD/NEA	EFF-2.4	ENDF-6	European Fusion files
Japan	JENDL-5	ENDF-6	Latest version released in 2021 of the Japanese library
USA	ENDF/B-IV	ENDF-4	Old but useful for reference
USA	ENDF/B-VIII.0	ENDF-6	The evaluations benefit from recent experimental data obtained in the U.S. and Europe, and improvements in theory simulation
USA	ENDL-84	ENDF-5	Livermore laboratory evaluation
Russia	BROND-2.2	ENDF-6	Neutron reaction data of the Russian Federation, released in 1992 and updated in 1993
China	CENDL-2	ENDF-6	It contains cross sections of all reactions, angular distributions and spectra of secondary neutrons from 54 nuclides from 10-5eV to 20MeV

most important isotopes for criticality calculations. The second one includes the 562 isotopes of the previous set, but it is completed by the additional 2251 isotopes. This set is recommended for more general purposes [8]. During the development of this Thesis, it was possible to contribute to the testing of the last version of this library and the results are reported in Section 8.

- The *Evaluated Nuclear Data File* (ENDF) library project is coordinated by the Cross Section Evaluation Working Group (CSEWG) and CSEWG. They released the new ENDF/B-VIII.0 library in February 2018, incorporating work from across the US and the international nuclear science community over the last six years. The library is being issued in the traditional ENDF-6 format, as well as in an alternative new Generalized Nuclear Database Structure (GNDS) format. The latest realised version is the ENDF/B-VIII.0 library which continues to evolve through close interactions with parallel organizations around the world, most notably with Europe (JEFF), Japan (JENDL) and

with South Korea. Collaborations with the International Atomic Energy Agency (IAEA) have had numerous impacts, most notably on Collaborative International Evaluation Library Organization (CIELO) nuclides, prompt fission neutron spectra (PFNS) evaluations, and dosimetry cross sections [9].

These libraries have been generated by different projects but they are not totally independent since certain evaluations appear in several different libraries. What ties a lot of these libraries together is their use of a common format known as the **ENDF-6 format** [4].

As already said, after the creation of a library, the data will be processed in files and formats which can be used by different codes such as transport codes. This step is not trivial and can have many impacts in the performances of transport codes. The International Atomic Energy Agency (IAEA) <sup>2</sup>, the Nuclear Energy Agency (NEA) or the National Nuclear Data Center (NNDC) <sup>3</sup> are the main organizations responsible for the distributions of the nuclear data libraries [12].

## 2.2 ENDF-6 format

The ENDF-6 format is the internationally agreed format for data files of evaluated nuclear reaction data [13]. Apart from the storage and retrieval of evaluated nuclear data, it was developed to be used for applications of nuclear technology. These applications control many features of the system including the choice of materials to be included, the data used, the formats used, and the testing required before a library is released. The structure of the **ENDF-6 Formats Manual** is divided in *Formats* and *Procedure*. The former describes how the data are arranged in the libraries and gives the formulas needed to reconstruct physical quantities, while the latter gives the rules that specify what data types must be included, which format can be used in particular circumstances, and so on.

The ENDF-6 format is a computer-readable format, it means that it can be used as the main input to nuclear data processing programs. It uses 80-character records. For historic reasons the parameters are defined in the old-fashioned form of FORTRAN variables. The structure of the ENDF-6 format is illustrated in Figure 2.1. Each file contains a library which may have several sections corresponding to different MAT (specific number which identifies a material) and each material section is structured into several so-called *Files* [14].

---

<sup>2</sup>The IAEA is the world's centre for cooperation in the nuclear field and seeks to promote the secure and peaceful use of nuclear technologies [10].

<sup>3</sup>The NNDC is an organization based in the Brookhaven National Laboratory that acts as a repository for data regarding nuclear chemistry [11].

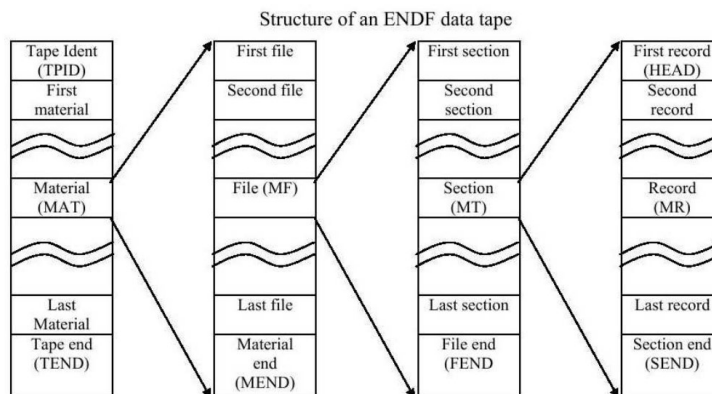


Figure 4: Structure of an ENDF data tape.

**Figure 2.1:** Structure of an ENDF-6 data tape [13]

In each File a certain class of information is stored and they are identified with the abbreviation MF which runs from 1 to 99. Some important examples are:

- File 1 (MF1) stores general information and the multiplicities of neutrons for prompt and delayed fission reaction;
- File 2 (MF2) stores information about the resonance parameters;
- File 3 (MF3) stores the reaction cross sections and auxiliary quantities;
- File 8 (MF8) stores information concerning the decay of the reaction products;
- Files 31-35 (MF31-35) stores the covariance information for MF1-5.

Each MF section is again divided in different subsections called MT, each of which runs from 0 to 999 and identifies a particular reaction or a particular type of auxiliary data. During the development of this thesis, a great effort was done to analyze the section MF8 of the ENDF-6 format, which can be divided into two main subsections:

- MT=454 and MT=459 contain independent and cumulative fission product yield data for fissionable materials;
- MT=457 contains the spontaneous radioactive decay data.

These data will be analyzed in details in Chapters 5 and 6.

## 2.3 Covariance matrix

The correlated uncertainties of different nuclear parameters are considered using the concept of **covariance matrix**. One of the important aspects of nuclear data and of cross sections in particular is that the various data tend to be correlated to an important degree through the measurement processes and the different corrections made to the observable quantities to obtain the microscopic cross sections. In addition to the uncertainties due to the basic data, the results of calculations have uncertainties due to imperfections in the calculational models used. In some situations "modeling uncertainties" may dominate the uncertainties in computed results, while in others they can be considered negligible compared to the effects of microscopic data uncertainties. In principle improving the models may reduce "modeling uncertainties", although sometimes at a large cost. The data uncertainties may also be reduced by performing better measurements, new kinds of measurements, or sometimes a more refined analysis of existing data.

Until the ENDF/B-IV (version IV of the ENDF/B library), the only means available to evaluators for communicating the estimated uncertainties in the evaluated data was through publication of the documentation of the evaluations. Then the Nuclear Data community have formed a Covariance Subcommittee to coordinate the efforts at standardizing statements made about the data uncertainties and correlations. The dominant reason for the inclusion of covariance files in the ENDF system is to enable estimation of the contribution of nuclear data uncertainties to uncertainties in calculates results for nuclear systems having broad (neutron) spectra. Therefore, in developing the ENDF formats, the highest priority was given to attain this goal. Indeed, the main purpose of the covariance information in ENDF-6 formats is to permit the propagation of nuclear data uncertainties for applications with broad neutron spectra [13].

It is appropriate to define uncertainty quantities. Each cross section or related quantity in an ENDF file represents a physical quantity that has a definite, though unknown true magnitude. The knowledge of each such quantity  $X$  is summarized by its *Probability Density Function (PDF)* defined so that  $f(X)\Delta X$  is the probability that the true numerical value of  $X$  lies in the range  $\Delta X$  about  $X$ . The *marginal density function*  $f(X)$  is the average over all other independent variables  $Y$ ,  $Z$ , etc. of the overall multivariate density function for the cross section data base. The shape of a density function depends on the experiments that have been performed, relevant to estimating the true values of the data elements. The density function has unit normalization for each variable. The **expected value**,  $\langle g(X) \rangle$ , of any function  $g(X)$  is given by the average value of that function over the marginal density function. The simplest example is the expected value of the quantity itself:

$$\langle X \rangle = \int X f(X) dX \quad (2.1)$$

The *true value* of a given quantity  $X$  can be expressed as the best estimate of its expected value  $\bar{X}$  plus its uncertainty  $\delta X$ :

$$X = \bar{X} + \delta X \quad (2.2)$$

Considering the second moments of the density function and the quantity  $F(X, Y)$  as the Cumulative Distribution Function (CDF) averaged over all variables other than  $X$  and  $Y$ , it is possible to define the covariance between  $X$  and  $Y$  as a measure of the relationship between them:

$$Cov(X, Y) = \langle \delta X \delta Y \rangle = \int \int (X - \langle X \rangle)(Y - \langle Y \rangle) F(X, Y) dX dY \quad (2.3)$$

The variance of  $X$ , as a measure of its variability, is:

$$Var(X) = Cov(X, X) = \langle \delta X \delta X \rangle \quad (2.4)$$

In matrix form, the covariance terms will cover the off-diagonal terms, while the variance terms will be in the diagonal. Knowledge of the covariance is crucial to the joint application of the quantities  $X$  and  $Y$  [13].

From these definitions, it is possible to state that the concept of covariance matrix defines a quantification of a lack of knowledge on a particular physical quantity and, as a mathematical object, it is symmetric and positive semidefinite, i.e., with only non-negative eigenvalue. Considering this concept in a physical way, round-off errors and collapse or extension into multi-group energy structures can lead to small negative eigenvalues, for which approximate solutions are stored in the nuclear data libraries.

## Chapter 3

# Nuclear data uncertainty propagation

In this Chapter, the basic physical aspects and methodologies used during the development of this thesis are reported.

### 3.1 Basic definitions

In this Section, the basic definition of the main physical quantities used in this Thesis are mentioned. The notation used and explained in this paragraph will be adopted in the following Sections.

The time will be indicated with  $t$ , the position with  $\bar{r} = (x, y, z)$ , the energy with  $E$  and the velocity with  $\bar{v}$ . The latter is a vector which direction is represented by the normalized vector  $\bar{\Omega} = \frac{\bar{v}}{|\bar{v}|}$ .

$$\begin{cases} \bar{\Omega} = \Omega_x \bar{1}_x + \Omega_y \bar{1}_y + \Omega_z \bar{1}_z \\ \Omega_x^2 + \Omega_y^2 + \Omega_z^2 = 1 \end{cases} \quad (3.1)$$

with  $\bar{1}_x, \bar{1}_y$  and  $\bar{1}_z$  the versors of the three space directions (x, y and z respectively in cartesian coordinate). Now it is possible to define the **density function**

$$n(\bar{r}, E, \bar{\Omega}, t) \quad (3.2)$$

where  $(\bar{r}, E, \bar{\Omega}, t)$  is called *phase space*. To evaluate the number of neutrons that are in the volume  $d\bar{r}$  with energy in the interval  $(E, E + dE)$  and direction in the small area  $d\Omega$ , the density function must be multiplied for the equivalent volume of interest:

$$n(\bar{r}, E, \bar{\Omega}, t) d\bar{r} dE d\Omega = \text{neutrons within } d\bar{r} \text{ } dE \text{ } d\Omega \text{ at time } t \quad (3.3)$$

### 3.1.1 Neutron interactions

Neutrons can have different interactions with particles surrounding them: scattering, fission, capture are some of them. Each kind of interaction has a certain probability of happening. In general, the probability per unit of path that the event 'x' occurs (i.e. the collision that generates the event 'x') is indicated with  $\Sigma_x$  and it is measured in  $cm^{-1}$ .  $\Sigma_x$  is called **macroscopic cross section**. Each interaction is due to the collision of neutrons with other nuclei of the medium, in fact neutron vs. neutron collisions are neglected. The area of the target involved in the collision is called **microscopic cross section**. It is a figurative way to represent the quantum effect of the mentioned collision. It is generally indicated with the symbol  $\sigma$  and it is measured in  $cm^2$  or in barn ( $1 \text{ barn} = 10^{-24} \text{ cm}^2$ ) [15]. There are several events of interest occurring during neutron collisions. In particular, *absorption* (including *fission* or *capture*) and *scattering* are the most important. A neutron that is absorbed ( $\Sigma_a$ ) by a target can generate fission ( $\Sigma_f$ ) or can be just captured by it ( $\Sigma_c$ ). Otherwise a neutron can just be scattered ( $\Sigma_s$ ) by the target and the collision may be elastic or inelastic. The macroscopic cross section is not a simple constant but depends on the position and on the energy of the neutron colliding on the target in an isotropic medium. Considering a non-isotropic medium, it depends also on the direction  $\bar{\Omega}$ . Talking about scattering, it can be useful to know not only the probability that a scatter event occurs, but also the probability for a neutron located in  $\bar{r}$  moving with direction  $\bar{\Omega}'$  and energy  $E'$  of being reissued in a certain cone  $d\Omega$  with energy in the interval  $(E, E + dE)$  [16]. In order to do so, it has been defined the **scattering probability density**  $f_s$  that depends on the position of the neutron, on the energy before ( $E'$ ) and after ( $E$ ) and on the direction before ( $\bar{\Omega}'$ ) and after ( $\bar{\Omega}$ ) the collision. In particular, in an isotropic medium, this probability does not depend on the incoming direction of the neutron (it is a rotational invariant in spherical geometry), so it will depend only on the angle that the two directions may form. It means that it is possible to consider just the dependence of the scalar product between the two directions.

$$f_s(\bar{r}, E' \rightarrow E, \bar{\Omega}' \cdot \bar{\Omega}) \quad (3.4)$$

Regarding fission, it is possible to define  $\nu(\bar{r}, E')$ , i.e. the expected **number of neutrons emitted in  $\bar{r}$**  after a fission event by a neutron with energy  $E'$  (before the collision), and the **fission spectrum**  $\chi(\bar{r}, E)$  which represents the probability density of being reissued within the interval  $(E, E + dE)$ . Moreover, fission can be considered isotropic, so the probability for a neutron of being reissued in a certain direction is equal for all direction (i.e.  $\frac{1}{4\pi}$ ) [17].

Knowing the cross section of each event is crucial to calculate the number of interactions of that type. It can be written as the total distance traveled by neutrons in a certain media multiplied by the probability for unit path of that kind

of interaction. The total distance traveled by neutrons is the multiplication of the total number of neutrons (equation 3.3) by the distance traveled at their speed,  $v$ , by the time  $dt$ .

$$n(\bar{r}, E, \bar{\Omega}, t)d\bar{r}dEd\Omega v dt \Sigma_x = \text{number of interactions 'x' in } d\bar{r}dEd\Omega dt \quad (3.5)$$

The product  $n(\bar{r}, E, \bar{\Omega}, t)v$  in nuclear physics is usually called **angular flux**  $\phi$ :

$$\phi(\bar{r}, E, \bar{\Omega}, t) = n(\bar{r}, E, \bar{\Omega}, t)v \quad (3.6)$$

In order to have the total amount of interactions in a finite volume in phase space, the sum of all the contributions must be performed, and so integrating:

$$\oint_{\Omega} \int_E \phi(\bar{r}, E, \bar{\Omega}, t)d\bar{r}dEd\Omega dt \Sigma_x = \text{total number of interactions 'x'} \quad (3.7)$$

## 3.2 The transport equation

In this Section the main ingredients needed to put down a model describing neutrons behavior in a reactor are analyzed. Let's start taking in consideration a little volume  $d\bar{r}$  and studying the variation in time of the number of neutrons that are in this volume due to collisions - without considering fission for the moment. It is possible to set up an equation like [16]:

$$\begin{aligned} & \text{neutrons at time } (t+dt) - \text{neutrons at time } (t) = \\ & (\text{neutrons moving in} - \text{neutrons moving out}) - (\text{removal due to captures}) + \\ & (\text{neutrons scattered in from the outside}) + \text{source} \end{aligned} \quad (3.8)$$

In math form it can be expressed as:

$$\begin{aligned} & [n(\bar{r}, E, \bar{\Omega}, t + dt) - n(\bar{r}, E, \bar{\Omega}, t)] = \\ & = -\nabla \cdot \bar{\Omega} \phi(\bar{r}, E, \bar{\Omega}, t)d\bar{r}dEd\Omega dt - \Sigma(\bar{r}, E)\phi(\bar{r}, E, \bar{\Omega}, t)d\bar{r}dEd\Omega dt + \\ & + \oint d\Omega' \int dE' \Sigma_s(\bar{r}, E')\phi(\bar{r}, E, \bar{\Omega}, t) f_s(\bar{r}, E' \rightarrow E, \bar{\Omega}' \cdot \bar{\Omega}) d\bar{r}dEd\Omega dt + \\ & + S(\bar{r}, E, \bar{\Omega}, t) d\bar{r}dEd\bar{\Omega} \end{aligned} \quad (3.9)$$

The notation adopted and the physical meaning of each term are the same as discussed in the previous Section, but a further comment is needed for the divergence term. It corresponds to the net number of neutrons that cross the surface going out of the volume. It can be seen as the surface integral of the net current density  $(\phi(\bar{r}, E, \bar{\Omega}, t) \cdot \bar{\Omega})$ , but exploiting the divergence theorem, it is reported as the volumetric integral of the divergence of the current density. In equation 3.9, the divergence theorem is used in differential form.

In the discussion so far, the fission term of the neutron transport equation was neglected. It can be expressed in the following way:

$$\oint d\Omega' \int dE' \Sigma_f(\bar{r}, E') \bar{\Omega}' \frac{\chi(\bar{r}, E)}{4\pi} \nu(\bar{r}, E') \phi(\bar{r}, E, \bar{\Omega}') d\bar{r} dE d\Omega \quad (3.10)$$

Each parameter was already explained in 3.1.

For what concerns initial conditions, in general it is not restrictive to say that they are known, while boundary conditions require more attentions. Let's suppose that the space domain is a *non re-entering (convex) and simply-connected* one. If outside the domain there is void, neutrons can leave it but once out they cannot bounce back because they cannot collide anymore, so it is possible to say that the incoming flux is equal to zero at the boundaries. Since air is a rarefied gas, it is not much different for a neutron if outside the domain there is air or void, so the previous condition remains valid also in this case. This boundary condition can be expressed in the following way [18]:

$$\phi(\bar{r}, E, \bar{\Omega}_{incoming}, t) = 0 \quad (3.11)$$

The transport equation can be analytically solved in simplified domains but, for what concerns nuclear studies domains, it can be not very simple so approximations could be needed. It is possible to write the transport equation in operational form, useful in the developing of solution methods. In Table 3.1 the definition of some operators to write the equation 3.9 in a more concise way is reported, considering steady state condition and without source term.

**Table 3.1:** Operator definitions useful to write the transport equation in a more concise way

Operator	Expression
Transport operator	$\hat{T} = \nabla \cdot \bar{\Omega} + \Sigma(\bar{r}, E)$
Leakage operator	$\hat{L} = \hat{T} - \hat{\theta}_s$
Scattering operator	$\hat{\theta}_s = \oint d\Omega' \int dE' \Sigma_s(\bar{r}, E') f_s(\bar{r}, E' \rightarrow E, \bar{\Omega}' \rightarrow \bar{\Omega})$
Fission operator	$\hat{F} = \oint d\Omega' \int dE' \Sigma_f(\bar{r}, E') \bar{\Omega}' \frac{\chi(\bar{r}, E)}{4\pi} \nu(\bar{r}, E') d\bar{r} dE d\Omega$

with these operators, the transport equation can be expressed as:

$$\hat{T}\phi = \hat{\theta}_s\phi + \hat{F}\phi \quad (3.12)$$

This equation is homogeneous, it has of course the zero solution, but it's not of practical interests. To find a non-zero solution it is possible to introduce an eigenvalue  $k$ , also called **multiplication factor**. It is a mathematical trick inserted

to find the non-trivial solution. This parameter can be seen as the ratio between the number of neutrons in one generation with respect to the number of neutrons in the preceding generation.

Once  $k$  is inserted, a solution of this equation is guaranteed and it is called *eigenfunction* [19].

- If  $k = 1$  the system is called *critical*, which means that the neutron population self-sustains itself;
- if  $k < 1$  the system is called *sub-critical*, which means that the fission process is not able to compensate the leakages, the neutron population is not self-sustaining;
- if  $k > 1$  the system is *super-critical* and the fission process is producing more neutrons than those that are lost.

With this parameter, equation 3.12 becomes 3.13.

$$\hat{T}\phi = \hat{\theta}_s\phi + \frac{1}{k}\hat{F}\phi \quad \text{or} \quad \hat{L}\phi = \frac{1}{k}\hat{F}\phi \quad (3.13)$$

### 3.3 The adjoint transport equation

In this Section a new physical concept is introduced: the **Importance function**

$$\psi(\bar{r}, E, \bar{\Omega}) \quad (3.14)$$

whose output is a scalar value. The physical meaning of the Importance function is to estimate the importance of neutrons. First, to derive the importance equation, the importance concept is addressed as the capability to make fission; later on, this concept will be extended in a more general way.

Considering  $N_0$  neutrons traveling along direction  $\bar{\Omega}$  with energy status  $E$ , it is possible to perform a steady-state balance of neutron importance between a point  $\bar{r}$  and a nearby one  $\bar{r} + ds\bar{\Omega}$  distant  $ds$  along the direction  $\bar{\Omega}$ . The importance of the neutrons introduced in  $\bar{r}$  with energy  $E$  and direction  $\bar{\Omega}$  is equal to the importance of the neutrons in  $\bar{r} + ds\bar{\Omega}$  that have not collided plus the importance of all generated neutrons. The generated neutrons considered are the scattered and the fission produced [20]. The Importance of the neutrons in  $\bar{r}$  with energy  $E$  and direction  $\bar{\Omega}$  is given by:

$$N_0\psi(\bar{r}, E, \bar{\Omega}) \quad (3.15)$$

The Importance of neutrons in  $\bar{r} + ds\bar{\Omega}$  that have not collided moving along  $ds$  is given by

$$[1 - \Sigma(\bar{r}, E)ds]N_0\psi(\bar{r} + ds\bar{\Omega}, E, \bar{\Omega}) \quad (3.16)$$

The scattering contribution is given by:

$$N_0 ds \oint d\Omega' \int dE' \Sigma_s(\bar{r}, E) f_s(\bar{r}, E \rightarrow E', \bar{\Omega} \cdot \bar{\Omega}') \psi(\bar{r}, E', \bar{\Omega}') \quad (3.17)$$

The fission contribution is given by:

$$\frac{1}{k} N_0 ds \oint d\Omega' \int dE' \Sigma_f(\bar{r}, E) \nu(\bar{r}, E) \frac{\chi(\bar{r}, E')}{4\pi} \psi(\bar{r}, E', \bar{\Omega}') \quad (3.18)$$

The overall balance can be written as:

$$\begin{aligned} N_0 \psi(\bar{r}, E, \bar{\Omega}) &= [1 - \Sigma(\bar{r}, E) ds] N_0 \psi(\bar{r} + ds \bar{\Omega}, E, \bar{\Omega}) + \\ &+ N_0 ds \oint d\Omega' \int dE' \Sigma_s(\bar{r}, E) f_s(\bar{r}, E \rightarrow E', \bar{\Omega} \cdot \bar{\Omega}') \psi(\bar{r}, E', \bar{\Omega}') + \\ &+ \frac{1}{k} N_0 ds \oint d\Omega' \int dE' \Sigma_f(\bar{r}, E) \nu(\bar{r}, E) \frac{\chi(\bar{r}, E')}{4\pi} \psi(\bar{r}, E', \bar{\Omega}') \end{aligned} \quad (3.19)$$

Simplifying the arbitrary number of neutrons  $N_0$ , dividing for  $ds$  and taking the limit for  $ds$  going to zero, the following importance equation is derived:

$$\begin{aligned} -\bar{\Omega} \cdot \nabla \psi(\bar{r}, E, \bar{\Omega}) + \Sigma(\bar{r}, E) \psi(\bar{r}, E, \bar{\Omega}) &= \\ &= \oint d\Omega' \int dE' \Sigma_s(\bar{r}, E) f_s(\bar{r}, E \rightarrow E', \bar{\Omega} \cdot \bar{\Omega}') \psi(\bar{r}, E', \bar{\Omega}') + \\ &+ \frac{1}{k} \oint d\Omega' \int dE' \Sigma_f(\bar{r}, E) \nu(\bar{r}, E) \frac{\chi(\bar{r}, E')}{4\pi} \psi(\bar{r}, E', \bar{\Omega}') \end{aligned} \quad (3.20)$$

An important consideration is that  $\psi$  is not a density function, it is a value, so the differentials  $dE' d\Omega'$ , inserted in the scattering and fission terms, are there even before the introduction of  $\psi$ : indeed, they are attached to the probability density functions  $f_s$  and  $\chi$  [20]. To solve equation 3.20, some boundary conditions are needed. Assuming the impossibility of any neutron to enter the domain from the external world (i.e. domain surrounded by vacuum), once a neutron leaves the domain is lost. This means that it is no more able to make any fission and in this contest its importance is zero. From a mathematical point of view, it is possible to write:

$$\psi(\bar{r}_s, E, \bar{\Omega}_{outgoing}) = 0 \quad (3.21)$$

From equations 3.11 and 3.21, it seems obvious that there is a kind of similarity between the importance equation and the transport equation. If a position in space that is the boundary of the domain is considered, then for every entering directions the angular flux will be zero; if now every outgoing direction is considered, the Importance will be zero. This behaviour leads to this statement: the product

between the angular flux and the importance evaluated in any position at the boundary is always zero whatever energy and direction.

$$\phi(\bar{r}_s, E, \bar{\Omega})\psi(\bar{r}_s, E, \bar{\Omega}) = 0 \quad \forall \bar{\Omega}, E \quad (3.22)$$

Equation 3.20 is also called **Adjoint transport equation**. An adjoint equation is a linear differential equation, usually derived from its primal equation using integration by parts [21]. To understand the meaning of the adjoint function, a simple example is proposed. Let  $f$  and  $g$  be two functions of one variable  $x$ . The scalar product of these two functions is:

$$(g, f) = \int dx g(x)f(x)\xi(x) \quad (3.23)$$

where  $\xi(x)$  is a weighting function, that could be equal to 1. Now if  $\theta$  is an operator,  $f$  and  $g$  are two functions in the  $x$  domain, then  $\theta^+$  is called the **adjoint operator of  $\theta$**  if this relation is true [22].

$$(g, \theta f) = (\theta^+ g, f) \quad (3.24)$$

The general way to find the adjoint of an operator is to apply the formal definition of adjointness (equation 3.24).

Coming back to the equation 3.20, it results an homogeneous equation so in every term there is an operator applied to  $\psi(\bar{r}, E, \bar{\Omega})$ . To find the link between the importance equation and the transport equation, the adjoint operator of each term of the importance equation must be computed as follows [20]:

- $\theta = \Sigma(\bar{r}, E)$ :

Considering the angular flux  $\phi$  and the importance function  $\psi$  and applying the definition of the adjoint operator  $(\psi, \Sigma\phi) = (\Theta^+\psi, \phi)$  the result is:

$$\begin{aligned} \oint d\Omega \int dE \int d\bar{r} \psi(\bar{r}, E, \bar{\Omega})[\Sigma(\bar{r}, E)\phi(\bar{r}, E, \bar{\Omega})] &= \\ &= \oint d\Omega \int dE \int d\bar{r} \phi(\bar{r}, E, \bar{\Omega})[\theta^+\psi(\bar{r}, E, \bar{\Omega})] \end{aligned} \quad (3.25)$$

The product operation is commutative and the equation is satisfied if

$$\theta^+ = \Sigma(\bar{r}, E) \quad (3.26)$$

which means

$$(\Sigma(\bar{r}, E))^+ = \Sigma(\bar{r}, E) \quad (3.27)$$

From formula 3.27, it is possible to conclude that the  $\Sigma$  operator is self-adjoint.

- $\theta = \oint d\Omega' \int dE' \Sigma_s(\bar{r}, E) f_s(\bar{r}, E \rightarrow E', \bar{\Omega} \cdot \bar{\Omega}')$ :

- $\theta = \frac{1}{k} \oint d\Omega' \int dE' \Sigma_f(\bar{r}, E) \nu(\bar{r}, E) \frac{\chi(\bar{r}, E')}{4\pi}$ :

Also the scattering term and the fission term are self-adjoint. The demonstration for these terms is the same as explained for the  $\Sigma$  operator and it is based on renaming the variables of the integral.

- $\theta = -\bar{\Omega} \cdot \nabla$ :

For the sake of simplicity, the derivation of this adjoint term is performed in the opposite way. Starting from the assumption that

$$(\bar{\Omega} \cdot \nabla)^+ = -\bar{\Omega} \cdot \nabla \quad (3.28)$$

the condition of adjointness is applied to verify that the assumption 3.28 is satisfied. This condition is the following:

$$(\psi, \bar{\Omega} \cdot \nabla \phi) = (-\bar{\Omega} \cdot \nabla \psi, \phi) \quad (3.29)$$

that in an extended form is written as

$$\begin{aligned} \oint d\Omega \int dE \int d\bar{r} \psi(\bar{r}, E, \bar{\Omega}) [\bar{\Omega} \cdot \nabla \phi(\bar{r}, E, \bar{\Omega})] &= \\ = \oint d\Omega \int dE \int d\bar{r} \phi(\bar{r}, E, \bar{\Omega}) [-\bar{\Omega} \cdot \nabla \psi(\bar{r}, E, \bar{\Omega})] & \quad (3.30) \end{aligned}$$

Gathering all the terms to the first member:

$$\begin{aligned} \oint d\Omega \int dE d\bar{r} [\psi \bar{\Omega} \cdot \nabla \phi + \phi \bar{\Omega} \cdot \nabla \psi] &= 0 \\ \oint d\Omega \int dE d\bar{r} \bar{\Omega} \cdot [\psi \nabla \phi + \phi \nabla \psi] &= 0 \\ \oint d\Omega \int dE d\bar{r} \bar{\Omega} \cdot \nabla (\psi \phi) &= 0 \\ \oint d\Omega \int dE d\bar{r} \nabla \cdot [\bar{\Omega} \psi(\bar{r}, E, \bar{\Omega}) \phi(\bar{r}, E, \bar{\Omega})] &= 0 \quad (3.31) \end{aligned}$$

At this point the *divergence theorem* can be applied, which states that the integral of the divergence of a vector in the volume is equal to the flux of that vector through the surface of that volume [23].

$$\int dE \oint d\Omega \int \bar{\Omega} \phi(\bar{r}_s, E, \bar{\Omega}) \psi(\bar{r}_s, E, \bar{\Omega}) \cdot \bar{n}(\bar{r}_s) dA(\bar{r}_s) = 0 \quad (3.32)$$

Where  $dA(\bar{r}_s)$  is an element of the surface surrounding the volume  $d\bar{r}$  and  $\bar{n}(\bar{r}_s)$  is the outgoing normal vector in every point of the surface. Using equation 3.22, it is possible to state that the adjointness condition is verified and assumption 3.28 is true.

With these demonstrations it is verified that the equation for the importance function is the adjoint equation of the transport equation and so:

$$\psi = \phi^+ \quad (3.33)$$

A more general definition for the importance function can be done introducing the concept of *detector*. It can be thought as the general target for neutrons. More precisely a detector is a volume in phase space to which a cross section can be associated:

$$\Sigma_d(\bar{r}, E, \bar{\Omega}) \quad (3.34)$$

In the balance equation, this detector can be seen as a source. This means that a balance should be performed considering a sub-critical system in which a source can be inserted. The condition of sub-critical system is mandatory since for just critical or super-critical system the introduction of a source would produce meaningless results as a negative solution, to compensate for the over production of neutrons, in order to achieve the equation balance. So the equation for the considered system can be written as:

$$\begin{aligned} -\bar{\Omega} \cdot \nabla \psi(\bar{r}, E, \bar{\Omega}) + \Sigma(\bar{r}, E) \psi(\bar{r}, E, \bar{\Omega}) = \\ = \oint d\Omega' \int dE' \Sigma_s(\bar{r}, E) f_s(\bar{r}, E \rightarrow E', \bar{\Omega} \cdot \bar{\Omega}') \psi(\bar{r}, E', \bar{\Omega}') + \\ + \oint d\Omega' \int dE' \Sigma_f(\bar{r}, E) \nu(\bar{r}, E) \frac{\chi(\bar{r}, E')}{4\pi} \psi(\bar{r}, E', \bar{\Omega}') + \Sigma_d(\bar{r}, E, \bar{\Omega}) \end{aligned} \quad (3.35)$$

With equation 3.35 it is possible to change the kind of detector and get different equations for the importance, meaning that there is no unique equation for the source importance problems.

## 3.4 Perturbation theory

During the normal life of a nuclear reactor it works in steady state for most of the time. However, sometimes some changes could be needed such as the movement of control rods. This Section focuses on the discussion of how the change of some quantities affect the others. These effects of change can be mainly of two types: changes can be produced by the operator or they can be related to the uncertainties on the basic nuclear data [24].

A list of some applications of perturbation theory is presented:

- Evaluation of effects of perturbations on integral parameters;
- Evaluation of effects of perturbations on neutrons and reaction rates distributions;

- Sensitivity/uncertainty analysis, i.e. uncertainty of material compositions;
- Studies of reactor control and safety;
- Nuclear data adjustment.

### 3.4.1 SPT - Standard Perturbation Theory

The main aim of Standard Perturbation Theory (SPT) is evaluating the perturbation of the multiplication factor  $k$  due to perturbation of some nuclear data — e.g. cross section  $\Sigma$ . At this scope it is possible to define the **reactivity**  $\rho$  and **sensitivity**  $S$  (of parameter  $k$  with respect to the cross section) as follows:

$$\rho = \frac{\delta k}{k} \quad (3.36)$$

$$S = \frac{\delta k/k}{\delta \Sigma/\Sigma} \quad (3.37)$$

Note that in the case of cross sections, if several materials are adopted, then different cross sections can be perturbed: thus  $\Sigma$  could be a vector and so for the multiplication factor  $k$ . For this reason sensitivity is in general a matrix. Starting from the criticality problem, it is possible to perturb all the terms [25].

$$\hat{L}\phi = \frac{1}{k}\hat{F}\phi \quad (3.38)$$

Indeed the perturbation of the operations will induce a perturbation to the flux, which will be indicated as follow:

$$\hat{L} \rightarrow \hat{L} + \delta\hat{L}; \quad \hat{F} \rightarrow \hat{F} + \delta\hat{F}; \quad \phi \rightarrow \phi + \delta\phi \quad (3.39)$$

To simplify the notation,  $k$  can be expressed as its inverse  $\lambda = \frac{1}{k}$  and the perturbed value is:

$$\lambda \rightarrow \lambda + \delta\lambda; \quad \delta\lambda = -\frac{1}{k^2}\delta k \quad (3.40)$$

Substituting 3.39 and 3.40 into 3.38, the perturbed equation of the criticality problem is:

$$\hat{L}\delta\phi + \delta\hat{L}\phi = \lambda\hat{F}\delta\phi + \lambda\delta\hat{F}\phi + \delta\lambda\hat{F}\phi \quad (3.41)$$

In order to solve equation 3.41, it is useful to solve the adjoint criticality problem and get the adjoint function  $\phi^+$  whose meaning was discussed in Section 3.3:

$$\hat{L}^+\phi^+ = \lambda^+\hat{F}^+\phi^+ \quad (3.42)$$

Since  $\lambda$  is a real number, it coincides with its adjoint  $\lambda = \lambda^+$ . Exploiting this relationship, it is possible to project equation 3.41 to  $\phi^+$  and integrate it over the phase space – i.e. to do the inner product between equation 3.41 and  $\phi^+$  [25]. Considering only the first order terms and so neglecting the higher order terms, the equation obtained is:

$$(\cancel{\phi^+, \hat{L}\delta\phi}) + (\phi^+, \delta\hat{L}\phi) = \cancel{\lambda(\phi^+, \hat{F}\delta\phi)} + \lambda(\phi^+, \delta\hat{F}\phi) + \delta\lambda(\phi^+, \hat{F}\phi) \quad (3.43)$$

The two terms cancelled are simplified thanks to the equation 3.42, indeed they can be written as  $(\hat{L}^+\delta\phi^+, \phi) = \lambda^+(\hat{F}^+\delta\phi^+, \phi)$ . By using the definition of adjoint operator and substituting 3.42, it is possible to obtain a suitable formula to evaluate the reactivity at a 1<sup>st</sup> order without finding  $\delta\phi$  that is:

$$\delta\lambda = \frac{(\phi^+, \delta\hat{L}\phi) - \lambda(\phi^+, \delta\hat{F}\phi)}{(\phi^+, \hat{F}\phi)} \quad (3.44)$$

or in terms of multiplication factor:

$$\frac{\delta k}{k} = \frac{\frac{1}{k}(\phi^+, \delta\hat{F}\phi) - (\phi^+, \delta\hat{L}\phi)}{\frac{1}{k}(\phi^+, \hat{F}\phi)} = \rho \quad (3.45)$$

Formula 3.45 allows to compute the perturbation on the multiplication factor, i.e. the reactivity inserted by that perturbation, for any kind of perturbation. To get  $\rho$ , the reference problem and the adjoint problem must be solved and the perturbations  $\delta\hat{L}$  and  $\delta\hat{F}$  must be computed. Equation 3.45 is valid for small perturbation (only first order terms have been used to derive it).

From Section 3.3, the adjoint function of angular flux was defined as the importance of neutrons. Thus, if  $\hat{F}\phi$  is the number of neutrons emitted by fission per unit of phase space and time, its inner product with the importance  $(\phi^+, \hat{F}\phi)$  is the total importance of all the neutrons produced by fission in the whole domain. With the same scheme, it is possible to say that  $(\phi^+, \delta\hat{L}\phi)$  is the total importance of the neutrons lost due to the change of  $\hat{L}$  and  $(\phi^+, \delta\hat{F}\phi)$  is the total importance of neutrons emitted by fission due to the change of  $\hat{F}$ . To understand the physical meaning of equation 3.45, it can be expressed in words [24]:

$$\rho = \frac{\text{change of importance due to perturbation}}{\text{importance of fissions}} \quad (3.46)$$

### 3.4.2 GPT- Generalized Perturbation Theory

The basic principle of the generalized perturbation theory is to study the perturbation of parameters that can be written as integrals of the solution of the reference equation [26].

Let's consider a system which is kept in steady state by the presence of a source  $S$  (this means the system is sub-critical). Defining the operator  $\hat{H} = \hat{L} - \hat{F}$ , the model behaviour can be described by equation 3.47.

$$\hat{H}\phi = S \quad (3.47)$$

Then a perturbation occurs, such that the operator  $\hat{H}$  and the source  $S$  are perturbed.

$$\hat{H} \rightarrow \hat{H} + \delta\hat{H} ; \quad S \rightarrow S + \delta S \quad (3.48)$$

The relevant perturbation under consideration can be seen as the variation of the integral quantity  $I$ , defined as:

$$I = (\mathbf{D}, \phi) \quad (3.49)$$

where  $\mathbf{D}$  is called *detector*. It is defined as an ideal instrument to measure the interested quantity. As the perturbations  $\delta\hat{H}$  and  $\delta S$  arise, the flux will be perturbed as  $\delta\phi$ . Assuming that the perturbation is only propagated to the flux and not to the detector, the perturbation of the quantity of interest will be:

$$\delta I = (\mathbf{D}, \delta\phi) \quad (3.50)$$

The aim of perturbation theory proposed with this approach is to compute the value of  $\delta I$  without the need of finding  $\delta\phi$  [27]. Substituting 3.48 into 3.47, the perturbed equation results:

$$\hat{H}\phi + \hat{H}\delta\phi + \delta\hat{H}\phi + \delta\hat{H}\delta\phi = S + \delta S \quad (3.51)$$

Simplifying the reference equation 3.47 and neglecting the second order terms, equation 3.51 becomes:

$$\hat{H}\delta\phi + \delta\hat{H}\phi = \delta S \quad (3.52)$$

Coherently with the philosophy of the perturbation theory, the next step is to solve another problem to get a solution which is valid for a various range of applications. For this purpose, the extra problem to be solved can be consider as the adjoint problem of the reference equation 3.47, with the system driven by the detector  $\mathbf{D}$  instead of the adjoint source.

$$\hat{H}^+\phi^+ = \mathbf{D} \quad (3.53)$$

An important consideration is that in the case of the homogeneous problem, the adjoint problem to be solved was unique. In the case of the detector analysis considered, the auxiliary problem to be solved is not unique as it changes with the detector chosen.

The next step is to project equation 3.52 on the solution of the adjoint problem  $\phi^+$ :

$$(\phi^+, \hat{H}\delta\phi) + (\phi^+, \delta\hat{H}\phi) = (\phi^+, \delta S) \quad (3.54)$$

Exploiting the definition of adjoint problem, the first term can be written in the following way:

$$(\phi^+, \hat{H}\delta\phi) = (\hat{H}^+\phi^+, \delta\phi) = (D, \delta\phi) = \delta I \quad (3.55)$$

Finally, the interested perturbation can be computed with equation 3.56.

$$\delta I = (\phi^+, \delta S) - (\phi^+, \delta\hat{H}\phi) \quad (3.56)$$

which is a formula that allows to compute the perturbation of the integral quantity of interest  $\delta I$ , knowing only the perturbing phenomena  $\delta\hat{H}$  and  $\delta S$  and the solutions of the adjoint and direct problems [27].

### 3.5 Perturbation Theory vs Total Monte Carlo

As already discussed in the Introductory Chapter, since the beginning of the century the nuclear science community is putting more attention to the assessment of nuclear data uncertainties. Nuclear data uncertainties are currently on the spotlight, due to the assessment of their impact on criticality safety analysis, and also in burn-up/depletion/activation analysis [28]. As of today, two methods can be used to propagate uncertainties from nuclear data to quantities of large scale systems: **Perturbation method** and **Total Monte Carlo (TMC)** [29]. The first method was explained in Section 3.4. The TMC method was developed more recently thanks to the huge increase in computer power of these last decades. It relies on a large number of calculations, all alike but with different random nuclear data in each of them. The result is a probability distribution from which different moments can be extracted [30]. Total Monte Carlo means that the random variation of nuclear data, experimental data, ENDF-6 data file creation, processing and applied reactor calculation are seen as a single loop in a Monte Carlo process [31]. An example of the propagation of cross sections uncertainties to evaluate the uncertainty on the multiplication factor parameter is reported in Figure 3.1 to compare the two methods. Moreover, to be comparable, the two approaches should start from a similar starting point. To ensure this, it is possible to generate these start ENDF files from the same set of runs using different codes, such as the TALYS code<sup>1</sup>. The TALYS system creates random ENDF nuclear data files based on random inputs [32]. At the end of the random file generation, the covariance

---

<sup>1</sup>TALYS: Nuclear Model Code System for Analysis and Prediction of Nuclear Reactions and Generation of Nuclear Data [32].

information is extracted and formatted into an ENDF format. This method allows to cover the top part of Figure 3.1, from the "n TMC input files", to the "1 ENDF file + covariances" and "n x ENDF random files". After this point, the "TMC box" in this Figure has two ramifications described in the following items. Both methods exploit the **MCNP** calculation. MCNP is a general-purpose Monte Carlo N-Particle code that can be used for neutron, photon, electron, or coupled neutron/photon/electron transport. It has predictive capability that can replace expensive or impossible-to-perform experiments. It is often used to design large-scale measurements providing a significant time and cost savings to the community [33]. In the case of the example analyzed this code is used to compute the values of  $k_{eff}$ , starting from the perturbed nuclear data and the related sensitivity.

- In *Perturbation method branch* (left side) the ENDF file is processed by NJOY<sup>2</sup> to obtain processed covariances and processed cross sections. The "Add perturbation", "MCNP input file + perturbation card" and "MCNP6" boxes in Figure 3.1 present the essential part of the sensitivity calculation. Exploiting version 6 of the MCNP code, the sensitivity profile  $S$  can be calculated. It is defined as the relative change in a response parameter  $R$  due to a relative change in a cross section in a particular energy group  $g$ . In the MCNP input file the relevant material is replaced by the perturbation cards, introducing a perturbation in one or more specific materials. Then the MCNP6 code is run with these modifications in the input file. The MCNP output gives the results of the perturbations with statistical uncertainties and a  $k_{eff}$  value in case of criticality benchmarks. Finally, to combine the sensitivity and covariance matrices, the *moment propagation equation* can be adopted obtaining the uncertainty on  $k_{eff}$  due to nuclear data;
- In the *TMC branch* (right side), each of the n random input ENDF files is processed by NJOY and the benchmark calculation is performed with MCNP6. At the end of the n calculations, n different  $k_{eff}$  values with their statistical uncertainties are obtained. It means that, from the calculated probability distribution of  $k_{eff}$ , the standard deviation can be obtained which corresponds to the uncertainty on  $k_{eff}$  due to the nuclear data [29].

Several comparisons were found in literature between the two methods. The TMC seems to provide a more general and exact answer, it does not require special codes, but it is more time-consuming. The Perturbation method considers a restricted number of nuclear data uncertainties, and it needs more processing and intermediate codes, but it is the fastest to produce results [29].

---

<sup>2</sup>NJOY: nuclear data processing code developed at Los Alamos National Laboratory [34].

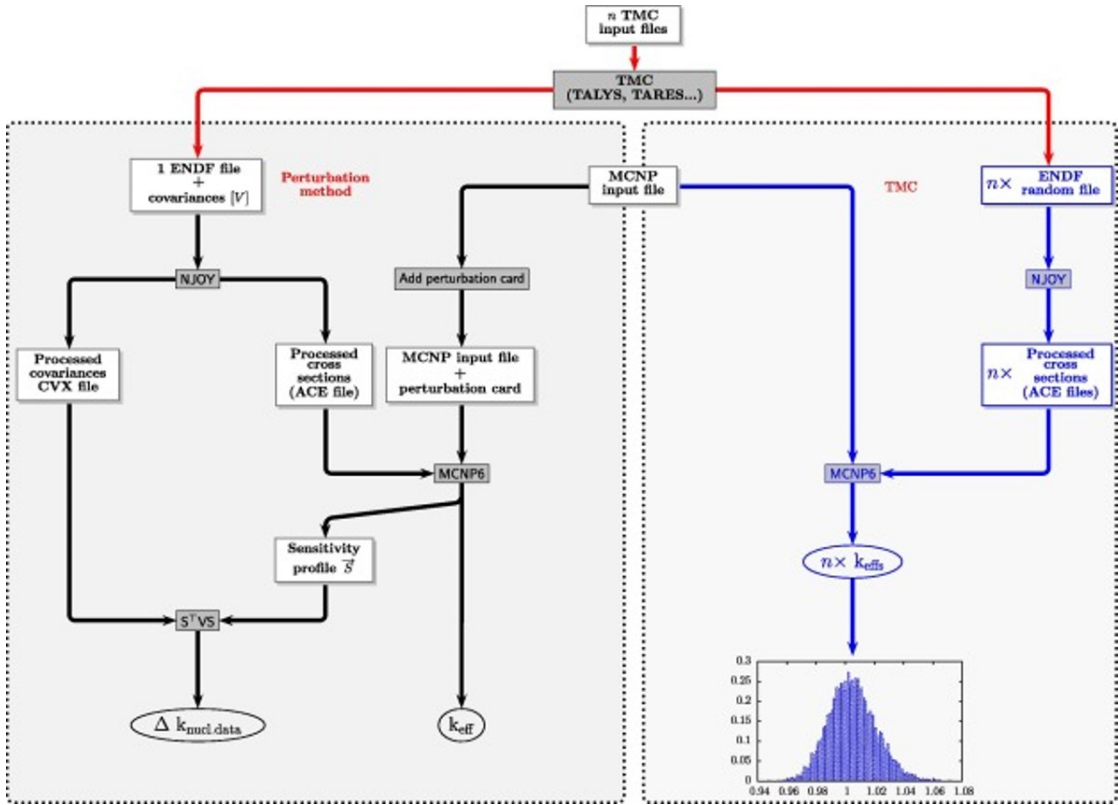


Figure 3.1: Flowchart of the uncertainty propagation from Total Monte Carlo and perturbation method [35]

### 3.6 Sensitivity and uncertainty analysis

The **Sensitivity Analysis (SA)** is the study of how the uncertainty in the output of a model can be apportioned to different sources of uncertainty in the model input. The **Uncertainty Analysis (UA)** refers to the quantification of uncertainty in the model output, based on the uncertainties of the input. A model can be seen as whatever stands between some input parameters and the related outputs. It can be:

- Diagnostic or prognostic: the first is related to a model used to understand a law, while the second is used to predict the behaviour of a system, given a supposedly understood law;
- Data-driven or law-driven: A data-driven model tries to treat the solution as a signal and to derive its properties statistically, while the law-driven model tries to put together accepted laws which have been attributed to the system, in order to predict its behaviour. The latter may have a greater capacity

to describe the system under unobserved circumstances, while data-driven models tend to adhere to the behaviour associated with the data used in their estimation. Statistical models are an example of data-driven models [36].

Of course, other categorizations of models are possible. The definition of the model input depends on the particular model under study. Concerning the uncertainty and sensitivity analysis, the inputs of the model can be defined as everything that can drive a variation in the output of the model. When the best parameter values and their uncertainty are known, it is possible to perform the uncertainty analysis by propagating the uncertainty in the parameter through the model. One possible way of doing this is through the Monte Carlo approach (or sampling based), in which the distribution function of the input parameters is taken under consideration. To explain the procedure, a simple scheme is reported for the uncertainty analysis of a model with a output  $y$  and three inputs  $(\alpha, \beta, \gamma)$ . The following scheme was then adapted and used to perform the uncertainty analysis in the model of Fission Pulse Decay Heat (FPDH), discussed in Chapter 7.

1. The input parameter  $\alpha$  is considered to be normally distributed with mean  $\bar{\alpha}$  and standard deviation  $\sigma_a$ . The same is done also for the other input parameters  $\beta$  and  $\gamma$ . For the sake of simplicity, for the moment, the input factors are considered independent of each other;
2. For each of these factors a sample from the respective distributions is drawn;
3. Step 2 is repeated  $N$  times to produce a set of row vectors  $(\alpha^{(j)}, \beta^{(j)}, \gamma^{(j)})$  with  $j = 1, 2, \dots, N$  in such a way that  $(\alpha^{(1)}, \alpha^{(2)}, \dots, \alpha^{(N)})$  is an array of samples from  $N(\bar{\alpha}, \sigma_a)$  (likewise for the distribution function of the other factors). Collecting the array of samples for each input parameter, the following matrix can be built:

$$\begin{bmatrix} \alpha^{(1)} & \beta^{(1)} & \gamma^{(1)} \\ \alpha^{(2)} & \beta^{(2)} & \gamma^{(2)} \\ \dots & \dots & \dots \\ \alpha^{(N-1)} & \beta^{(N-1)} & \gamma^{(N-1)} \\ \alpha^{(N)} & \beta^{(N)} & \gamma^{(N)} \end{bmatrix} \quad (3.57)$$

4. In the last step, the model is computed for all vectors  $(\alpha^{(j)}, \beta^{(j)}, \gamma^{(j)})$  thereby producing a set of  $N$  values of the model output  $y_j$ :

$$\begin{bmatrix} y^{(1)} \\ y^{(2)} \\ \dots \\ y^{(N-1)} \\ y^{(N)} \end{bmatrix} \quad (3.58)$$

These four steps constitute the uncertainty analysis. From these it is possible to evaluate the average output, its standard deviation (which corresponds to its uncertainty), plot the distribution itself and so on. Note that, for the purpose of the uncertainty analysis just described, only the estimated parameters  $\alpha$ ,  $\beta$  and  $\gamma$  were considered as relevant inputs. All other possible types of information fed into the model, like the observations or the internal model variables, are disregarded. Of course a further step could be added at the beginning of the scheme to collect all the uncertainties coming from the different uncertainty sources and perform the uncertainty propagation taking all of them into account.

### 3.7 Global vs Local sensitivity analysis

Most of the sensitivity analyses met in literature are based on the concept of derivatives. Indeed the derivative  $\delta Y_j / \delta X_i$  of an output  $Y_j$  versus an input  $X_i$  can be thought as a mathematical definition of the sensitivity of  $Y_j$  with respect to the input  $X_i$ . This approach is also known as **Local sensitivity analysis**. The fatal limitation of this approach is that the derivatives are only informative at the base point where they are computed and do not provide for an exploration of the rest of the space of the input factors. In opposite, with the so called **Global sensitivity analysis**, it is possible to examine the sensitivity with regard to the entire parameter distribution. It focuses on the variance of model outputs and determines how input parameters influence the output parameters. It is a central tool in sensitivity analysis since it provides a quantitative and rigorous overview of how different inputs influence the output. Global SA is often preferred when possible, due to its greater detail, but for a large system it is very computationally expensive. Local SA method can be preferred because it requires less computational power [37]. The sensitivity coefficient in case of Global SA must be normalized by the input-output standard deviations: in this way all the distribution is taken into account.

$$S_{Z_i}^\sigma = \frac{\sigma_{Z_i} \delta Y}{\sigma_Y \delta Z_i} \quad (3.59)$$

This aspect changes the point of view of sensitivity: with the Global sensitivity analysis it is possible to access the variance fraction of the output explained by the variance of the input [38]. Monte Carlo analysis is a common approach for global methods. As already said, Monte Carlo analysis is based on performing multiple evaluations with randomly selected values of model inputs, and then using the results of these simulations to determine both uncertainty in the prediction of model outputs and assign to each model input its contribution to the variance in model outputs [39]. To investigate the behaviour of the model in the Global analysis usually a *scatterplot* is adopted by projecting in turn the N values of the

selected output  $Y$  against the  $N$  values of each of the  $Z$  input factors. In Figure 3.2, an example with some of them is reported.

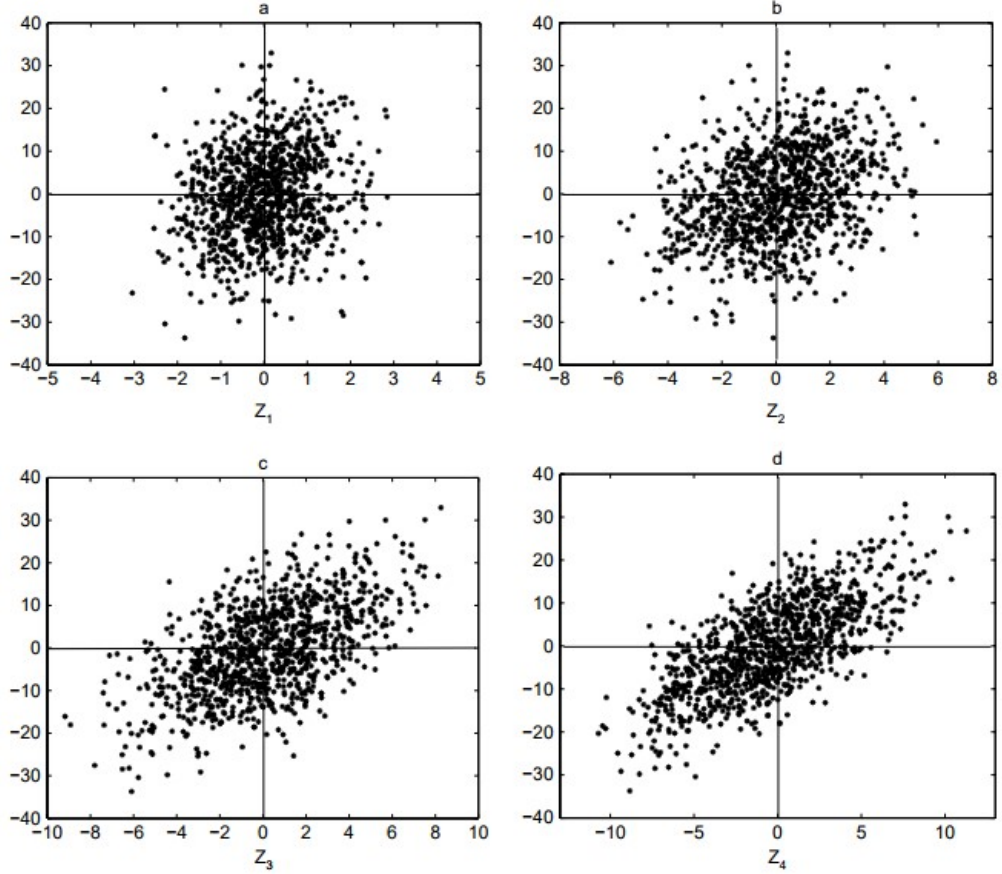


**Figure 3.2:** Scatterplots of  $Y$  versus  $Z_1, Z_2, Z_3, Z_4$  [36]

The Figure 3.2 shows that  $Y$  is more sensitive to  $Z_4$  than it is to  $Z_3$ . The ordering of the input factors by their influence on  $Y$  is

$$Z_4 > Z_3 > Z_2 > Z_1 \tag{3.60}$$

Such a conclusion can be drawn from this Figure as there is a better pattern in the plot for  $Z_4$  than for  $Z_3$  and so on. However, using the derivative approach of  $Y$  versus  $Z_i$ , the standard deviation of the input parameters and so their distribution is not taken into account and relation 3.60 is not so straightforward to get [36].

## Chapter 4

# Contributions to SANDY development

From Section 2.2 it emerges that the data stored in ENDF-6 format are restricted by constraining formatting rules and it is difficult to handle them without suitable tools. To manipulate these data it is possible to use different processing codes and then use these data as inputs for many user applications. In this processing procedure SANDY is inserted. It is a Monte Carlo sampling-based code developed to perform the nuclear data uncertainty propagation in nuclear codes. SANDY can generate random nuclear data samples, exploiting the basic theory of stochastic sampling, that reproduce the covariance information stored in the ENDF-6 files. Such random data are then rewritten in perturbed ENDF-6 or Point-wise ENDF-6 files (PENDF) [40]. These steps are schematized in Figure 4.1.

The files processed will become the input of different nuclear data codes; they are suitable for Monte Carlo uncertainty propagation calculations, where a given model is solved repetitively, each time adopting a different file. From the statistical analysis of the resulting output predictions, it is possible to calculate the distributions of any calculated quantities, including their mean, variance and any other moments [41].

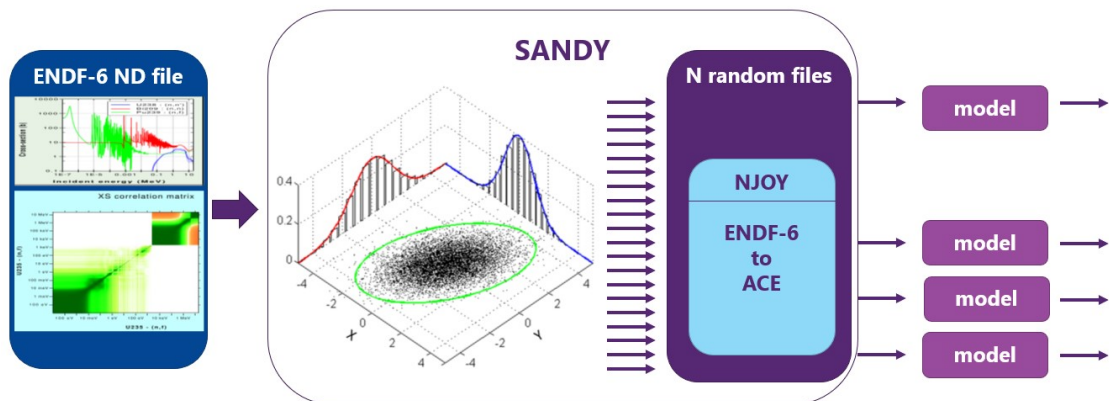
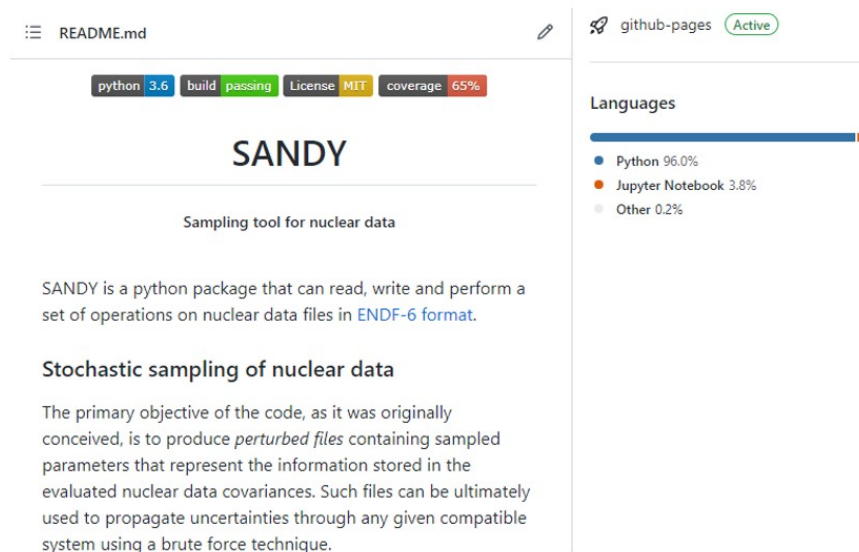


Figure 4.1: SANDY's workflow [35]

## 4.1 Development of SANDY

SANDY is created as an high-level Python interface to parse ENDF-6 files, collect nuclear data, build covariance matrices, draw samples from probability distribution and perform other nuclear data-related tasks. To coordinate the work among different SANDY developers, GitHub is used. It is a provider of Internet hosting for software development and version control using Git, an open source distributed system designed to handle from small to very large projects with speed and efficiency. It is possible to use it for the storage of different projects, collaborative development, download, hosting/website publishing and versioning [42].

Exploiting this software, continuous integration (CI) with GitHub actions is also performed, allowing developers to frequently merge code changes into a central repository where tests are then run. The version control system is also supplemented with other checks like automated code quality tests, syntax style review tools, and more. This helps guarantee a certain level of quality assurance of the SANDY code.



**Figure 4.2:** SANDY’s documentation on GitHub platform [43]

## 4.2 Working scheme

After the interaction with the ENDF-6 format to extract the requested data, SANDY sampled the nuclear parameters into random sets according to the multivariate probability distribution of the uncertain variables. The samples are randomly selected using a sampling algorithm, according to the specified probability distribution. It is guaranteed that the random samples are distributed in the input phase space according to the original covariance matrix information. At the end of the process, the random nuclear data samples are written in copies of the original data file, so keeping the original format. Response uncertainties calculated with SANDY take into account first and higher order effects and are not limited by constraints of linearity. Cross sections and other energy-dependent data are not approximated by multigroup energy structures but they are propagated as pointwise, exploiting the Total Monte Carlo scheme.

Currently, SANDY can produce random perturbed nuclear data files for:

- Nubar (MF31)
- Cross sections (MF33)
- Angular distributions (MF34)
- Energy distributions (MF35)
- Fission yields (MF8) (detailed discussion in Chapter 6)

- Decay data (MF8) (detailed discussion in Chapter 5)

SANDY retrieves the best estimates and uncertainties/covariances directly from the libraries, so it interacts only with the ENDF-6 nuclear data files and it remains independent of the model and of the numerical solver. This tool is therefore able to quantify the uncertainty on the model responses and it can also estimate the importance of the nuclear data on the response uncertainty.

### 4.3 Sampling procedure

To implement statistical sampling, an assumption on the input parameter distribution is required. Gaussian distribution is generally assumed [44] as it guarantees maximum entropy to the parameter values and since a set of random variables tends to be distributed normally according to the Central Limit Theorem (CLT). On the one hand, the bias brought by this assumption should be assessed, on the other hand, the gaussian distribution assumption implies the possibility of having negative sampled values, which is not always physical for nuclear data.

In SANDY the correlated sampling procedure is performed through covariance matrix diagonalization, which only allows to preserve the normal shape of the distribution, as such a shape is the only one to be preserved when convoluted [45], according to the CLT.

A linear combination of normally distributed random variables is also normally distributed, so if  $\vec{\xi}$  is a set of normally distributed variables, each with zero mean and unit standard deviation, then set of samples with target mean and standard deviation can be computed as in equation 4.1,

$$\vec{x}^{(m)} = A \cdot \vec{\xi}^{(m)} + \vec{\mu} \quad (4.1)$$

where matrix A is such as to preserve the mean values, standard deviations and the correlations between the components of  $\vec{x}$  and  $\vec{\mu}$  is the vector of the expected values of  $\vec{x}$ .

$$\mathbb{E}(\vec{\xi}) = 0 \quad (4.2)$$

$$\mathbb{E}(\vec{\xi} \vec{\xi}^T) = \mathbb{1} = \begin{bmatrix} 1 & 0 \\ 0 & 1 \end{bmatrix} \quad (4.3)$$

Matrix A is the lower-triangular decomposed covariance matrix of  $\Sigma$  and the product  $A \cdot \vec{\xi}^{(m)}$  results in correlated sets of randomly distributed values centered in zero and with covariance matrix  $A \cdot A^T = \Sigma$ . This dot product is a linear operation, which makes  $\vec{x}$  converge to the normal distribution. More intuitively, it can be considered as:

$$\begin{aligned}
 x_1 &= A_{1,1}\xi_1 \\
 x_2 &= A_{2,1}\xi_1 + A_{2,2}\xi_2 \\
 x_3 &= A_{3,1}\xi_1 + A_{3,2}\xi_2 + A_{3,3}\xi_3 \\
 &\dots \\
 x_n &\xrightarrow{n \rightarrow \infty} \mathfrak{N}
 \end{aligned}$$

Each parameter  $x_n$  results from a sum of distributions and the CTL states that the distribution of sample means approximates a normal distribution as the sample size gets larger, regardless of the population's distribution [46].

SANDY works with relative covariance matrix, this means that equation 4.1 is adapted to handle relative terms in this way:

$$\vec{x}^{(m)} = (A_{relative} \cdot \vec{\xi}^{(m)} + 1) \cdot \vec{\mu} \quad (4.4)$$

where the matrix  $A_{relative}$  is computed in such a way as to satisfy the product  $A_{relative} \cdot A_{relative}^T = \Sigma_{relative}$ , with  $\Sigma_{relative}$  the covariance matrix built with relative variance — i.e., relative uncertainties with respect to the best estimates.

Evaluated covariance matrices can present correlations out of bounds — i.e., lower than -1 or larger than 1. This results in non-physical negative eigenvalues during the sampling procedure, for which reason SANDY "adjusts" the evaluated covariance matrices. This is done by setting to zero the negative eigenvalues and then recomposing the adjusted covariance matrix  $\tilde{\Sigma}$ .  $\tilde{\Sigma}$  is semi-positive definite by construction and it is decomposed as in equation 4.5,

$$\tilde{\Sigma} = V \cdot E \cdot V^{-1} = V \cdot \sqrt{E} \cdot \sqrt{E} \cdot V^{-1} \quad (4.5)$$

where  $V$  is the matrix of eigenvectors  $v_i$  of  $\tilde{\Sigma}$ , and  $E$  is the diagonal matrix whose elements are the eigenvalues of  $\tilde{\Sigma}$ . To obtain matrix  $A$  of equation 4.1, the QR decomposition of the  $\sqrt{E}$  matrix is computed and equation 4.5 can be rewritten as in equation 4.6

$$\tilde{\Sigma} = V \cdot \sqrt{E} \cdot \sqrt{E} \cdot V^{-1} = (QR)^T \cdot (QR) = R^T Q^T \cdot QR \quad (4.6)$$

The  $Q$  matrix is a unitary matrix, so the latter equation leads to write the approximation of covariance matrix in the form  $\tilde{\Sigma} = R^T \cdot R$ . Setting  $R^T = A$ , an analogous form to the Cholesky factorization for semi-positive defined matrices is obtained. Thanks to the linearity of the operation, the covariance matrix of  $\vec{x}$  will approximate  $\tilde{\Sigma}$  — the higher the number of considered samples the better the approximation—, indeed, for the moment propagation, it is possible to write:

$$\mathbb{E}(\overline{A\xi}) = A \mathbb{E}(\vec{\xi}) = 0 \quad (4.7)$$

$$\mathbb{E}((A \vec{\xi})(A \vec{\xi})^T) = A \mathbb{E}(\vec{\xi} \vec{\xi}^T) A^T = A \cdot A^T = \Sigma \quad (4.8)$$

With explicitly given  $A$  and  $\vec{\mu}$ , arbitrary random multivariate normally distributed samples can be produced by employing equation 4.1.

### 4.3.1 Truncation of negative values

The normal distribution is the distribution at maximum entropy, which means the one that makes the fewest assumptions about your data (the one with maximal information entropy) [47]. This is therefore a conservative guess when only the best estimate and the standard deviation or covariance matrix of a distribution are provided. This is often the case for nuclear data. The usual choice of multivariate normal distribution sampling is also well justified by the CLT, according to which, when manipulated, the distributions tend to converge to the normal one. Still, negative samples can be computed when sampling a normal distribution. This can lead to non physical values for many nuclear data such as the cross sections, the decay constants, the fission yields, etc... For this reason, usually the normal distribution is truncated, removing the negative values. If the random variable has been truncated only from below, some probability mass has been shifted to higher values, giving a first-order stochastically dominating distribution and hence increasing the mean to a value higher than the expected original normal distribution. Likewise, if the random variable has been truncated only from above, the truncated distribution has a mean less than original one. Regardless of whether the random variable is bounded above, below, or both, the truncation is a mean-preserving contraction combined with a mean-changing rigid shift, and hence the variance of the truncated distribution is less than the variance of the original normal distribution [48].

Concerning the sampling procedure of nuclear data, the mean of the distribution coincides with the best estimate of the nuclear datum provided by the libraries. To preserve the mean value of the distribution, the truncation procedure must be symmetrical, i.e. truncation on both sides of the distribution must be performed. To avoid these negative samples, two main options were considered in the development of the sampling procedure in SANDY:

- method 1: all truncated values are set equal to the mean value of the distribution;
- method 2: all the truncated values are set equal to the values at the boundaries of the distribution.

In both cases, the truncation procedure results in a reduction of the standard deviation. A further investigation was performed to see which method deviates less

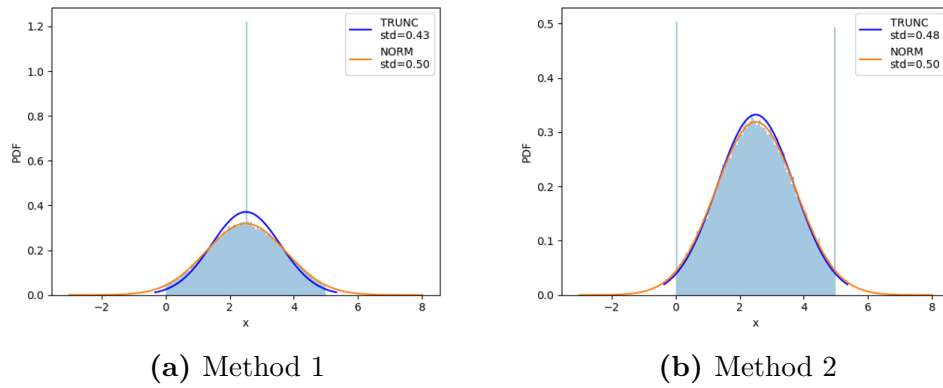


**Figure 4.3:** Methods to handle negative samples with Normal PDF

from the standard deviation of the original distribution and the result is shown in Figure 4.4.

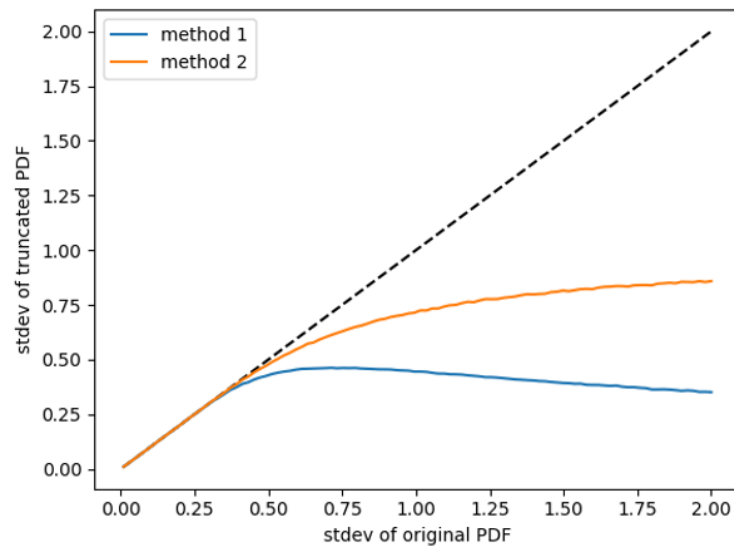


**Figure 4.4:** Standard deviation of the original PDF vs. standard deviation of the truncated PDFs

When the variance of the original normal distribution increases, the second method results in a lower reduction of the variance so this method was selected to be implemented in the SANDY sampling procedure.

The work done for this implementation during the development of this Thesis was

also presented during the JEFF-Nuclear data week of April 2022, reported in [49].

### 4.3.2 Change of the input parameter distributions

As already said in section 4.3, considering the distribution of the input parameters as a Gaussian is the first assumption made in the sampling procedure. One might then want to assess the bias given by this assumption considering different distributions. This kind of analysis is out of the scope of this work, yet a contribution to the implementation of the sampling according to the lognormal and to the uniform distribution was part of the effort of this thesis work. This was done in collaboration with Federico Grimaldi. These two distributions were selected among different options to avoid negative samples (in case of lognormal) and for the easy implementation (in case of uniform).

The implementation of the sampling according to the lognormal distribution was implemented according to [50]. This distribution is defined in the interval  $[0, +\infty]$ , so the probability to have negative values in this case is zero. For large standard deviations, the lognormal distribution becomes highly asymmetric, with a significantly higher tail than normal distribution. In opposite, for small standard deviations, the lognormal looks like a normal distribution. This behaviour is shown in Figure 4.5.

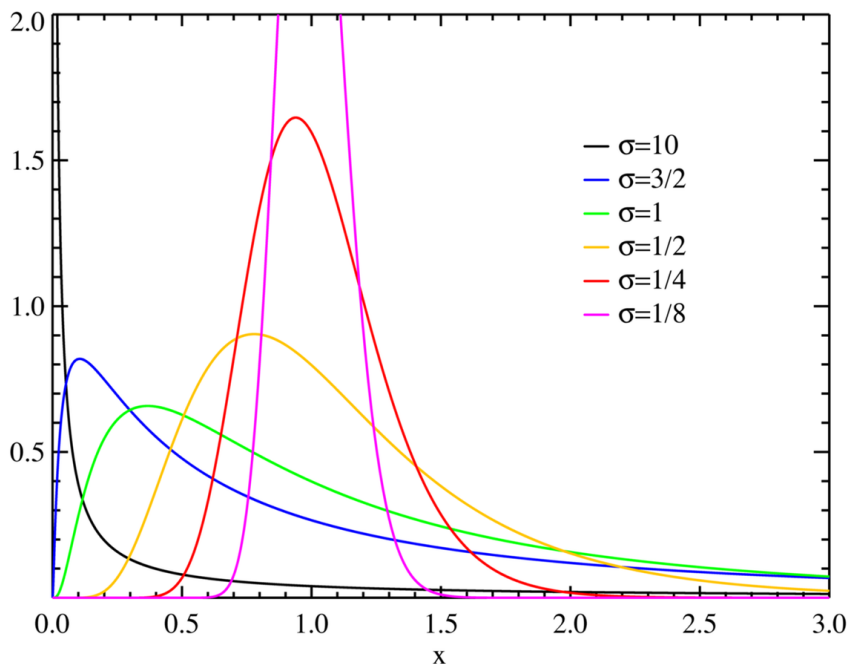


**Figure 4.5:** Lognormal distribution [51]

A transformation of the covariance matrix and the mean values is needed to obtain lognormally distributed correlated samples. The link between the mean value and the standard deviation ( $\mu$ ,  $\sigma$ ) of the normal distribution and the ones of the lognormal distribution ( $\langle x \rangle$ ,  $\sigma_x$ ) is expressed by the following two equivalent equations 4.9 and 4.10.

$$\sigma = \sqrt{\ln\left(1 + \frac{\sigma_x^2}{\langle x \rangle^2}\right)} \quad (4.9)$$

$$\mu = \ln(\langle x \rangle) - \frac{\sigma^2}{2} = \ln(\langle x \rangle) - \frac{1}{2}\ln\left(1 + \frac{\sigma_x^2}{\langle x \rangle^2}\right) = \ln\left(\frac{\langle x \rangle^2}{\sqrt{\langle x \rangle^2 + \sigma_x^2}}\right) \quad (4.10)$$

This modification of the standard deviation and the mean value allows to repeat the procedure described in section 4.3 for the normal distribution using the transformed covariance matrix. This results in the underlying normal distribution of the target lognormal distribution, such that 4.11 holds

$$\mathcal{L}\text{og}\mathfrak{N} = e^{\mathfrak{N}} \quad (4.11)$$

where  $\mathcal{L}\text{og}\mathfrak{N}$  is the lognormal distribution with the covariance matrix from the ENDF-6 file and  $\mathfrak{N}$  is the underlying normal distribution.

The transformation of the covariance matrix is needed because of the implemented procedure. After the sampling scheme is performed with the underlying mean and covariance matrix, the exponential is computed to get the lognormal distribution centered in the original mean and with the original covariance matrix.

The consideration about the dot product  $A \cdot \vec{\xi}^{(m)}$  in the explanation in Section 4.3 is of major importance when trying to sample non-normal distributions. An example of this also is given by the uniform distribution  $\mathfrak{U}$ . The sum of uniform distributions converges to the Irwin–Hall distribution [52].

This makes impossible to perform such a sampling in a straightforward way as it was for  $\mathfrak{N}$ , highlighting the need of a change in the covariance matrix or the impossibility for such an implementation. The investigation of the possibility to compute uniformly distributed multivariate correlated samples is left out of the scope of this work while non-correlated uniform sampling was implemented in SANDY — i.e. diagonal covariance matrix is considered in that case.

To access the impact of the choice of the input parameter sampling distribution, the nuclide concentration uncertainty results of the UAM Benchmark Exercise I-1 "Cell Physics", obtained sampling the independent fission yields from normal, lognormal and uniform distributions were analysed. This investigation is reported in Appendix A.

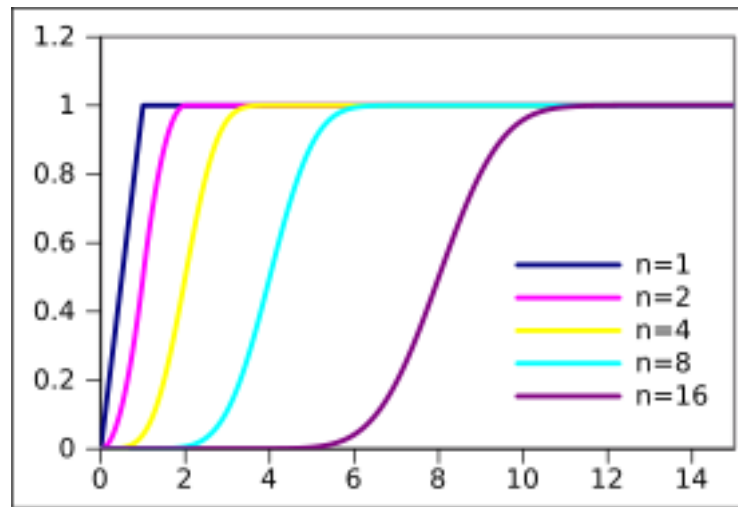


Figure 4.6: Irwin–Hall distribution [53]

## 4.4 Generalized Least Squares update technique

As already discussed in Chapter 1, nuclear data communities have embraced the concept of covariance matrix to collect the uncertainties of the nuclear data. Usually the best estimates of nuclear parameters can be obtained by performing experiments. Importantly, the raw data from measurements, such as detector counts, must always be transformed and corrected to reflect the properties of the nuclei, which are independent of the applied experimental technique. For this reason, the corrected data from experiments are assessed another time by evaluators. As a first step of an evaluation, evaluators collect and compare available experimental data. Depending on the outcome of this investigation, experimental data are then corrected if possible or discarded. A correction may be the adjustment of an estimate or of the associated uncertainty. This can be done with the **Generalized Least Squares technique** [54]. This is an adjustment technique that states that the information on some prior system parameters can be improved with the addition of new knowledge for which relationships between data and parameters are established [55]. This method represents a modification of Ordinary Least Square (OLS) which takes into account the inequality of variance in the observations. It is mainly used to deal with situations in which the OLS estimator is not BLUE (Best Linear Unbiased Estimator) because one of the main assumptions of the Gauss-Markov theorem, namely that of homoscedasticity — i.e. constant variance’s error — and absence of serial correlation, is violated. The **Gauss-Markov** (GM) theorem states that for an additive linear model, and under the ”standard” GM assumptions, OLS estimator has the lowest sampling variance within the class of linear unbiased

estimators. The standard GM assumptions are:

1. Linearity: the parameters we are estimating using the OLS method must be themselves linear;
2. Randomity: our data must have been randomly sampled from the population;
3. Non-Collinearity: the regressors being calculated are not perfectly correlated with each other;
4. Exogeneity: the regressors are not correlated with the error term;
5. Homoscedasticity: the error of the variance is constant.

If heteroscedasticity is present, so the variances of the observed values are unequal, the GLS estimator is BLUE. For this theorem, the updated values will have the minimum variance or the narrowest sampling distribution. More specifically, when your model satisfies the assumptions, GLS estimates follow the tightest possible sampling distribution of unbiased estimates compared to other linear estimation methods [56].

Many practitioners use the Generalized Least Squares (GLS) formulas to combine experimental data and results of model calculations in order to determine reliable estimates and covariance matrices. A prerequisite to apply the GLS formulas is the construction of a prior covariance matrix for the observables from a set of model calculations. The method described is suitable to handle problems in which relationships between the observables and the parameter to be estimated are inherently linear or non-linear problem which are first linearized by means of Taylor series expansion [57], so they are in the form:

$$y - y_a = S \cdot (\theta - \theta_a) \quad (4.12)$$

where  $\theta$  are the parameters of the system,  $\theta_a$  the prior estimates of  $\theta$ ,  $y$  the responses of the constraining equation,  $y_a$  the responses of the constraining equation to the prior estimates  $\theta_a$  and  $S$  are the sensitivity coefficients of the response  $y - y_a$  to the parameters  $\theta - \theta_a$  [58].

It is assumed that no correlations existed between the prior and the new information. Then, further information  $\eta$  could be introduced in order to derive refined values for the parameters  $\theta$ , with all the available uncertainty information properly incorporated into the formalism. The updating process is the following:

$$\theta - \theta_a = V_a - S^T \cdot (S \cdot V_a \cdot S^T + V)^{-1} \cdot (\eta - y_a) \quad (4.13)$$

$$V_s = V_a - V_a \cdot S^T \cdot (S \cdot V_a \cdot S^T + V)^{-1} \cdot S \cdot V_a \quad (4.14)$$

where  $V_a$  is the covariance matrix of the prior estimates of the parameters  $\theta$ ,  $V$  is the covariance matrix of the introduced data fitting the constraining system  $\eta$ , and  $V_s$  is the updated covariance matrix of the system parameters  $\theta$  [59]. The uncertainty reduction is highlighted in the equation 4.14, where the diagonal and off-diagonal terms are respectively:

$$\mu_{ii} = \sigma_i^2 \left( 1 - \frac{\sigma_i^2}{\sigma^2 + \sum_j \sigma_j^2} \right) \quad (4.15)$$

$$\mu_{ij} = -\frac{\sigma_i^2 \sigma_j^2}{\sigma^2 + \sum_j \sigma_j^2} \quad (4.16)$$

with  $\sigma_i$  the standard deviation of the  $i$ -th parameter and  $\sigma$  the standard deviation of the introduced data fitting the constraining system. Sum  $\sum_j \sigma_j^2$  includes all the other correlated parameters [60]. The derivation of these formulas is reported in Appendix B.

Part of the work of this thesis was devoted to insert the procedure for this updating scheme in SANDY. Then it was used to obtain an estimate of the fission yields covariance matrix and it is discussed in Chapter 6.

## Chapter 5

# Perturbation methodology of decay data

In this Chapter, the implementation of the covariance propagation and local/global sensitivity capabilities - based on stochastic sampling - for radioactive decay data in SANDY is described.

Decay data are defined as those parameters relating to the normal radioactive decay modes of a nuclide. They include half-life, total decay energies and branching fractions, alpha-particle energies and emission probabilities, beta-particle energies, emission probabilities, and transition types, electron-capture (and positron) energies, transition probabilities, and transition types, gamma-ray energies, emission probabilities and internal conversion coefficients, Auger and conversion-electron energies and emission probabilities, X-ray energies and emission probabilities, characteristics of spontaneous fission, delayed-neutron energies and emission probabilities, delayed-proton energies and emission probabilities [61].

Radionuclidic decay data are also used in many types of non-nuclear applications such as chemical experiments, metallurgical and mining industries, medical treatments and functional studies, quality control, health, safety, etc. A nuclide is a neutral atom, specified by the mass number  $A$  and atomic number  $Z$  of its nucleus, which is either stable or lives long enough to be classified as radioactive. Figure 5.1 shows the stable nuclides represented by black squares, while the radioactive ones, experimentally identified, are plotted by the light-shaded area [62].

For burnup/inventory/transmutation calculations, radioactive Decay Data libraries are needed, indeed they provide the radioactive decay data, such as decay constants, half-lives, branching ratios or decay energies, which drive part of the burnup/depletion equations [63]. Very often the decay data stored in the libraries are not so accurate due to a lack of experimental information and they are accompanied by very large uncertainties. The covariance information for the evaluated data

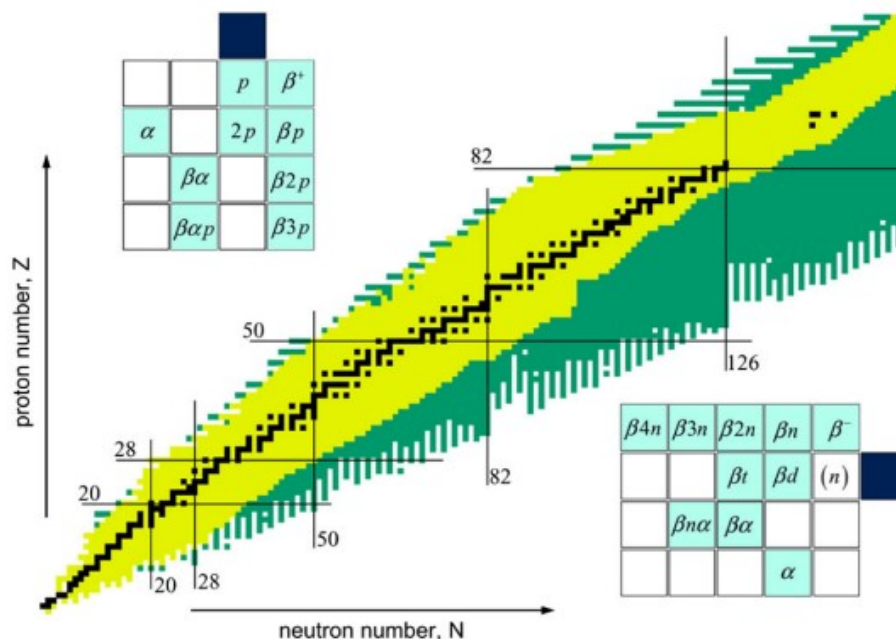


Figure 5.1: Nuclide chart [63]

is absent in the currently commonly used formats, so we don't have information about the correlated uncertainties of some decay data. When the uncertainty of the reference data used in the experiment predominates, the results of measurements are highly correlated and cannot be processed assuming statistical independence. Besides that, direct inclusion of balance relations in the evaluation procedure leads to a strong correlation between some resulting evaluated characteristics. For this reason the evaluated data reported without covariance information should be considered as incomplete [64].

## 5.1 Algorithm to obtain perturbed decay data in SANDY

The decay data analyzed during the development of the decay data sampling procedure in SANDY are *decay constant*, *branching ratio* and *decay energy*, which are the ones more relevant in nuclear spent fuel characterization.

As discussed in Chapter 4, the SANDY code is written in python and it is composed by different scripts with different python classes and methods. The algorithm to obtain perturbed decay data touches four main classes of this code:

- `sandy.Endf6`: container for ENDF-6 file text grouped by MAT, MF and MT numbers;
- `sandy.DecayData`: container of radioactive nuclide data for several isotopes;
- `sandy.decay._DecayBase`: base class to perturb decay data, it acts as a container of best estimates and uncertainty of decay data as a pandas dataframe;
- `sandy.CategoryCov`: container of covariance matrices.

A typical Unified Modeling Language (UML) Class diagram with the python classes used in the perturbation algorithm of decay data implemented in SANDY, their attributes and main operations (or methods) is reported in Figure 5.2.

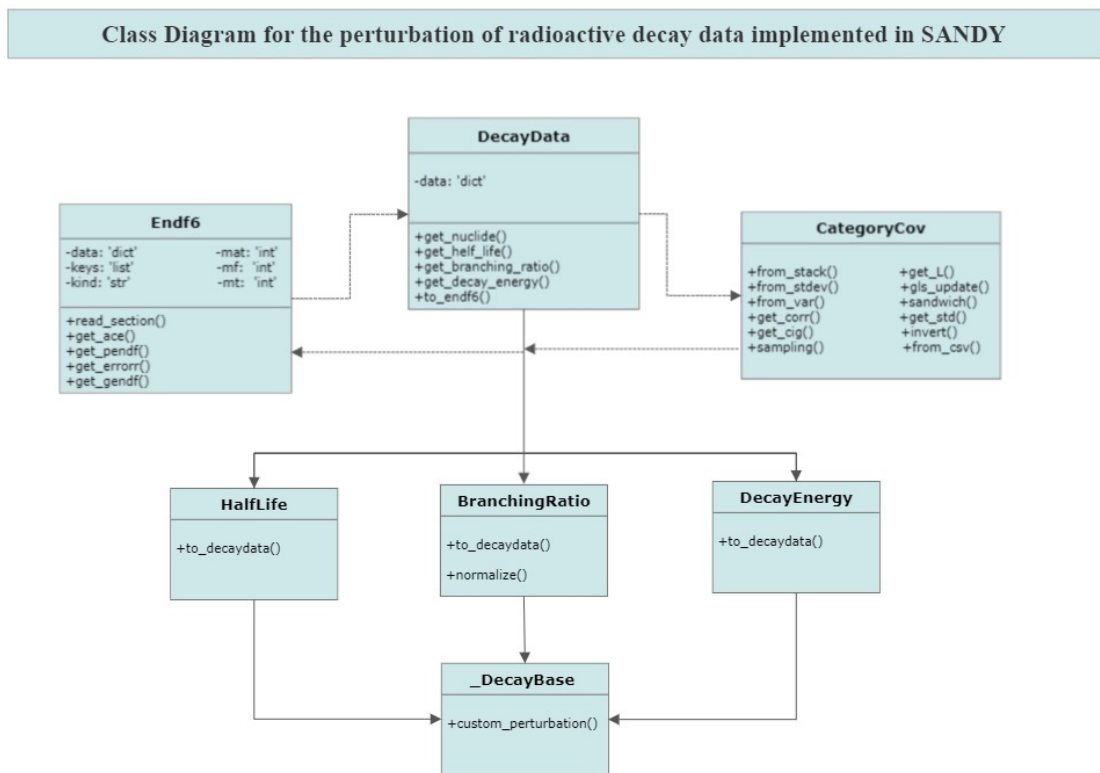


**Figure 5.2:** UML Class diagram with the main python classes, attributes and methods used for the implementation of the algorithm for the perturbation of radioactive decay data implemented in SANDY

The procedure starts with the reading of the ENDF-6 file directly from the libraries to retrieve the best estimates and the related uncertainties information. The decay data information are stored without the covariance matrix needed to perform the sampling procedure implemented in SANDY. For this reason the uncertainties are taken as standard deviations and, divided by the best estimates, will be used to build a relative diagonal covariance matrix. Then the correlations between the decay data are inserted, if present, by imposing some physical constraints discussed one by one in the following Sections. Once the relative covariance matrix is obtained, the sampling procedure can be performed and it will give the perturbation coefficients that must be multiplied by the best estimates to obtain the radioactive perturbed decay data. The last step of the algorithm focuses on the writing of the perturbed values in ENDF-6 format into a file that will be used as input for different nuclear data codes.

The explained steps are summarized in Figure 5.3.

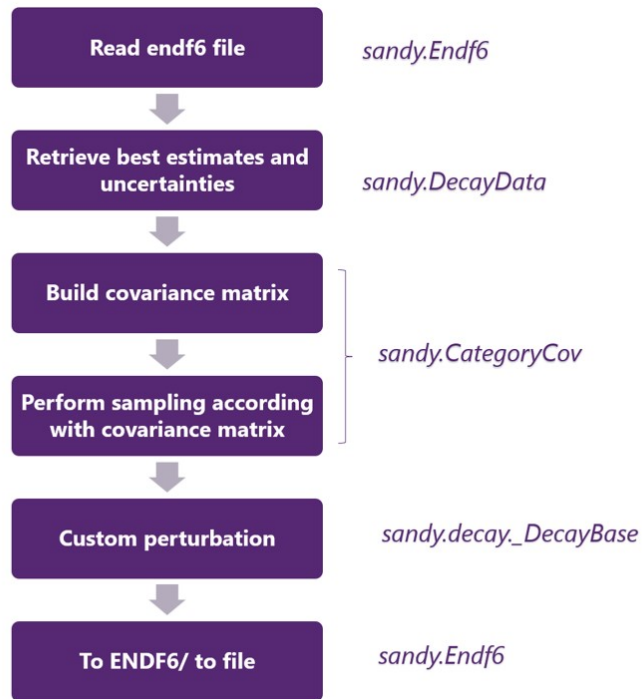


**Figure 5.3:** Algorithm to obtain perturbed decay data



Of course, if a nuclide has two decay modes and the corresponding branching ratios have equal uncertainties, it is possible to assume that the evaluation was performed by taking into account the above constraint: the sampling can be done for one variable and the other is evaluated from the constraint. In opposite, if a nuclide has two decay modes with different uncertainties in the branching ratios or if a nuclide has more than two decay modes, the constraint can be enforced by updating the covariance matrix according with the GLS method or with the normalization method. The differences between the two mentioned methods are reported in Section 5.3.1. At the end, the normalization method, which results easier to implement, was selected to be inserted in SANDY.

### 5.3.1 Generalized least squares update vs normalization procedure

The GLS method was already discussed in section 4.4 and the updating formulas reported there were used to update the covariance matrix of the branching ratios. Concerning the normalization method, it consists of the normalization of each set of samples, i.e. dividing each set for the sum of all the perturbed branching ratios. The main difference between the two methods is related to the fact that with the 4.4 method, the sampling procedure will be implemented with the updated covariance matrix. In the other case, it will be performed with the diagonal covariance matrix, so between non-correlated variables, and then the constraint will be added for each set of samples.

To report an example of the covariance matrix of sampled branching ratios obtained, the branching ratios of  $^{235}\text{U}$  and  $^{236}\text{U}$  from the JEFF-3.3 library were perturbed. Figure 5.5 reports the correlation matrix of 50 sampled branching ratios of these nuclides without the insertion of the constraint.

Figure 5.6 shows a visual comparison between the correlation matrices coming from the updated GLS covariance matrix and the covariance matrix after the normalization of 50 sampled branching ratios of  $^{235}\text{U}$  and  $^{236}\text{U}$ .

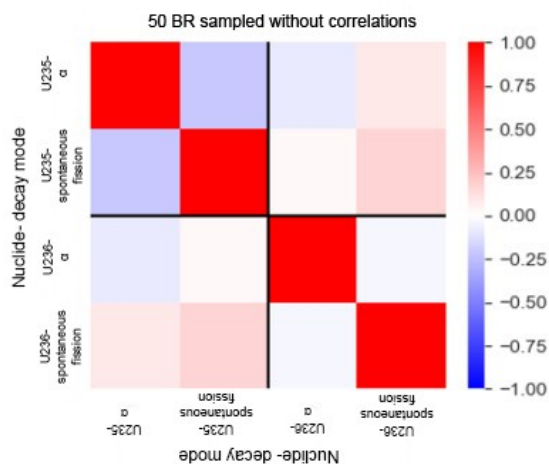


Figure 5.5: Correlation matrix of 50 samples branching ratios without correlations

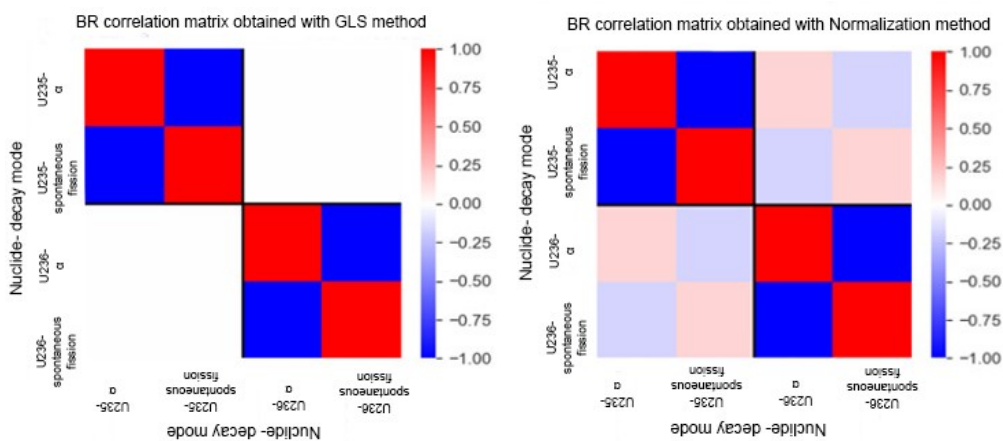


Figure 5.6: Comparison of correlation matrices of branching ratios obtained with GLS and Normalization method

## 5.4 Decay energy

The decay energy is the energy released from a nuclide having undergone one or more of the possible radioactive decays. In ENDF-6 file, these energies are grouped as average decay energies for decay heat application, for three general radiation types:  $E_{LP}$  (for light particles),  $E_{EM}$  (for electromagnetic radiation), and  $E_{HP}$  (for

heavy particles), followed by the individual components.

$$\begin{aligned}
 E_{LP} &= E_{\beta^-} + E_{\beta^+} + E_{e^-} + \dots \\
 E_{EM} &= E_{\gamma} + E_{x\text{-ray}} + E_{\text{annih.rad.}} + \dots \\
 E_{HP} &= E_{\alpha} + E_{\text{spont.fission}} + E_p + E_n + \dots
 \end{aligned}
 \tag{5.3}$$

The sum of these three general quantities is the total average energy (neutrino energies excluded) available per decay to the decay heat problem.

Not all the isotopes have an uncertainty for their decay energy stored in the ENDF-6 files, so a study of which isotopes have no uncertainty data is important because they can affect the final results of the uncertainty propagation calculations. For this purpose, the nuclides without uncertainties in their decay energies were studied for two nuclear data libraries and the results are reported in Table 5.1.

Library	Total # of isotopes	# of isotopes with no uncertainty in decay energy
JEFF-3.3	4908	3391
ENDF/B-VIII.0	5114	3398

**Table 5.1:** Number of isotopes without uncertainties in their decay energies for the analysed libraries

In JEFF-3.3 about 70 % of the isotopes have no decay energy uncertainty information and about 65 % in ENDF/B-VIII.0. To identify which isotopes have this lack of information, they were classified according to half life groups reported in Table 5.2. The result is reported in Figure 5.7.

The most relevant nuclides in nuclear spent fuel characterisation have large half lives, so they belong to groups 1 or 2. In this range, the total number of isotopes without uncertainties is around 320 for JEFF-3.3 and 300 in ENDF/B-VIII.0. The bulk of the isotopes with no uncertainty in decay energy is between the fifth and eighth groups, corresponding to isotopes with short half-lives which are poorly characterised, with partially known (even non-existent) decay schemes that arise from a serious lack of measured data [61].

Group	$T_{1/2}$ [s]
1	$> 10e7$
2	$[10e7; 10e5]$
3	$[10e5; 10e3]$
4	$[10e3; 10e2]$
5	$[10e2; 10]$
6	$[10; 1]$
7	$[1; 0.1]$
8	$[0.1; 10e-2]$
9	$[10e-4; 10e-6]$
10	$< 10e-6$

**Table 5.2:** Half life groups

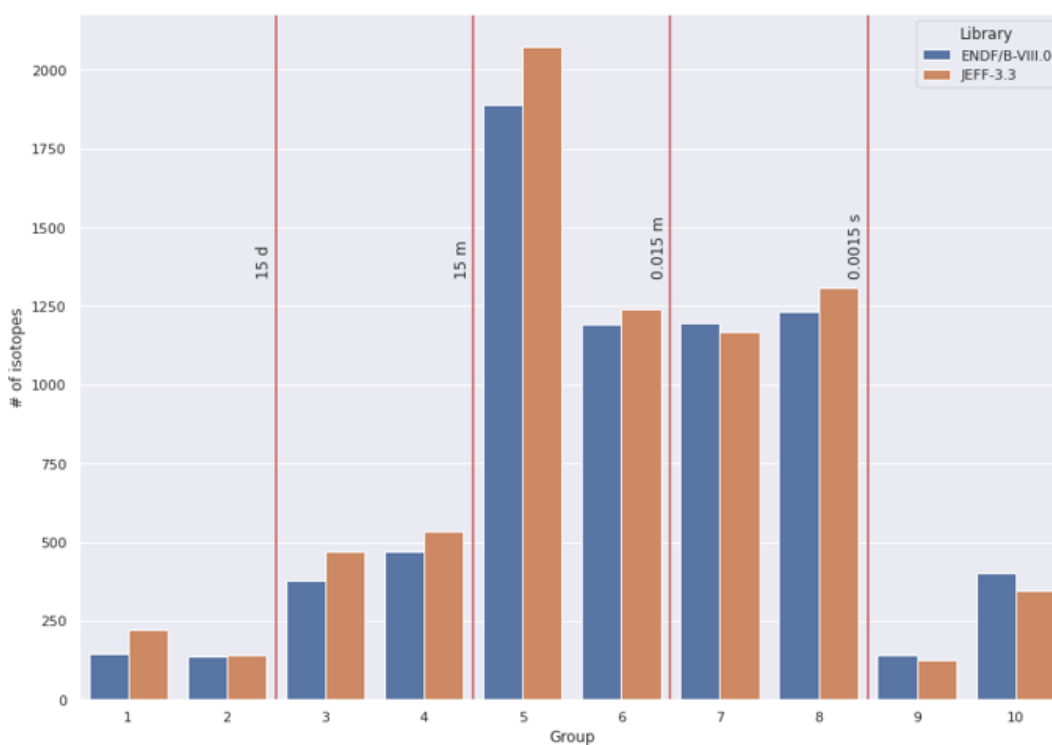


**Figure 5.7:** Number of isotopes with no uncertainty in their decay energy, classified in half life groups reported in Table 5.2

## Chapter 6

# Perturbation methodology of fission yields

In this Chapter, the implementation of the sampling procedure for fission yields inserted in SANDY is described.

When fission happens, a nucleus undergoes a deformation that leads to the scission of the nucleus into at least two fragments. These fragments have high excitation energy and undergo prompt neutron and photon emission. When the prompt neutron emission has ceased, the fragments are referred to as "products". The probability that a particular fission product will be produced directly from a fission event is called an **independent yield** (IFY). It can be written as the product of three factors [60]:

$$IFY(A, Z, M) = Y(A) \cdot f(A, Z) \cdot r(A, Z, M) \quad (6.1)$$

where:

- $Y(A)$  is the total **mass fission yield**(MFY), i.e. the sum of independent fission yields of all fission products with mass number  $A$ , before delayed neutron emission;

$$Y(A) = \sum_{A_i=A} IFY(A_i, Z, M) \quad (6.2)$$

- $f(A, Z)$  represents the **fractional independent yield** of all isomers with mass  $A$  and charge  $Z$ ;
- $r(A, Z, M)$  is the **anisomeric yield ratio** and represents the fraction of fission products  $(A,Z)$  produced as isomeric state  $M$ .

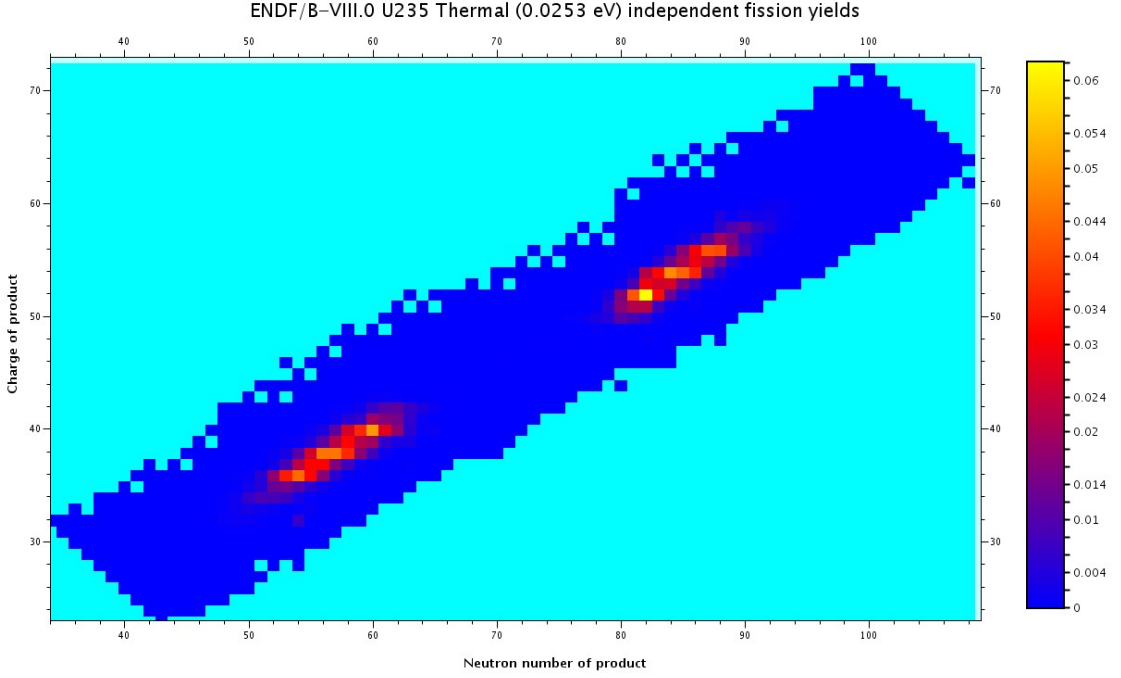


**Figure 6.1:** Independent fission yield distribution for a thermal fission of  $^{235}\text{U}$ . Nuclear data is taken from the ENDF/B-VIII.0 library [68]

The probability that a particular fission product will exist at some point in time after fission, either due to direct production from fission or due to product ion from the decay of a parent fission product, is called a **cumulative yield**(CFY) [69]. CFYs have a strong relationship with fission products decay chains, indeed they can be calculated from IFYs and decay data branching fractions using the so-called *Q-matrix* approach [70]. From the definition, the CFY can be obtained by calculating the probability that an independent product will follow a decay path leading to a cumulative product using Equation C.2.

$$CFY_i = IFY_i + \sum_{j \neq i} b_{j \rightarrow i} CFY_j \quad (6.3)$$

where  $b_{j \rightarrow i}$  the branching ratio of isotope j decay mode to isotope i. In matrix form, equation C.2 becomes:

$$CFY = Q \cdot IFY \quad (6.4)$$

The derivation of this formula is reported in Appendix C. Q-matrix is equal to  $Q = (1 - B)^{-1}$  and B is the diagonal matrix of the collection of all branching ratios, so in terms of IFY:

$$IFY = (1 - B) \cdot CFY \quad (6.5)$$

The **chain fission yield** (ChFY) is defined as the total yield for a given decay chain after both prompt and delayed neutron emission.

$$ChFY(A) = \sum_{A_i=A} IFY(A_i) \quad (6.6)$$

At first sight it may be confused with the mass fission yield  $Y(A)$ , indeed the two can differ by a few percent as the second does not include the contribution of delayed-neutron emission [70].

Fission product yields are required at several stages of the nuclear fuel cycle, indeed they are needed for calculating the accumulation and inventory of fission products. Concerning the reactor design and operation, fission yields are used in criticality and reactivity calculations, for fuel and reactor core management, for reactor safety and in determining limits of safe operation in new plants and for nuclear materials transport [71].

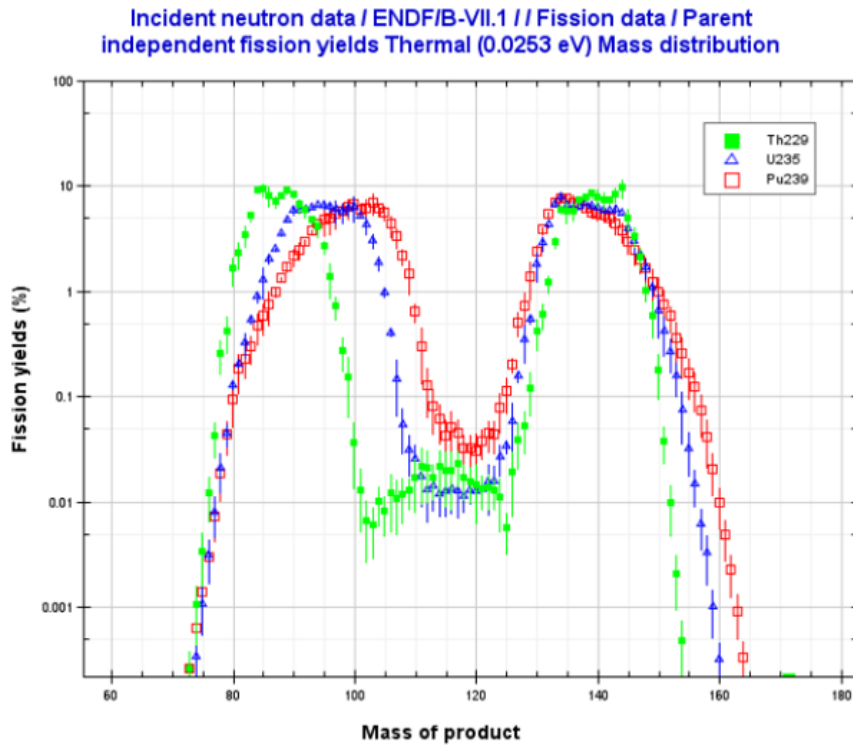


**Figure 6.2:** Mass distribution of fission product yields for thermal neutron fission of  $^{235}\text{U}$ ,  $^{229}\text{Th}$  and  $^{239}\text{Pu}$  [68]

All the libraries analyzed in Section 2.1 store the recommended independent and cumulative fission yields with their uncertainties, whereas the chain yields are provided only in the literature.

## 6.1 Algorithm to obtain perturbed fission yield in SANDY

Part of the work of this thesis was related to update the procedure to obtain perturbed fission yields in the newly version of SANDY, according with the new Python classes and methods implemented.

The algorithm to obtain perturbed fission yields refers to three main python classes inserted in SANDY:

- `sandy.Endf6`, already used for the sampling of decay data;
- `sandy.Fy`: container of independent and cumulative fission yields for several isotopes;
- `sandy.CategoryCov`: already used for the sampling of decay data.

Again a UML Class diagram with the classes used in the perturbation algorithm of fission yields implemented in SANDY, their attributes and main operations (or methods) is reported in Figure 6.3.

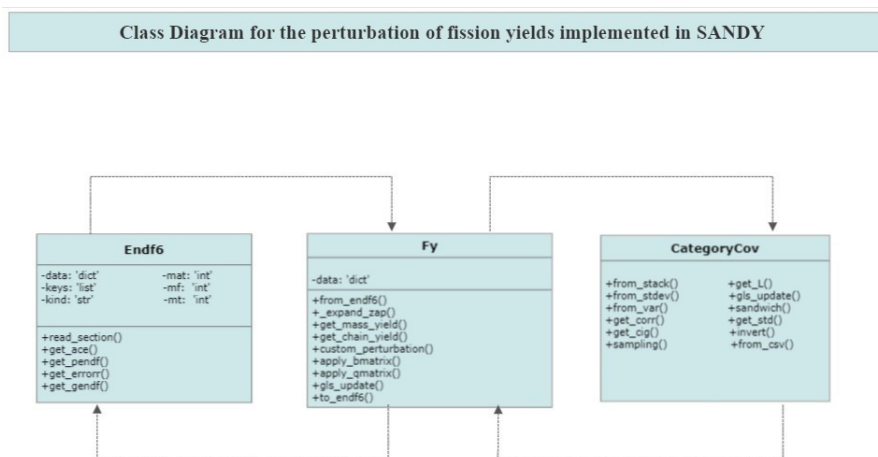


**Figure 6.3:** UML Class diagram with the main python classes, attributes and methods used for the implementation of the algorithm for the perturbation of fission yields implemented in SANDY

The steps to follow are the same already presented for the Decay Data in Section 5.1. Even in this case, the full covariance matrix is not stored in the ENDF-6 file, in which all the uncertainties are available. Taking again them as standard deviations, it is possible to build the variance matrix needed for the sampling procedure. However, because of the constraints and of the physics that governs the fission, the fission yields must be correlated and several institutions and projects are putting a great effort to develop methodologies to generate full covariance matrices. For this purpose, the procedure to update the diagonal covariance matrix with the GLS method explained in [60] was inserted in SANDY.

## 6.2 Generalized Least Squares update of independent fission yields covariance matrix

As already said in the previous Section, independent fission yields are constrained by physical conditions or conservation equations. In a fission event, at least two fission products must be produced. Therefore, binary fission yields should sum to two (*normalization of the independent yield*):

$$\sum_i IFY_i = 2 \quad (6.7)$$

The conservation of mass and charge numbers can be expressed as:

$$\sum_i A_i IFY_i = A_{CN} - \nu_p(E) - A_{LCP} \quad (6.8)$$

$$\sum_i Z_i IFY_i = Z_{CN} - Z_{LCP} \quad (6.9)$$

In the *mass conservation equation* 6.8,  $Z_i$ ,  $A_i$  and  $A_{CN}$  are the proton and the nucleon numbers of the  $i$ -th fission product and the latter of the compound nucleus.  $\langle A_{LCP} \rangle$  is the average mass number of light-charged particles from ternary fission such as proton, triton, and  $\alpha$  particles, respectively.  $\nu_p$  stands for the prompt neutron multiplicity [71]. In the *charge conservation equation* 6.9,  $Z_{CN}$  and  $Z_{LCP}$  are the charge numbers of the compound nucleus and average  $Z$  value of the light-charged particles, respectively. Another constraint that is possible to add is the *chain yield relationship* given by equation 6.6. All the mentioned constraints are linearized and can be expressed in matrix form, reported in Table 6.1, where the **Design matrix** corresponds to the sensitivity matrix used in the GLS procedure, explained in Section 4.4.

Sequential GLS updating steps can be applied to the independent fission yields and their variance matrices in an iterative way. An example of this procedure was performed during the development of this thesis, exploiting the last constraint, to

Constrain	Linear relation	Design matrix
normalization	$I^T IFY = 2$	$I^T$
mass conservation	$A^T IFY = A_{CN} - \nu_p(E) - A_{LCP}$	$A^T$
charge conservation	$Z^T IFY = Z_{CN} - Z_{LCP}$	$Z^T$
chain yield relation	$D^T IFY = ChIFY$	$D^T$

**Table 6.1:** Summary of the reported equations for the constraints that can be used to create covariances with Generalized Least Squares method for independent fission yields.

update the thermal fission yields covariance matrix of  $^{235}\text{U}$ . The updating GLS covariance matrix formula 4.14 becomes:

$$V_{IFY_{post}} = V_{IFY_{prior}} - V_{IFY_{prior}} \cdot D^T \cdot \left( D \cdot V_{IFY_{prior}} \cdot D^T + V_{Ch_{extra}} \right)^{-1} \cdot D \cdot V_{IFY_{prior}} \quad (6.10)$$

The extra information for the evaluation of the chain yields and their related covariance matrix  $V_{Ch_{extra}}$  are taken from the IAEA document [72]. By using evaluated chain fission yields to modify independent fission yield data, a deeper knowledge on the first is assumed. This is a consistent assumption since the chain fission yield and uncertainties are evaluated mostly directly from the measurements, while the independent fission yields are not [71].

To understand the impact of the difference between the chain fission yields and the mass fission yields, the IFY covariance matrix was updated considering the design matrix coming from the chain yield relationship 6.6 ( $D_c$ ) and mass fission yield relationship 6.2 ( $D_m$ ). Both matrices have the mass numbers in the rows and the nuclides along the columns. The main difference between the two is related to the fact that the chain yield takes into account the delayed neutron emission, this means that the sensitivity of an isotope must be evaluated considering the decay products of this isotope. On the contrary, the mass yield sensitivity was evaluated based only on the information stored in the Fission Yield section of the ENDF-6 file, i.e., considering only the correlations between the fission products of  $^{235}\text{U}$ . This explains why the chain yield sensitivity matrix correlates more nuclides with respect to the other. Indeed,  $D_c$  matrix has 1 in the row of that nucleus if it is stable or in the mass number of the products in which it decays and it has the fraction in the rows, which represents the probability of decaying along that path, if that nucleus has more than one path to decay. To highlight the fact that a nuclide results correlated to more nuclides in the chain yield case, a comparison between the two correlation matrices of the two design matrices is show in Figure 6.4. In this Figure the "Nuclide Index" is an index assigned to each nuclide and it is sorted by atomic number, mass number, and isomeric number in ascending order. With these design matrices the IFY covariance matrix was computed with equation

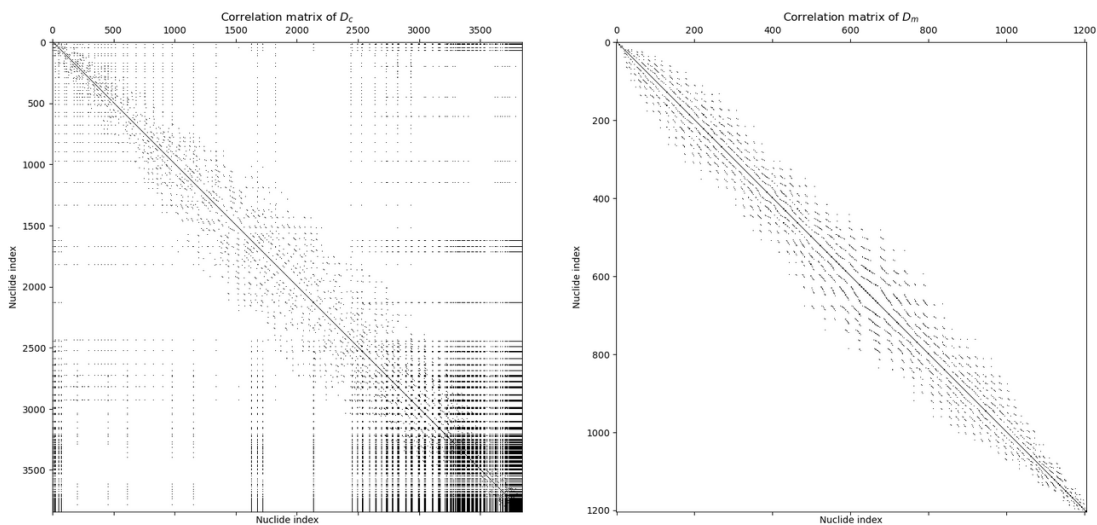


**Figure 6.4:** Comparison between correlation matrices of the two sensitivity matrices  $D_c$  and  $D_m$

6.10. Some nuclides were selected among the fission products of thermal fission of  $^{235}\text{U}$  to have a more clear visualization of the added correlations in a spy plot, reported in Figure 6.5.

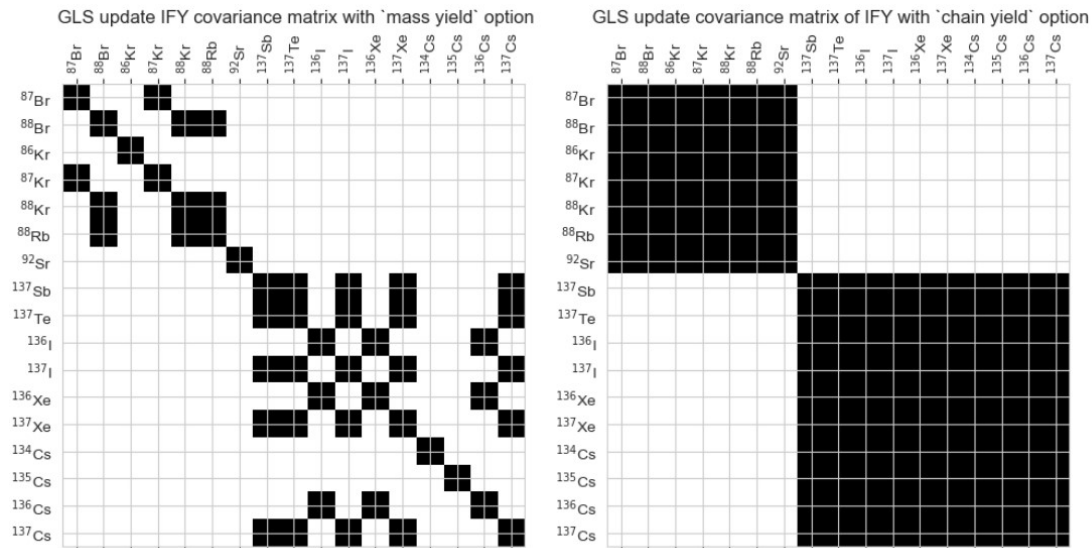


**Figure 6.5:** Comparison between IFY updated covariance matrices

The difference between the two matrices is already explained by the sensitivity

matrices. Indeed the  $D_c$  matrix results much more dense with respect to the  $D_m$  matrix, which means that more off-diagonal terms are present. As already explained, this is because, with the chain fission yields constraint, more nuclides result correlated to take into account the emission of delayed neutrons and so considering the possible decays of each nuclide. Delayed neutrons originate in the decay by neutron emission of nuclei produced in the  $\beta^-$  decay of certain fission products with gradually decreasing intensity over a period of minutes. As an example, one of the fission products is  $^{87}\text{Br}$ , containing too many neutrons and is consequently a  $\beta^-$  emitter with a half-life of 55.7 s, decaying to  $^{87}\text{Kr}$ . The latter is evidently formed in a highly excited state, with sufficient energy to permit it immediately to eject a neutron and leave a stable  $^{87}\text{Kr}$ . Another Delayed neutron precursor is  $^{137}\text{I}$  with a half-life of 22.7 s [73]. From Figure 6.5 it is possible to see that with the mass yield relation, the  $^{87}\text{Br}$  results correlated just with the nuclides with the same mass number (87) while, with the chain yield case, the other decay modes are taken into account. Indeed, this nuclide can undergo a beta decay with the production of  $^{87}\text{Kr}$  (branching ratio = 0.9749), but also a beta decay followed by the neutron emission, producing  $^{86}\text{Kr}$  (branching ratio = 0.0251).  $^{87}\text{Kr}$  can be also formed after beta decay plus neutron emission of  $^{88}\text{Br}$ . The latter nuclide can also decay in  $^{88}\text{Kr}$  and finally  $^{88}\text{Rb}$  is formed. All these decay schemes are considered in the case of chain yield relation, adding the correlations between these nuclides. The same consideration can be done for  $^{137}\text{I}$ : it undergoes beta decay with a branching ratio equals to 0.935, producing  $^{137}\text{Xe}$  and this is considered in both covariance matrices; it can also undergo a beta decay followed by a neutron emission with a branching ratio equals to 0.0251, producing  $^{136}\text{Xe}$  and this is not considered with the update performed with the mass yield relation. It is possible to see that all the other decay schemes connected to  $^{137}\text{I}$  are considered with the chain yield sensitivity in Figure 6.5.

### 6.2.1 Uncertainty reduction

Not only does the GLS method produce correlations between independent fission yields, but it also updates their variances. As already explained in Section 4.4, such an update consists in a reduction of the original values also due to the fact that the correlations added between the IFYs result in general negative correlations. The negative correlations expected (anti-correlations) can result from conservation equations. On the other hand, some chain yields with relatively large evaluated uncertainties may be expected to introduce positive correlation between the components of their corresponding chains. Still, that happens only in few cases, with anticorrelations generally dominating the updating steps. In Figure 6.6 a comparison between the original uncertainty and the updated one of some nuclides subjected to uncertainty reduction is reported. The amplitude of the uncertainty

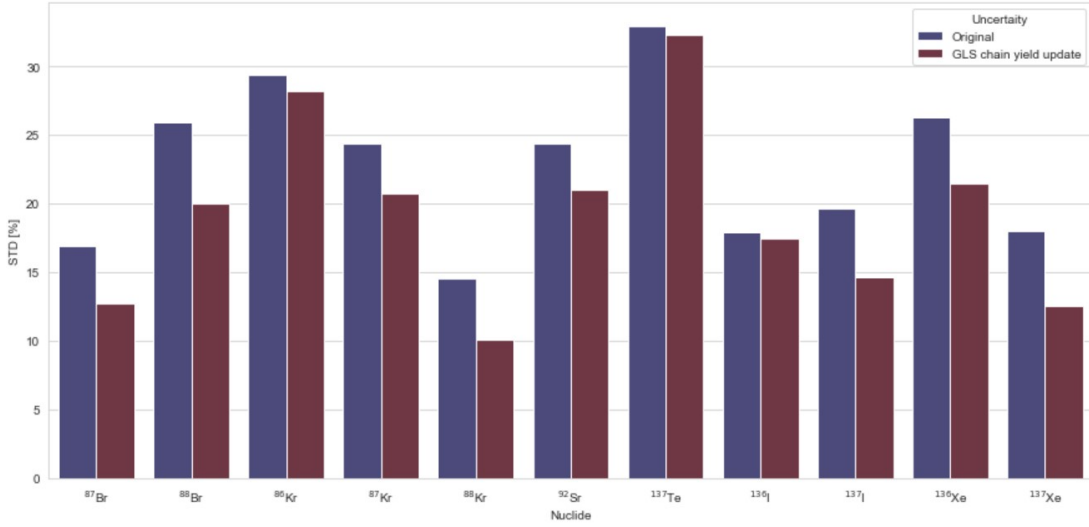


**Figure 6.6:** Independent fission yield uncertainties reduction for some JEFF-3.3  $^{235}\text{U}$  thermal fission data. The reduction is caused by the GLS update of the covariance matrix.

reduction is again explained by the updated covariance matrix: more negative correlations are added, more the uncertainty is reduced. An example is the nuclide  $^{137}\text{Xe}$ , indeed it results negative correlated with a lot of nuclides. Following its decay chain it can be correlated through a sequence of beta decays to  $^{137}\text{Cs}$ ,  $^{137}\text{Ba}$  and  $^{137m}\text{Ba}$ . It can also be produced after the beta decay of  $^{137}\text{I}$  that can also emit a neutron producing  $^{136}\text{Xe}$  and finally  $^{136}\text{Ba}$ . The other uncertainty reductions can be explained following the decay path and production of the other nuclides.

### 6.3 Cumulative fission yields covariance matrix

The evaluation of the covariance matrix of the cumulative fission yields can be done with an indirect measurement through the **moment propagation equation**, also called **sandwich rule**, derived in Appendix D. It states that the variance of the response  $R(\alpha_1, \dots, \alpha_k)$ , taken as a linear function of the input parameters  $\alpha_1, \dots, \alpha_k$ , can be computed with equation 6.11:

$$V_R = S^T V_p S \quad (6.11)$$

where  $S$  is the sensitivity matrix composed by sensitivity coefficients, i.e. the partial derivatives of  $R$  with respect to the input parameters and  $V_R$  and  $V_p$  are the response and parameter covariances respectively [74]. In case of CFY covariance matrix, exploiting the linear relation C.1, the sensitivity matrix corresponds to the

Q-matrix and the parameter covariance matrix is the independent fission yields covariance matrix. To see the consistency of this constraint in the nuclear data stored in the libraries, the IFYs of  $^{235}\text{U}$  thermal fission were computed from equation 6.5, taking the CFYs values from the library and the B matrix from SANDY. The results are compared with the data stored in the JEFF-3.3 library in Figure 6.7.

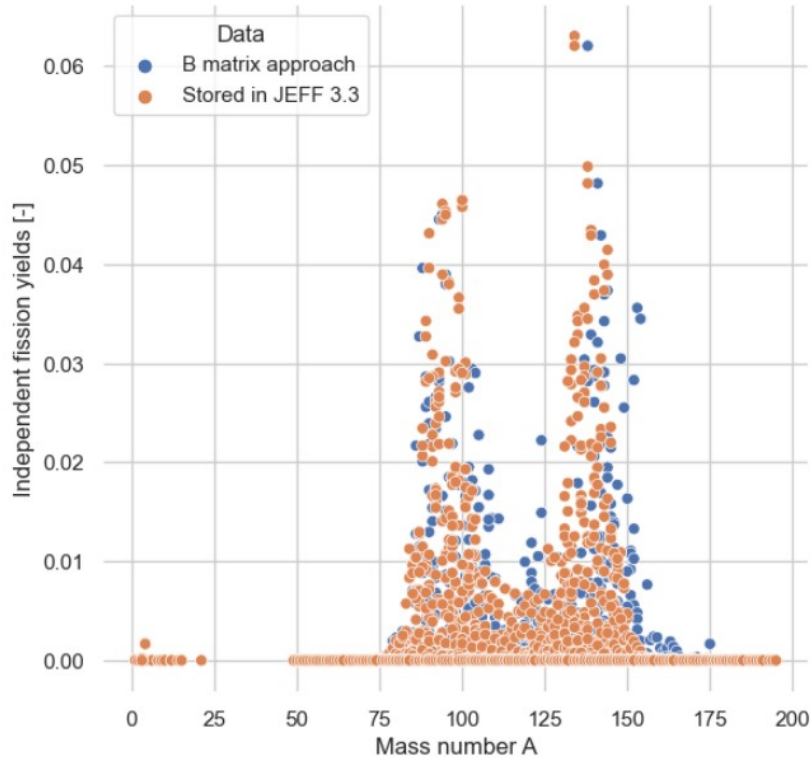


**Figure 6.7:** Comparison between evaluated IFY with B matrix approach and IFY stored in the JEFF-3.3 library

From Figure 6.7, the mass distributions of the IFYs evaluated with the B matrix approach and IFYs stored in the JEFF-3.3 library seem quite coincident, which means that the consistency between the evaluation of these IFYs and the physical constraint 6.5 is satisfied.

The uncertainty propagation of the original independent data taken from some libraries can lead to very large cumulative yield uncertainties in comparison to the values obtained from the experiments. For this reason, the JEFF evaluators corrected the cumulative yield uncertainty quantification formula using a least square approximation, introducing the contribution of the chain yields uncertainty [75]:

$$\delta CFY_j = \sqrt{\left( \left( 1 - \frac{CFY_j}{ChFY} \right) \sum_i Q_{i,j} \delta IFY_i \right)^2 + \left( \frac{CFY_j}{ChFY} \delta ChFY \right)^2} \quad (6.12)$$

This correction includes a weighting factor determined by the ratio chain/cumulative yields, which allows for the strict correlations between the two types of yield. Indeed, the cumulative yield represents the total number of atoms of that nuclide produced over all time after one fission: if the nuclide is stable and at the end of a mass chain, the cumulative yield is the total number of atoms remaining per fission, and is termed the chain yield [76].

The covariance matrix of the cumulative fission yields obtained from thermal fission of  $^{235}\text{U}$  was computed exploiting the moment propagation equation and considering the diagonal IFY covariance matrix. The nuclear data is retrieved from the JEFF-3.3 library. The result is presented in Figure 6.8. "FY Index" is an index assigned to each fission product and is sorted by atomic number, mass number, and isomeric number in ascending order. Thus in this case, for the 984 fission products, FY Index 0 has the lightest Z and A while FY Index 983 has the heaviest Z and A.

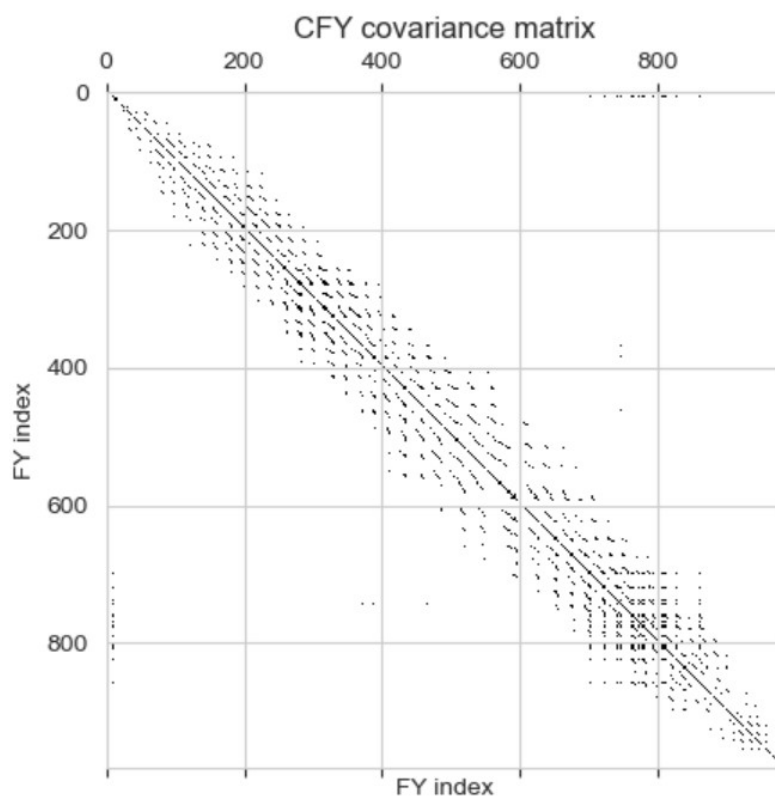


**Figure 6.8:** Cumulative fission yields covariance matrix

The CFY covariance matrix results similar to the independent fission yield covariance matrix updated with the chain yield information. This is due to the link between the cumulative and chain yields. Indeed the two take into account the correlations between the nuclides caused by their decay paths but the chain yield also adds the uncertainties which come from the chain yield evaluations (extra information). This link is highlighted by the fact that the unstable neutron-rich fission isomers mostly decay through  $\beta$ -particle emission, without any mass change [66].

# Chapter 7

## Fission pulse decay heat

In this Chapter the perturbation methodologies presented in Chapter 5 and 6 were exploited to perform the uncertainty quantification (UQ) studies to assess the impact of decay data and fission yields uncertainties on fission pulse decay heat results.

When a nuclear reactor is shut down, following some period of operation, there are various nuclear species and processes that remain which are capable of generating heat. The main sources of this heat are:

- Heavy elements - actinides: It is possible, through  $(n, \alpha)$ ,  $(n, \gamma)$  and  $(n, 2n)$  reactions and subsequent alpha and beta decay, to create numerous heavy elements and actinides during reactor operation. Then, following reactor shutdown, there remain many radioactive species which arise as a result of neutron-induced transmutation of the fuel constituents. The radiation subsequently emitted, in the form of alpha, beta and gamma rays, is an important component of reactor heat. The contribution of actinides to decay heat is a function of a number of different features such as specific power, initial enrichment, and accumulated burnup. Transmutation of actinides by neutron capture is the production mechanism of interest, and this production is more significant for fuel that has sustained a high neutron flux during its operating history [77].
- Fission products: During reactor operation fission products, in addition to their direct formation, may be produced as a result of neutron capture  $(n, \gamma)$  in a neighbouring isobar. Unstable nuclides will undergo radioactive decay while many, along with numerous stable fission products, will also be depleted through neutron capture. When the reactor is shut down, many radioactive fission products remain which, in their subsequent decay, produce the most important component of reactor decay heat [78].

- Decay of activated structural materials can also release heat but it is a minor contributor to overall decay heat.

Many aspects of the nuclear fuel cycle require accurate knowledge of the decay heat liberated at various times following reactor shutdown, such as safety analyses of nuclear power plants and nuclear waste disposal. It is significant to predict decay heat accurately and to quantify its uncertainty. These attempts contribute to make safety margin rational and then to improve the reliability of design. In general in decay heat analyses there are two basic concepts whose properties are utilized extensively: the instantaneous burst of fissions and the infinite irradiation in which there is neither build-up nor depletion of fission products as a result of neutron absorption [78].

The decay data and fission yields data of fission products are important for the analysis of the reactor decay heat and the radioactive inventory of the fission products in nuclear reactors. The accuracy of such a calculation as the decay heat depends on the adopted data. Although there are about 1000 fission products produced after fission, their decay data are not always reliable ones [79]. Roughly speaking, about a half of them has no measured or poorly measured decay data because of the difficulty to obtain experimentally the data with short half-lives. It is not suitable to use such deficient decay data for decay heat calculation at short cooling times after fission when the nuclides with short half-lives mainly contribute to the decay heat [80]. For this reason, an uncertainty quantification analysis is necessary to quantify the reliability of the calculation, indeed the uncertainty on decay heat raises from the propagation of variance and covariance values of the nuclear data.

The Fission Pulse Decay Heat (FPDH) is an idealised concept where an instantaneous burst of fissions occurs, typically in an individual nuclide. It can be defined as the the heat generated by radioactive decay after a single atom of a specific material fissions [81].

## 7.1 Set-up of the model

The decay heat at time  $t$ ,  $DH(t)$ , is calculated by integrating the nuclide-wise decay heat by a following equation:

$$DH(t) = \sum_{i=1} \lambda_i N_i(t) E_i \quad (7.1)$$

where  $\lambda_i$  is the decay constant,  $N_i(t)$  is the concentrations of isotopes involved in the calculation and  $E_i$  is mean decay energy of nuclide  $i$ . The time-evolution of radioactive material subject to pure decay is described by the system of ordinary differential burn-up equations (ODEs) in equation 7.2.

$$\frac{dN_i(t)}{dt} = -\lambda_i N_i(t) + \sum_j \lambda_j \beta_{ji} N_j(t) \quad i = 1, \dots, M \quad (7.2)$$

where  $\beta_{ji}$  is the branching ratio which indicates the decay mode and the fraction of decays that converts isotope  $j$  into  $i$  and  $M$  defines the size of the system which will be equal to the number of considered isotopes.

The analytical solution of this ODE system is generally complicated because the matrix governing the system is usually large and sparse and the problem is stiff [82]. For this reason, several numerical methods have been developed and incorporated to depletion codes.

In this thesis the model adopted simulates the FPDH for a thermal fission event of  $^{235}\text{U}$ . Radioactive decay and fission yield data that will be perturbed are taken from the libraries, whereas cross-sections do not take part in this kind of calculation. The code used to perform this calculation was ALEPH-2. **ALEPH** is a general purpose burn-up code merging Monte-Carlo radiation transport and ORIGEN-2.2 depletion codes, developed at SCK CEN since 2004. The new version of the code, ALEPH-2 was used in this thesis. It has decay heat and FPDH calculation capabilities and resorts to the highly accurate Runge–Kutta method RADAU5 to solve ODE systems [83]. In the fission pulse decay heat calculations, only the depletion calculations are done: 200 depletion steps were selected for this model, from 0 to  $10^6$  s logarithmically spaced. In these calculations, the initial nuclide composition is the independent fission yields of the considered fissionable nuclide [84].

## 7.2 Results

In this section plots and results of FPDH calculations for  $^{235}\text{U}$  thermal fission with uncertainty quantification are presented. To guarantee coherence in the calculations, all the simulated values have been compared with Tobias' compiled data [78], as they were previously used for the test and validation of the decay and fission yield data sub-libraries of JEFF-3.1.2 [75]. To validate the model built, the FPDH was computed with the best estimates of the nuclear data taken from JEFF-3.3 library and the result was also compared with the data from two standards: American(ANS5.1) [85] and Japanese(AESJ) [86]. This comparison is shown Figure 7.1, where the evaluated FPDH results in good agreement with the standards.

As stated before,  $^{235}\text{U}$  thermal FPDH calculation with uncertainty quantification was performed using the JEFF-3.3 library, first with the propagation of decay data uncertainties and then propagating the fission yields uncertainties. The sensitivity

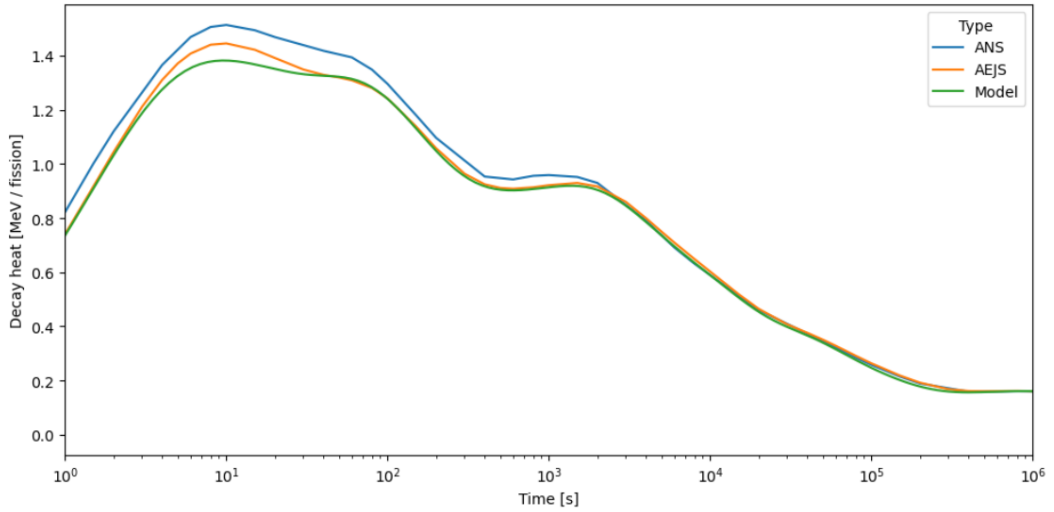


**Figure 7.1:** Comparison of evaluated FPDH and data taken from the ANS5.1 and AESJ standard

analysis was also explored to study the individual contribution of each nuclide and to quantify the most relevant isotopes.

### 7.2.1 Perturbation of decay data

Radioactive Decay Data present in the decay heat calculations are half lives, branching ratios and decay energies. To propagate the uncertainties of these data, the sampling procedure was performed with 200 samples and the convergence of means and standard deviations of the perturbed data was checked.

The Figure 7.2 shows the uncertainty estimates in  $^{235}\text{U}$  decay heat due to those in the radioactive half life, branching ratio and decay energy. Concerning the uncertainty coming from the half lives, this component seems the most relevant at the beginning of the cooling time considered. This is due to the fact that 259 out of 983 fission products of  $^{235}\text{U}$  thermal fission (about 25%) are short lived nuclides, so they disappear almost instantaneously and their half lives are difficult to measure [78]. For this reason, the half life of these nuclides is subjected to higher uncertainty with respect to the one of the long lived nuclides. This explains the overall decreasing trend of the uncertainty propagated from the half life. Yet, some oscillations arise from large uncertainties in the half lives of some not instantaneously-decaying nuclides. The most relevant ones are reported in Table 7.1.

**Table 7.1:** Nuclides with higher contribution in half life uncertainty

Nuclide	Half life [s]	Uncertainty [%]
<sup>147</sup> Xe	0.13	62
<sup>89</sup> Se	0.4	10
<sup>76</sup> Ni	0.47	83
<sup>84m</sup> As	0.65	23
<sup>102</sup> Nb	1.3	15
<sup>162</sup> Sm	2.4	21
<sup>145</sup> La	24.8	8
<sup>130m</sup> Sn	102	6
<sup>145</sup> Pm	104	6
<sup>144</sup> In	144	4
<sup>71</sup> Zn	147	4
<sup>99m</sup> Nb	156	8
<sup>170</sup> Ho	166	5
<sup>69</sup> Cu	171	5
<sup>174</sup> Er	192	7
<sup>84</sup> Se	195	3
<sup>84m</sup> Br	360	4
<sup>108m</sup> Rh	360	5
<sup>130m</sup> Sb	378	4
<sup>129m</sup> Sn	432	4
<sup>167</sup> Ho	11160	3
<sup>90m</sup> Y	11484	2
<sup>111m</sup> Pd	19800	2
<sup>156</sup> Sm	33840	2
<sup>127</sup> Sb	332640	3

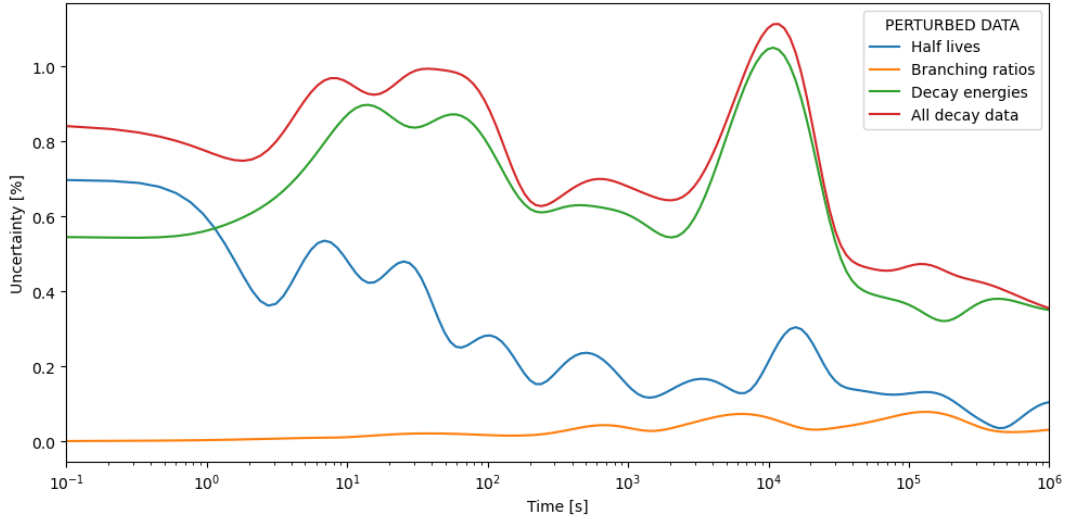


**Figure 7.2:** Uncertainty FPDH with various uncertainty contributions

The Figure 7.3 shows the uncertainty estimates in  $^{235}\text{U}$  fission pulse due to those in the radioactive decay energies. This is the highest contribution in almost all the cooling time considered. As mentioned in Section 5.4, a lot of decay energy uncertainties are not provided for many nuclides. To quantify the impact of the missing information in the output uncertainty, the sampling procedure was performed with the data available in the JEFF-3.3 library and adding the average uncertainty per decay when missing. The comparison between the resulting output uncertainty after the two sampling procedures performed is presented in Figure 7.3. The average uncertainty per decay among the data taken from JEFF-3.3 library for the fission products of  $^{235}\text{U}$  thermal fission, is reported in Table 7.2. In the case analyzed, 329 out of 983 fission products are stored in the library without uncertainty in their decay energies. As expected, with the insertion of the decay energies' uncertainties, the FPDH uncertainty increases (more uncertainties are propagated). The contribution of isotopes with no uncertainty on their decay energies increases the mean FPDH uncertainty of about 6 %. The difference is more relevant up to 1 second, in which it is almost 15 %. This is due to the fact that a lot of nuclides without uncertainty in their decay energies are short lived nuclides.

A sensitivity analysis was performed to understand which nuclides have an higher contribution to the FPDH uncertainty, and so the presence of some peaks in the distribution of Figure 7.3. A list of these isotopes with their uncertainty is reported in Table 7.3.

The Figure 7.4 shows the uncertainty estimates in  $^{235}\text{U}$  decay heat due to

**Table 7.2:** Average decay energy uncertainty per decay mode between the data taken from JEFF-3.3 library for the fission products of  $^{235}\text{U}$  thermal fission

Decay mode	Average uncertainty [%]
alpha	10
beta	5.6
gamma	5.4

**Table 7.3:** Nuclides with higher contribution in decay energy uncertainty

Nuclide	Decay mode	Decay Energy [eV]	Uncertainty [%]
$^{57}\text{Cr}$	Beta decay	1.94927e+06	13.96
$^{57}\text{Cr}$	Gamma decay	4.62212e+05	16.07
$^{59}\text{Mn}$	Beta decay	2.05981e+06	11.37
$^{69}\text{Cu}$	Beta decay	8.86523e+05	10.74
$^{115}\text{Ag}$	Beta decay	1.07923e+06	18.15
$^{115m}\text{Cd}$	Gamma decay	3.29355e+04	23.37
$^{121m}\text{In}$	Beta decay	1.51563e+06	21.43
$^{121m}\text{In}$	Gamma decay	6.43700e+04	13.03
$^{123}\text{Sn}$	Gamma decay	6.89212e+03	15.81
$^{125}\text{Sn}$	Gamma decay	3.33552e+05	10.72
$^{129m}\text{Sn}$	Gamma decay	1.70746e+06	10.44
$^{131}\text{Sb}$	Beta decay	5.76152e+05	14.05
$^{129m}\text{Te}$	Beta decay	2.62993e+05	45.29
$^{129m}\text{Te}$	Gamma decay	3.76553e+04	32.56
$^{134m}\text{I}$	Beta decay	8.67145e+04	16.61
$^{138}\text{Xe}$	Beta decay	6.41877e+05	14.10
$^{145}\text{Ce}$	Gamma decay	6.01026e+05	13.28
$^{150}\text{Pm}$	Beta decay	7.67614e+05	10.05
$^{156}\text{Sm}$	Beta decay	2.04310e+05	13.57
$^{156}\text{Sm}$	Gamma decay	1.14170e+05	10.54
$^{157}\text{Eu}$	Beta decay	3.92770e+05	10.63
$^{162}\text{Gd}$	Beta decay	3.39540e+05	11.32
$^{167}\text{Ho}$	Beta decay	2.26888e+05	31.34

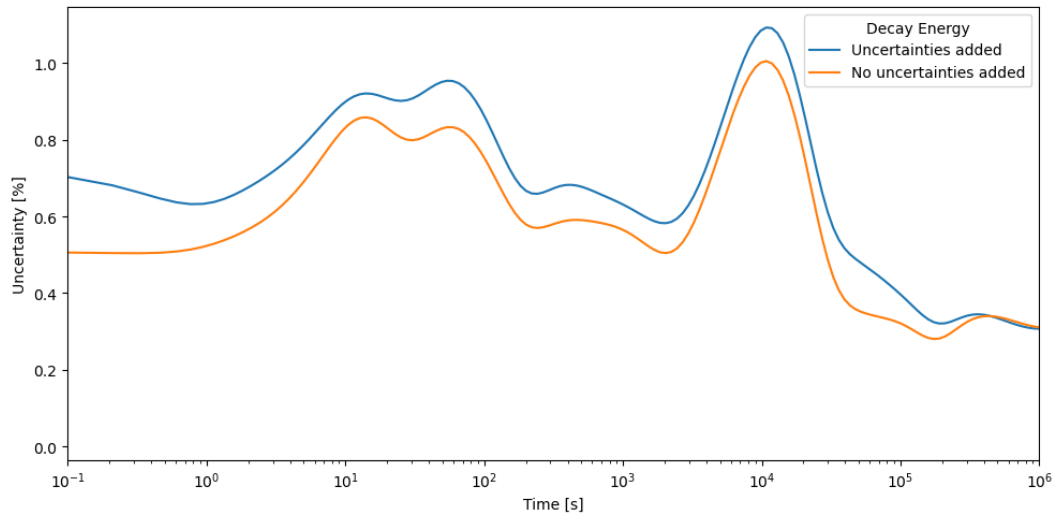


**Figure 7.3:** Comparison between the propagated uncertainty from the decay energies uncertainties available in the JEFF-3.3 library and adding the average uncertainty per decay when missing

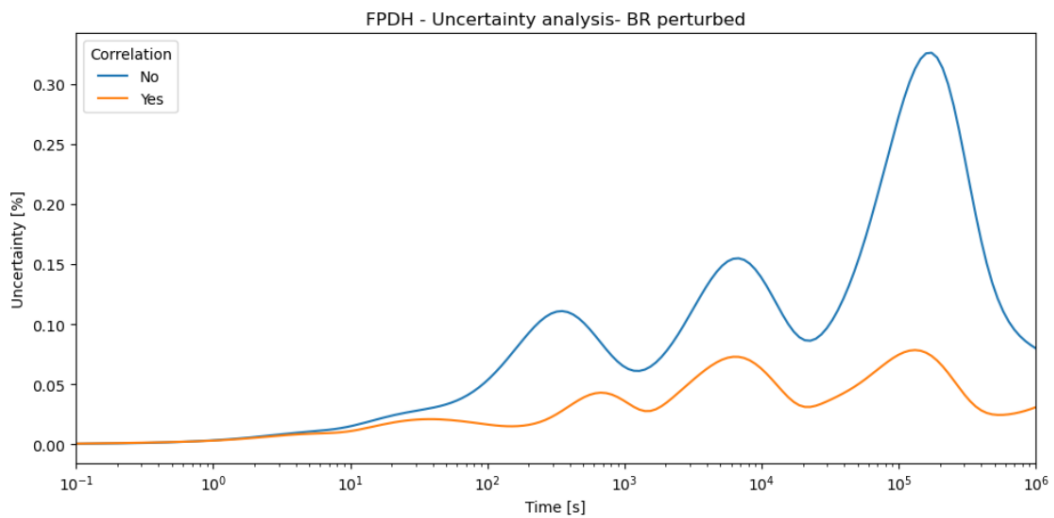


**Figure 7.4:** Comparison between the propagated uncertainty from correlated and non-correlated branching ratios

radioactive branching ratios. This component tends to be relatively insignificant for all the considered cooling times — i.e., of the order of 0.05% or smaller, corresponding to less than 5% of the total uncertainty, if correlated sampling is considered. The sampling procedure was implemented with and without the

correlations in the branching ratio covariance matrix and the comparison is reported in the mentioned Figure. From this Figure it is evident that, with the insertion of correlations between the branching ratio samples, the FPDH uncertainty decreases. For example, in the highest peak in Figure 7.4 at  $10^5$  seconds, the uncertainty on FPDH is reduced of about 80 %. This trend of uncertainty reduction is negligible in the first 10 seconds of the considered cooling time. However, the branching ratios uncertainty contribution remains low with respect to the total FPDH uncertainty, even without considering the correlations between the branching ratios, with the exception of one peak. Indeed for the non-correlated sampling, this contribution is 0.3 % at  $10^5$  seconds (highest peak), which means almost 30 % of the total FPDH uncertainty at that time. The uncertainty reduction is due to the insertion of the correlations. Indeed, the constrain 5.2 added to get the full covariance matrix introduces negative correlations. The **uncertainty propagation law** states that, for a function  $y = f(x_1, x_2)$ , the combined standard uncertainty of the measurement result  $y$ , designated by  $u_c(y)$  and taken to represent the estimated standard deviation of the result, is the positive square root of the estimated variance  $u_c^2(y)$  obtained from:

$$u_c^2(y) = \sum_{i=1}^N \left(\frac{\delta f}{\delta x_i}\right)^2 u_{x_i}^2 + 2 \sum_{i=1}^{N-1} \sum_{j=i+1}^N \frac{\delta f}{\delta x_i} \frac{\delta f}{\delta x_j} u(x_i, x_j) \quad (7.3)$$

where  $\frac{\delta f}{\delta x_i}$  corresponds to the sensitivity coefficient of  $f$  with respect to  $x_i$ ,  $u(x_i)$  is the standard uncertainty associated with the input estimate  $x_i$  and  $u(x_i, x_j)$  is the estimated covariance associated with  $x_i$  and  $x_j$  [87]. In case of branching ratios, the parameter  $y$  is the FPDH and  $u_c(y)$  is its related uncertainty, while  $x_i$  corresponds to the  $i$ -th branching ratio and  $u(x_i, x_j)$  is the covariance between the  $i$ -th and  $j$ -th branching ratios. The equation 7.3 explains the uncertainty reduction: if  $u(x_i, x_j)$  is negative, this term will be subtracted from the total uncertainty  $u_c(y)$ . This happens in the case of correlated samples, while in the opposite case  $u(x_i, x_j)$  will be equal to 0: this means that  $u_c(y)$  will be larger.

The three bumps reported in Figure 7.4 are related to three main decay chains. These physical mechanisms are preserved independently from the considered covariance matrix, so they are visible in both curves. In these peaks the sensitivity of the decay heat with respect to the branching ratio results to be larger. Moreover, to investigate the uncertainty reduction and the presence of these bumps, a sensitivity analysis was performed and the resulted main important nuclides are reported in Table 7.4. For some nuclides subjected to high uncertainty reduction, a comparison between the original uncertainty and the reduced one is reported in Figure 7.5. The original uncertainties are the ones obtained from the non-correlated samples, i.e. the uncertainties stored in the JEFF-3.3 library. The reduced uncertainties were calculated from the set of correlated samples, so they are the standard deviations of the correlated distributions. The selected nuclides are the ones for which the

relative difference between the original uncertainty and the reduced one, with respect to the original branching ratio uncertainty, is larger than 10%. These nuclides decay in correspondence to the times where the peaks are present in Figure 7.4. In Figure 7.5, "IT" stands for *Isomeric transition* while 0 and I correspond respectively to the first isomeric and ground state.

**Table 7.4:** Nuclides with higher contribution in branching ratio uncertainty

Nuclide	Decay mode	Branching Ratio [-]	Uncertainty [%]
<sup>129</sup> Sb	Beta decay	0.16	6.62
<sup>129m</sup> Te	Beta decay	0.37	45.94
<sup>129m</sup> Te	Isomeric transition	0.63	26.98
<sup>90m</sup> Rb	Isomeric transition	0.026	15.38
<sup>129m</sup> Sn	Beta decay(I isomeric state)	0.31	9.67
<sup>129m</sup> Sn	Beta decay	0.69	4.34
<sup>129m</sup> Sb	Isomeric transition	0.15	13.33
<sup>133m</sup> Te	Beta decay	0.825	3.63
<sup>133m</sup> Te	Isomeric transition	0.75	17.14
<sup>90</sup> Kr	Beta decay(I isomeric state)	0.128	4.68
<sup>130m</sup> Sn	Beta decay(I isomeric state)	0.16	12.5
<sup>89</sup> Br	Beta decay + n emission	0.14	2.83
<sup>132m</sup> I	Isomeric transition	0.86	2.32
<sup>132m</sup> I	Beta decay	0.14	14.28
<sup>117m</sup> In	Isomeric transition	0.47	3.14
<sup>117m</sup> In	Beta decay	0.53	2.83

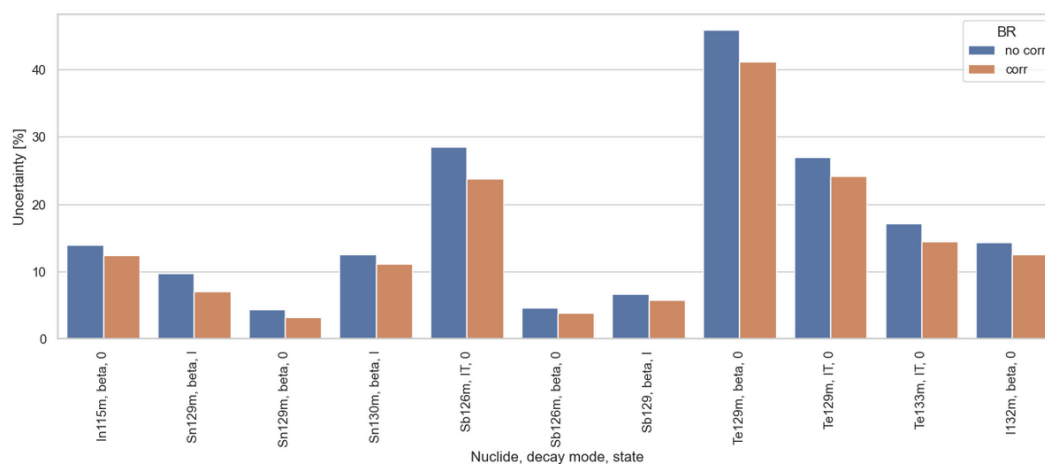


**Figure 7.5:** Comparison between the original branching ratio uncertainty and the reduced one of some nuclides

## 7.2.2 Perturbation of fission yields

Fission yield data are of critical importance in decay heat applications [80]. As already said in Chapter 6, these data are stored in the libraries without covariance matrix. In the same Chapter, the GLS update procedure was discussed to build a fission yield covariance matrix adding a physical constrain, according to [60]. The sampling procedure to propagate the uncertainty of fission yields in the fission pulse decay heat calculation was performed considering the diagonal covariance matrix, with the uncertainty coming from the JEFF-3.3 library, and the updated covariance matrix discussed in 6.2. 200 samples were adopted for this analysis and the convergence of means and standard deviations of the perturbed data was checked for each simulation.

The Figure 7.6 shows the uncertainty estimates in  $^{235}\text{U}$  decay heat due to those in fission yields, considering the correlated and non-correlated sampling procedures. From a visual comparison between this Figure and Figure 7.2, it is evident that the contribution of uncertainties coming from the fission yield data is higher than the one coming from the radioactive decay data. The uncertainty propagation performed with the uncertainties of correlated IFYs results in a reduction of the FPDH uncertainty with respect to the case of non-correlated IFY uncertainties taken from JEFF-3.3. This is due to the fact that with the GLS update technique, negative correlations are introduced into the off-diagonal terms of the IFY covariance matrix and the variance is reduced, as discussed in Chapter 4.4. FPDH calculations turn out to be very sensitive to nuclides with large IFYs, and this has a bearing on the statistics of decay heat [60]. A sorted list of nuclides whose IFYs contribute the most to thermal FPDH calculations for  $^{235}\text{U}$  over all times was compiled after

a sensitivity analysis and is proposed in Table 7.5.

Nuclide	FY [-]	FY uncertainty [%]
<sup>87</sup> Br	0.012767	16.92
<sup>88</sup> Kr	0.020639	14.57
<sup>89</sup> Kr	0.034248	10.29
<sup>91</sup> Rb	0.021575	21.41
<sup>92</sup> Sr	0.016104	24.34
<sup>93</sup> Sr	0.02905	18.31
<sup>94</sup> Sr	0.046061	10.54
<sup>95</sup> Y	0.010776	31.55
<sup>97</sup> Zr	0.011501	28.96
<sup>104</sup> Mo	0.010521	15.86
<sup>131</sup> Sb	0.013297	18.93
<sup>132</sup> Sb	0.01179	18.49
<sup>133</sup> Sb	0.024142	20.16
<sup>132</sup> Te	0.015042	24.02
<sup>133</sup> Te	0.011536	12.88
<sup>133m</sup> Te	0.02785	12.88
<sup>135</sup> I	0.024635	21.81
<sup>137</sup> Xe	0.029632	17.99
<sup>139</sup> Cs	0.011949	29.69
<sup>140</sup> Cs	0.018194	25.11
<sup>142</sup> Ba	0.027621	17.60
<sup>148</sup> Ce	0.010936	13.52

**Table 7.5:** List of the nuclides with higher contribution in the uncertainty of <sup>235</sup>U Fission Pulse Decay Heat

From Figure 7.6, it can be also noticed that after 10<sup>3</sup> seconds the difference between the FPDH uncertainty calculated with correlated and non correlated IFY uncertainties increases. As already explained in Section 6.2.1, this is due to the fact that a lot of fission products, that contribute to the decay heat at that time, are negatively correlated and are subjected to a larger uncertainty reduction. The identification of these nuclides was done and reported in Figure 7.7.

An example of the reduced uncertainty is given by <sup>131</sup>Sb. For this nuclide a lot of negative correlations are added with the performed GLS update technique. It takes into account its beta decay scheme, which leads to the production of <sup>131</sup>Te, <sup>131m</sup>Te, <sup>131</sup>I up to the stable <sup>131</sup>Xe.

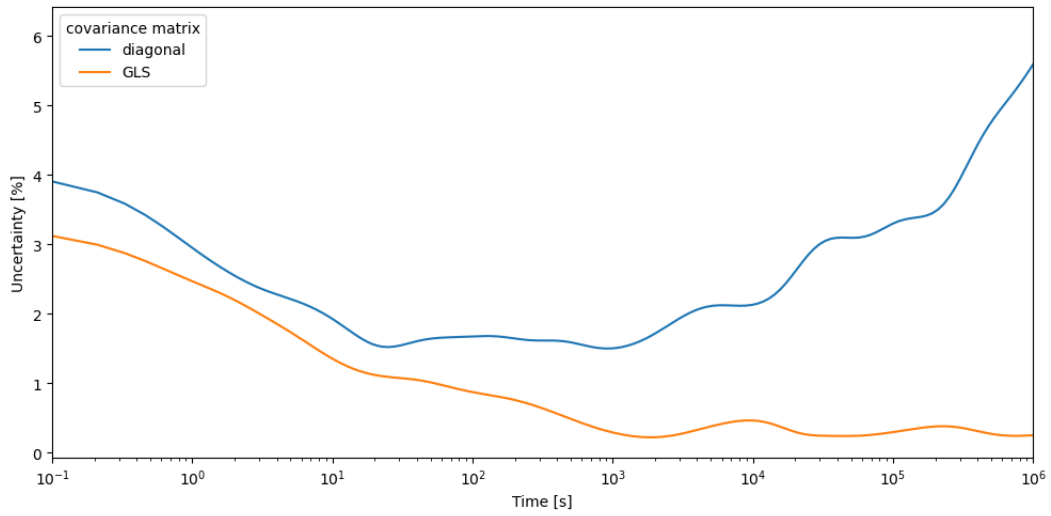


**Figure 7.6:** Uncertainty of  $^{235}\text{U}$  FPDH evaluated from the uncertainty propagation of FYs with diagonal and GLS covariance matrices

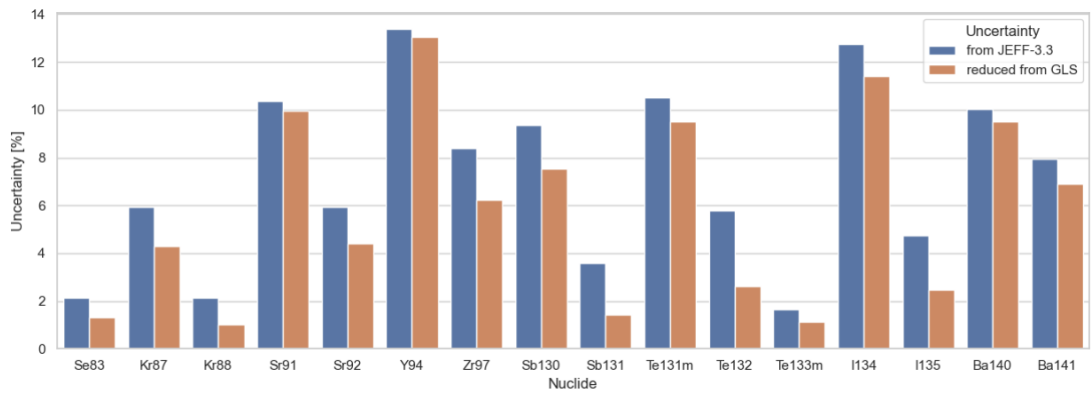


**Figure 7.7:** Comparison between the original fission yield uncertainty stored in JEFF-3.3 and the reduced one of some nuclides of interest in FPDH uncertainty after  $10^3$  seconds of cooling time. The reduced uncertainties come from the GLS update technique.

## Chapter 8

# Fission yield evaluations performed by CEA

During the development of this thesis, it was also possible to have access to the fission yields evaluations for the thermal neutron induced fission of  $^{235}\text{U}$  provided by CEA, and to test their realised correlation matrices. To update the fission yields evaluations the first point for CEA was to evaluate the mass yields after prompt neutron emission and 12 experimental datasets were considered for  $^{235}\text{U}$  thermal fission. Then, for each mass, nuclear charge distribution and isomeric ratio are based on the JEFF-3.3 library. It was also necessary to apply a "regularization" to these results because the data points from the 12 experimental datasets were not always comparable with each other. For this adjustment, four options have been explored:

- Conservative sorting 1 (C1): the 12 datasets are used by adding 2.5% uncertainty to all data points, in order to make them compatible. Only the mass 153 presents a mismatch with the second conservative sorting;
- Conservative sorting 2 (C2): Same as the C1, except for the mass  $A=153$ , where data from 2 datasets were excluded;
- Strict sorting 1 (S1): Instead of adding independent uncertainty, only some experiments are selected. Measurements that did not pass the tests per datasets and the tests per mass were excluded;
- Strict sorting 2 (S2): Same as S1, but different datasets were selected.

All the CEA proposed evaluations comply with standard conservation rules (mass, charge, isomeric, cumulative relationship) and come along with covariance

matrices (gaussian-like distribution is imposed in the generation process). FY correlations come as a by-product of normalization (or regularization).

The covariance matrix obtained with C1 approach is reported in Figure 8.1, where "FY index" is an index assigned to each fission product and is sorted by atomic number, mass number and isomeric number in ascending order.

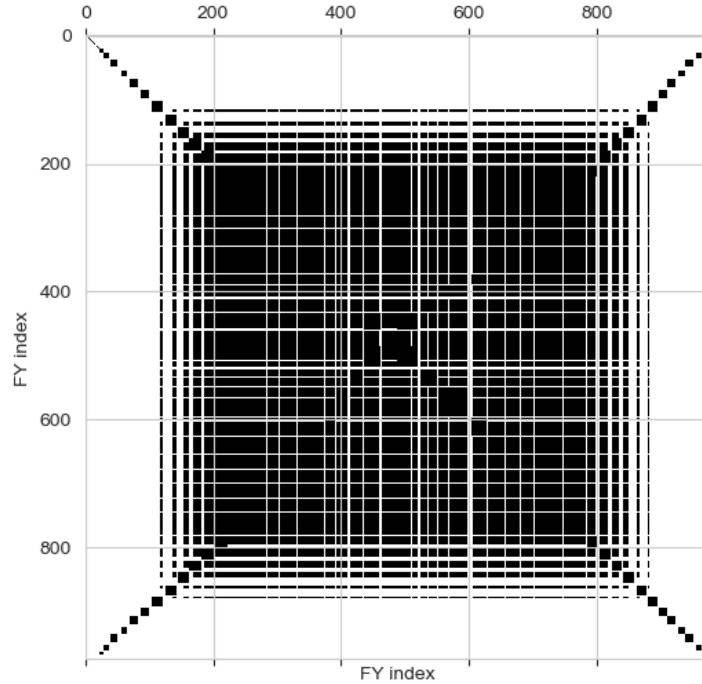


**Figure 8.1:** Covariance matrix obtained from the correlation matrix released by CEA with C1 approach

## 8.1 Propagation through FPDH model

All these covariance matrices were used to perform the sampling procedure through the FPDH model described in the previous chapter, exploiting the sampling methodology developed during this Thesis. The output uncertainty results, coming from the propagation of the uncertainties stored in the different CEA matrices, are compared in Figure 8.2. In this Figure the FPDH uncertainty coming from the non-correlated sampling procedure (i.e. from a diagonal matrix built considering only the IFY uncertainties from JEFF-3.3) is also reported in blue.

Even in this case, the correlated FY uncertainties lead to a FPDH uncertainty reduction with respect to the non-correlated ones. This reduction is higher after  $10^3$

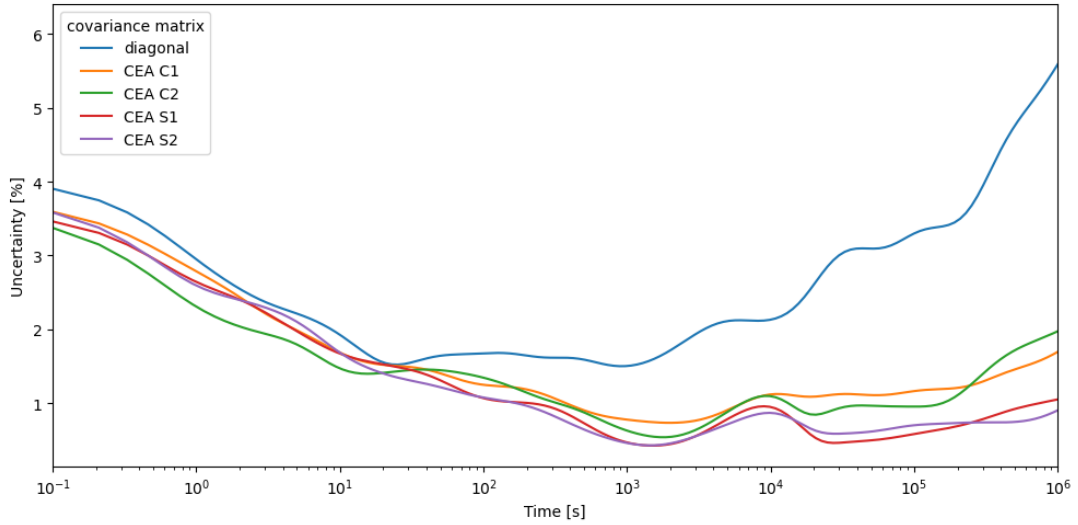


**Figure 8.2:** Uncertainty of FPDH evaluated from the uncertainty propagation of FYs with diagonal and CEA covariance matrices

seconds of cooling time. Also in this case, the insertion of negative correlations will lead to an uncertainty reduction in the fission yields of some nuclides. The insertion of different correlations gives a relevant impact after  $10^3$  seconds, where the matrix evaluated with C1 or C2 approaches leads to the highest FPDH uncertainty in comparison with the other CEA matrices. This is due to the fact that they consider data with a larger standard deviation, i.e. a more sparse dataset. This reduction is still lower with respect to the one obtained with the implemented GLS update proposed. This is due to different constraints added between the independent fission yields and the different measurements of the chain yields considered. The trend between C1 and C2 is inverted after  $10^5$  seconds. This is probably caused by the decay schemes of the nuclides with  $A=153$ , such as  $^{153}\text{Sm}$  that presents the largest IFY uncertainty in C2.

## 8.2 Propagation through UAM Pincell and Turkey Point models

Further analyses were done to test these covariance matrices. Two case studies were considered in the presented work: the first one was the UAM Benchmark Exercise I-1 "Cell Physics", described in [88]. It is a typical fuel rod from the TMI-1 PWR,  $15 \times 15$  assembly design. The configuration is shown in Figure 8.3a. The fuel adopted is  $\text{UO}_2$  with an initial enrichment of 4.85 w/o. Periodic boundary conditions are assumed. The Hot Full Power (HFP) condition for fuel pin-cell

test problem is analyzed in this work, where the average power density is equal to 33.58 W/g initial uranium. The final burnup achieved is 61.28 GWd/t, keeping the average power density constant during the whole burn-up period of 1825 days. The decay of the inventory is then followed for 300 years.

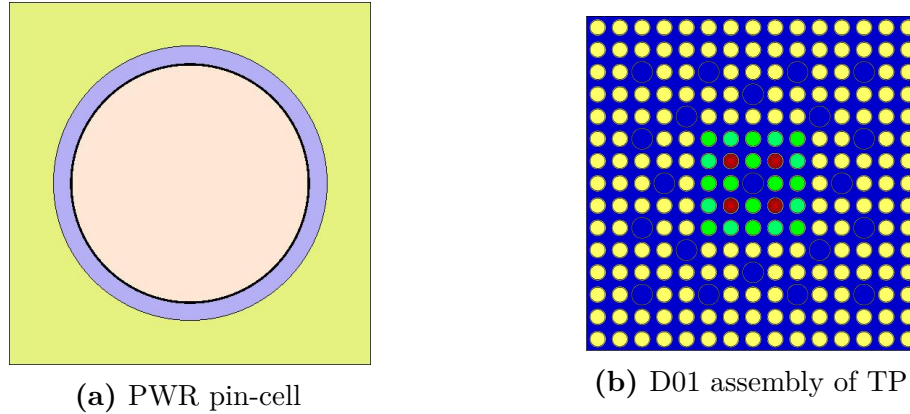


**Figure 8.3:** Geometry configurations of the analyzed models

The other model designed was the one of Turkey Point Unit 3 reactor, benchmarked in [89]. It is a PWR in the United States designed by Westinghouse Electric Corp with a net generating capacity of 699 MWe. The sample 15 from fuel rod G9, irradiated in the assembly D01 is considered. The configuration of the 15 x 15 assembly, showing the location of the measured fuel rod in red, is reported in Figure 8.3b. Exploiting the symmetry of the geometry, an eighth of the domain was modelled. The fuel used is  $\text{UO}_2$  with an initial  $^{235}\text{U}$  enrichment of 2.587 w/o. Reflective boundary conditions are set to the assembly. The specific power is assumed to be constant for the three considered cycles and equals 32.235 W/g initial uranium. A final sample burn up of 30.44 GWd/t is achieved for the selected sample, which is consistent with the expected one — 30.72 GWd/t. The results of the inventory were compared with the measured data found in SFCOMPO database [90]. This comparison is reported in Figure 8.4, where the error bar represents the experimental error as one standard deviation.

The burnup calculation of the two models is performed with Serpent 2 [91]. The independent fission yield uncertainties evaluated by CEA were propagated to the neutron multiplication factor  $k_{eff}$  and the nuclide inventory of the samples. The uncertainty results are reported for a selected set of nuclides, consisting in the ones with higher impacts in burnup and criticality calculations [92].

Before the uncertainty propagation, the CEA evaluations were compared with the values stored in the JEFF-3.3 and JEFF-3.1 libraries. The major important discrepancies for spent nuclear fuel characterization are reported in Figure 8.5. Most of the deviations are in the range of the standard deviation. The largest

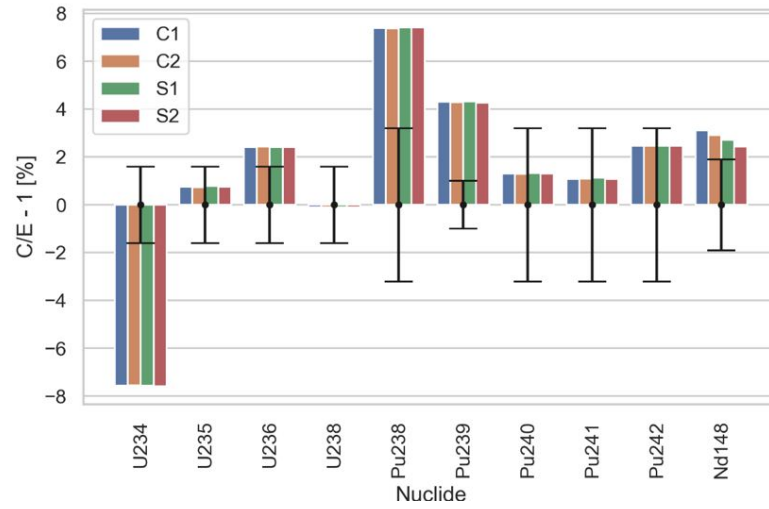


**Figure 8.4:** Comparison of the model results (C) against the reference results (E).

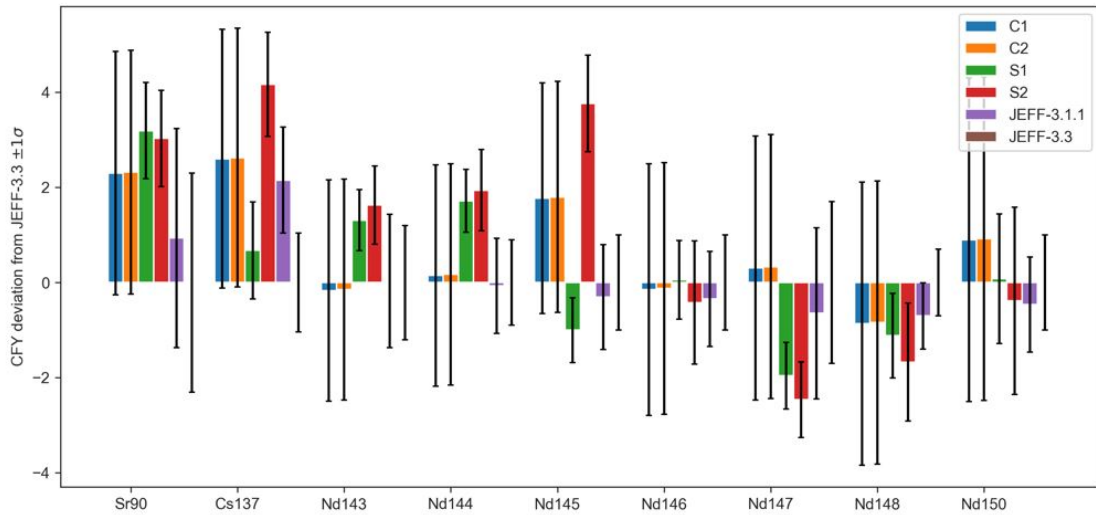


**Figure 8.5:** Comparison of CFYs evaluated by CEA and stored in JEFF-3.1.1 against the values in JEFF-3.3. The uncertainties are reported as error bars

deviation was detected in  $^{137}\text{Cs}$  and  $^{145}\text{Nd}$ , about 4% larger in S2 compared with JEFF-3.3.

### 8.2.1 Uncertainty evaluation on *keff*

200 samples were used for the uncertainty analysis, after a convergence check of the mean and standard deviation with respect to the CEA evaluated IFY best estimates

and uncertainties. In Figure 8.6 the results of the uncertainty propagation on the  $keff$  parameter through the the Pincell model are showed. These are reported in the form of discrepancies (in pcm) with respect to the uncertainty results obtained propagating the IFY values stored in JEFF-3.1.1. Statistical error is reported in the form of error bars. The uncertainty deviation results higher at low burnup:

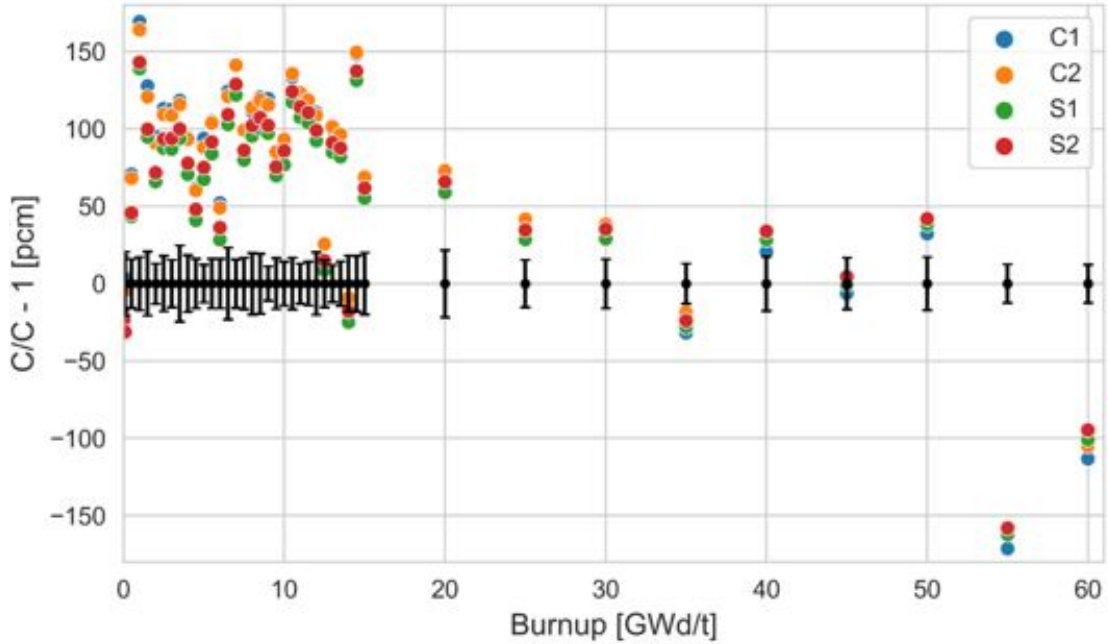


**Figure 8.6:** Discrepancies (in pcm) on  $keff$  parameter uncertainty (also called C/C-1) obtained propagating the CEA IFY uncertainties with respect to ones obtained propagating the IFY uncertainties stored in JEFF-3.1.1

this is due to the fact that in this range the analyzed parameter is more sensitive to the  $^{235}\text{U}$ , while for higher burnup the effects of Pu and other nuclides become more relevant but they are not perturbed in this analysis. A more clear visualisation of the resulted  $keff$  uncertainty is reported in Figure 8.7. The largest uncertainty is coming from JEFF-3.3 represented in purple, due to the lack of correlations between the fission yields. All the CEA evaluated uncertainties reduce the output uncertainty of about 100 pcm at low burnup. No relevant differences were found between the  $keff$  uncertainties obtained propagating the different CEA matrices. Even in this case the decreasing trend of the curve is visible due to the more relevant contribution of Pu at higher burnup. To highlight this aspect, the contribution of different fissioning systems to the  $keff$  variance was accessed propagating first only the  $^{235}\text{U}$  IFY uncertainty and then adding one by one the contribution of the thermal fissions of  $^{239}\text{Pu}$  and  $^{241}\text{Pu}$  and finally the fast fission of  $^{238}\text{U}$ , all coming

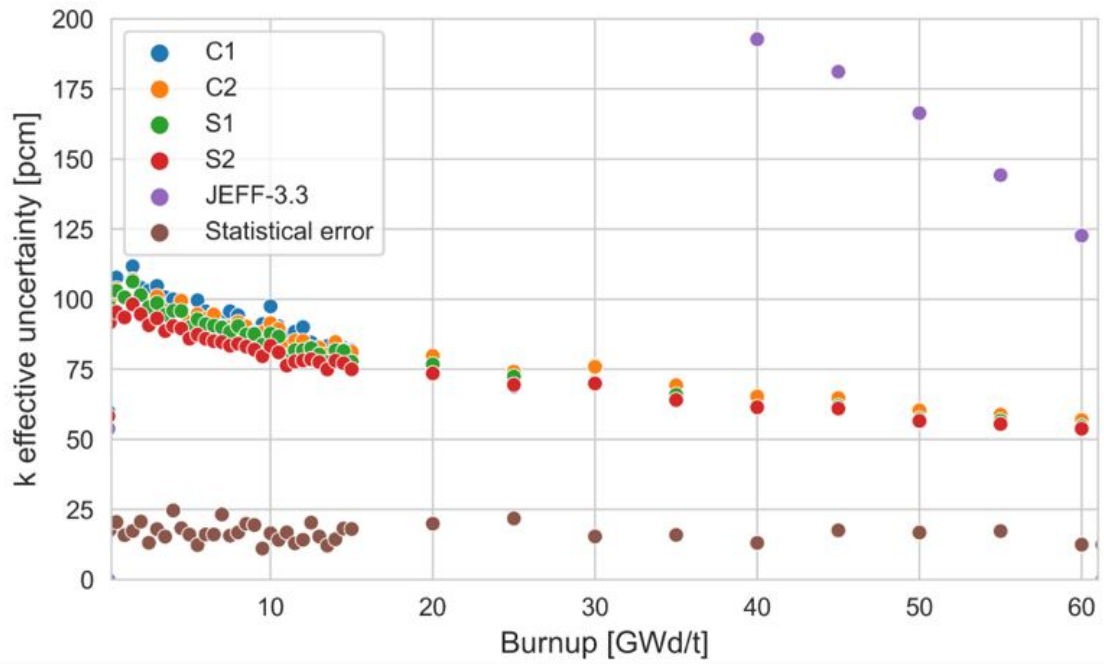


Figure 8.7: FY uncertainty propagation to  $k_{eff}$

from the values stored in JEFF-3.3 library. This analysis is showed in Figure 8.8.

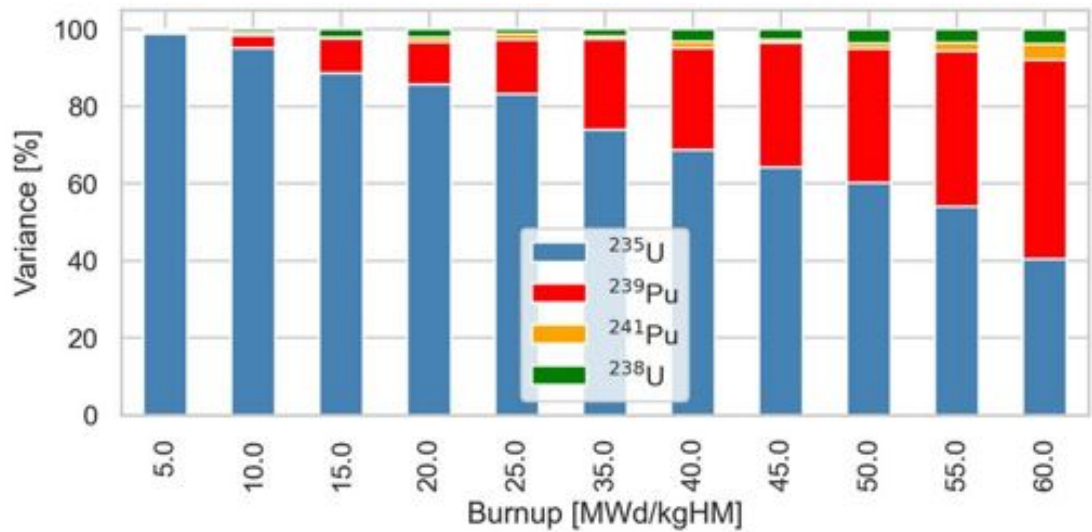
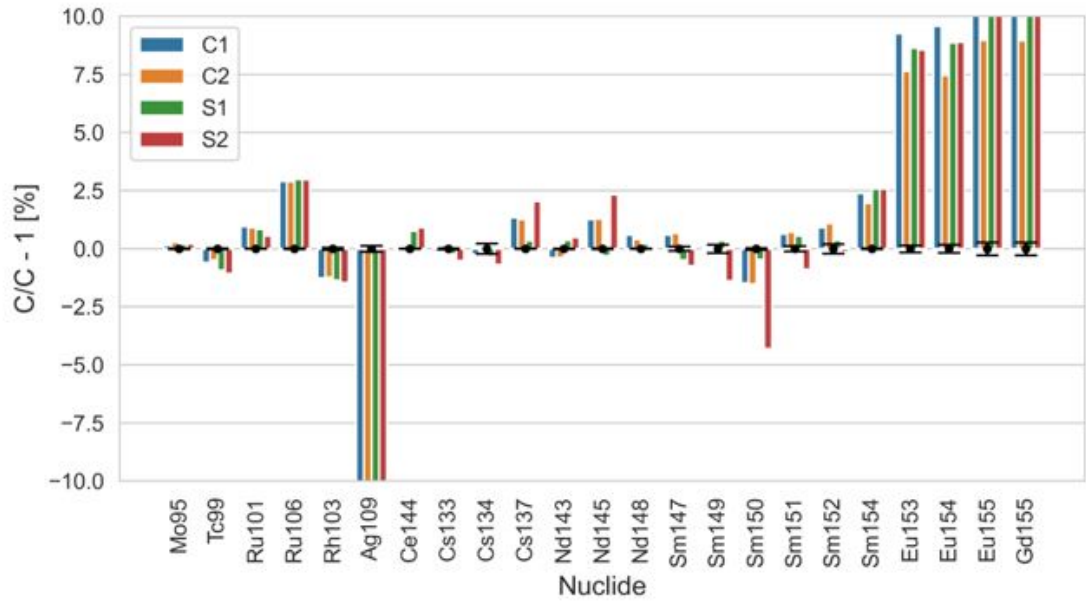


Figure 8.8: Contribution of different fissioning systems to the variance of  $k_{eff}$

## 8.2.2 Uncertainty evaluation on nuclide concentrations

The deviations of the uncertainties of the nuclide vector coming from the perturbation of the CEA matrices with respect to the perturbation of the values from JEFF-3.1.1, resulted from Turkey Point model at 30 GWd/t, are visible in Figure 8.9. The Nd and Cs will build up linearly with burnup, so they should deviate

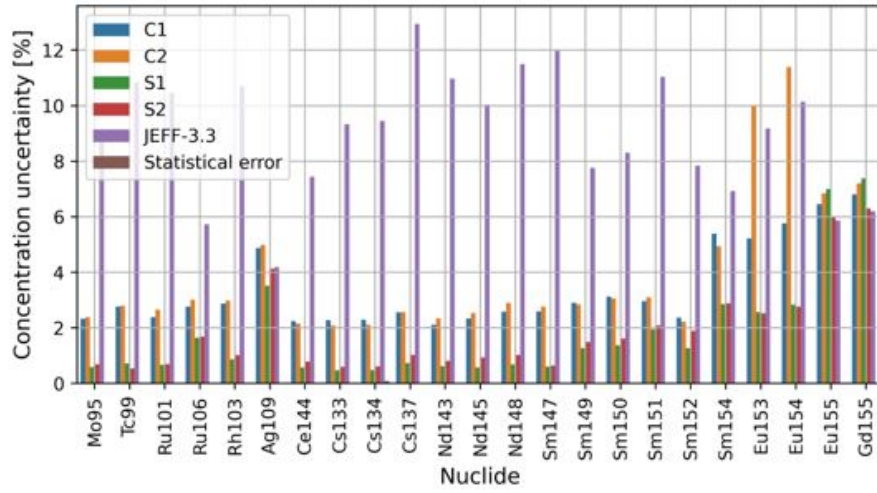


**Figure 8.9:** Nuclide vector deviations from JEFF-3.1.1

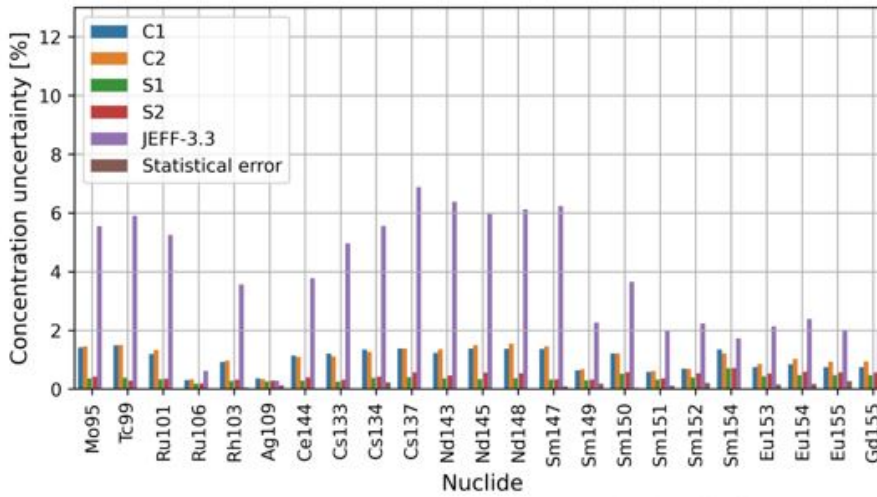
almost like the cumulative fission yields deviate. Indeed the visible trend is the same reported in Figure 8.5, where the cumulative fission yield deviations are reported. The analysis of the uncertainty on nuclide vector was done for the Pincell model up to 5 GWd/t (where the  $^{235}\text{U}$  contribution results more relevant) and up to 30 GWd/t for the Turkey Point model (at the experimental measurement time). The uncertainty results are showed in Figure 8.10.

As expected, it is evident a large reduction of the output uncertainty with respect to the results obtained with JEFF-3.3 and overall C1 and C2 show the largest uncertainty, in the range of 2-4 %. In some cases S1 and S2 go up, probably due to the selection of the databases in their generation that include some mismatches for mass  $A=153$ .

The same analysis of variance performed in the evaluation of  $k$  effective uncertainty was done for this case, taking the IFY uncertainties of  $^{235}\text{U}$ ,  $^{239}\text{Pu}$ ,  $^{241}\text{Pu}$  and  $^{238}\text{U}$  from JEFF-3.3 for Pincell model at 5 GWd/t and 60 GWd/t. From Figure 8.11 it is possible to see that at 5 GWd/t the uncertainty is basically totally due to the contribution of  $^{235}\text{U}$  IFYs, with the exception of  $^{109}\text{Ag}$  where capture reactions



(a) PWR pin-cell at 5 GWd/t

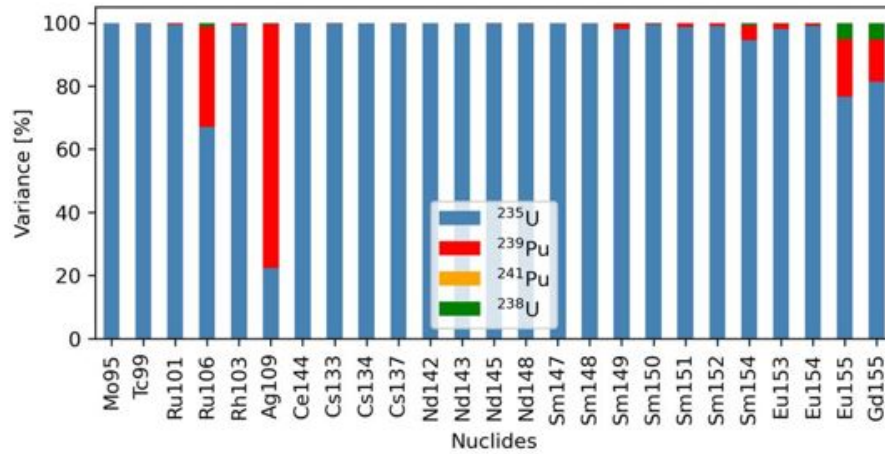


(b) D01 assembly of TP at 30 GWd/t

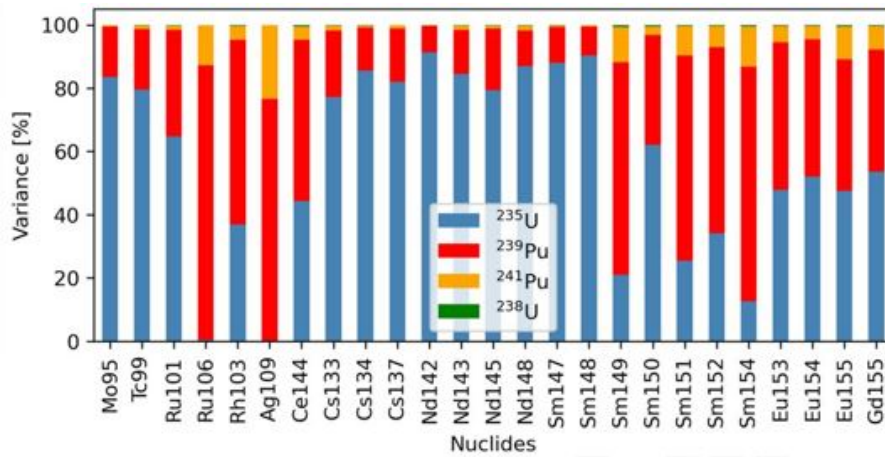
**Figure 8.10:** Uncertainty on nuclide vector

are involved and the direct production from  $^{235}\text{U}$  is very low. At 60 GWd/t the variance contribution of  $^{235}\text{U}$  is still important but there is a relevant contribution coming from  $^{239}\text{Pu}$  and  $^{241}\text{Pu}$ .

The nuclear community expressed the need for full fission yield covariance matrices in core and fuel cycle analysis, to take into account complete uncertainty data. The tests done until now with the CEA covariance matrices highlight the significant reduction of the FY uncertainty contribution to  $k_{eff}$  and nuclide vector uncertainty [93]. Several efforts are being spent to generate reliable FY covariances



(a) Pin-cell at 5 GWd/t



(b) Pin-cell at 60 GWd/t

**Figure 8.11:** Fraction of variance due to the different fissioning systems

by CEA hoping to include them in the next version of the JEFF library. Moreover, the CEA evaluations of some important nuclides for the spent nuclear fuel characterization, used to carried out this work, are now available in SANDY in <https://github.com/luca-fiorito-11/sandy/tree/develop/notebooks>.

The results of this analysis were presented during the JEFF Nuclear Data Week of November 2022, reported in [94].

# Chapter 9

## Conclusions

This thesis presents a methodology for propagating radioactive decay data and fission yields in calculations that involve ENDF-6 files as inputs, in conjunction with a review of the state-of-the-art of nuclear data and their uncertainties. In particular, decay data more relevant in nuclear spent fuel characterization were analyzed. The revision of these data is centered on the JEFF-3.3 and ENDFB-VIII.0 nuclear data libraries. It is found that for many isotopes, uncertainties on their decay energies are lacking and this lack has an impact on decay heat calculations related to fission products. Also, the uncertainties on branching ratios are not always consistent with a proper update of the uncertainties using the normalisation constraint to one. Indeed, for the probability nature of the branching ratios, the sum of all the branching ratios for each nuclide has to be equal to one. Finally, a comparison between two methodologies for the uncertainty propagation was discussed (Perturbation Theory and Monte Carlo sampling) and the sensitivity and uncertainty quantification were presented. These knowledge were the basis of the added contributions in the development of the SANDY code.

The sampling procedure adopted in SANDY is based on Monte Carlo sampling and its implementation is completely described: from the processing of nuclear data to statistical analysis. Improvements have been made to the methodology, such as the possibility to chose between different distribution for the input parameters. The assumption of the Gaussian distribution for the input parameters is analyzed and the truncation of the negative samples, which can result nonphysical for some nuclear data, is discussed.

Inconsistencies between independent and cumulative fission yield uncertainties and the lack of covariance for both gave rise to another improvement in the SANDY code. Indeed, it was also inserted the implementation of fission yield covariance data generation capability based on Bayesian/GLS updating scheme according with the algorithm described in [60].

The perturbation methodologies for decay and fission yield data were tested propagating the uncertainties of these data through the model of fission pulse decay heat. For this analysis the data of  $^{235}\text{U}$  thermal fission were taken from JEFF-3.3 library. ALEPH code was used for the depletion calculation. In this frame several uncertainty quantifications were computed and analyzed:

- All the radioactive decay data were perturbed;
- Only the decay constants of the  $^{235}\text{U}$  thermal fission products were perturbed;
- Comparison of the perturbation of only the branching ratios with and without the insertion of correlation between them;
- Comparison between the propagated uncertainty from the decay energies uncertainties available in the JEFF-3.3 library and adding the average uncertainty per decay when missing;
- Only the fission yields were perturbed, considering the diagonal matrix, i.e., without the insertion of correlations;
- The fission yields were perturbed with the insertion of correlation based on the implemented GLS update technique;
- The fission yields were propagated using the available covariance matrices produced by CEA.

The results of all these calculations were commented and validated comparing the FPDH uncertainty with the results found in literature. After the uncertainty quantification, also the sensitivity analysis was performed where the nuclides with the higher contributions in the FPDH uncertainty were identified and reported in Tables in Chapter 7. The decay uncertainties result in negligible impact in all the response functions, while the fission yield uncertainties give a significant contribution.

The sampling methodology was further improved to add the possibility to sample from the CEA covariance matrices. The analyses done during the their testing brought to the consideration of the influence of different fissioning systems, predicting the possible future interest for  $^{239}\text{Pu}$  thermal FY evaluation and covariance data. All the samples used for this work were released to the NEA community during the JEFF week of November 2022.

In conclusion, the addition of correlations reduces the uncertainties on the response function, therefore the uncertainties stored in the libraries seem overestimated. This aspect highlights the need of full covariance matrices for more accurate calculations.

There are several points where further investigations can be carried out. Regarding state-of-the-art of nuclear data uncertainties, the performance of major

evaluated nuclear data libraries can be compared. Considering the sampling procedure, the methodology adopted in SANDY can be compared with other tools used for the nuclear data uncertainty propagation and based on the Perturbation Theory. Moreover, a detailed analysis of the bias introduced by the choice of the sampling distribution of the input parameters can be done, considering the added options in the SANDY of the lognormal and uniform distributions. Furthermore, other distributions can be analyzed such as the symmetrical beta distribution.

In addition to the possibility to obtain perturbed radioactive decay and fission yields data with the added methodologies, several sets of 200 samples were produced for each of the mentioned calculations to perform these analyses. The perturbed ENDF-6 files are now available at the SCK-CEN center and can be used for further analyses of different models. This can help to perform different uncertainty quantifications. Providing realistic uncertainties can have a major impact on important scientific research program directions and technological applications. Indeed, if a quantity is thought to be known to a high-degree of accuracy, the need for further research may be hampered. Conversely, if the uncertainty is believed to be large, significant efforts may be spent to improve our knowledge of it. In nuclear field and in particular in spent nuclear fuel characterization, this can have a great impact in economical and security aspects, to minimize risks, reduce safety and security margins, and optimize the production of electricity while minimizing the production of nuclear waste, or possibly optimizing its destruction.

# Appendix A

## Impact of PDFs when propagating fission yield uncertainties in burnup calculations

In this Section a preliminary calculation of the bias introduced by the choice of the nuclear data distributions as input parameters for uncertainty quantification in burnup calculations is assessed.

To do so, an uncertainty analysis is carried out propagating the thermal neutron-induced  $^{235}\text{U}$  independent fission yields from ENDF/B-VII.1, suitable candidates because of their large evaluated uncertainties. Their values were sampled according to normal, lognormal and uniform distributions, exploiting to the sampling methodologies explained in Chapter 4.3.2. The uncertainties are propagated through the UAM Pincell model to the nuclide compositions. The model adopted is described in Chapter 8 and the nuclides selected in this analysis are the ones with higher impacts in burnup and criticality calculations [92]. The results are reported in Figure A.1.

No significant differences were found in the output uncertainties evaluated changing the input distributions to sample from. In general an higher uncertainty is expected considering the lognormal distribution. This trend is due to the distribution cut performed in the sampling procedure for normal and uniform distributions to avoid negative samples, which decreases the standard deviation. However this effect in this case is overall negligible, since it accounts for less than 2% for each nuclide concentration.

A more detailed analysis of the output distribution was done for  $^{148}\text{Nd}$ , which

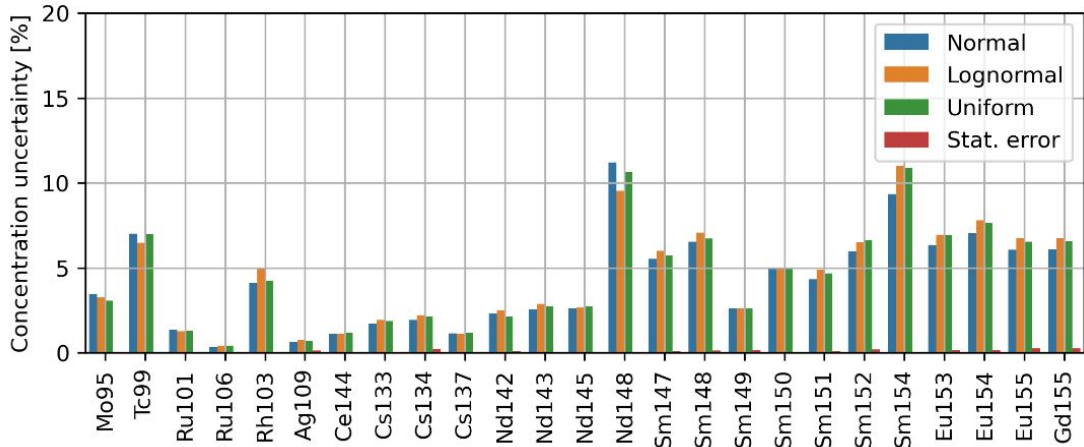
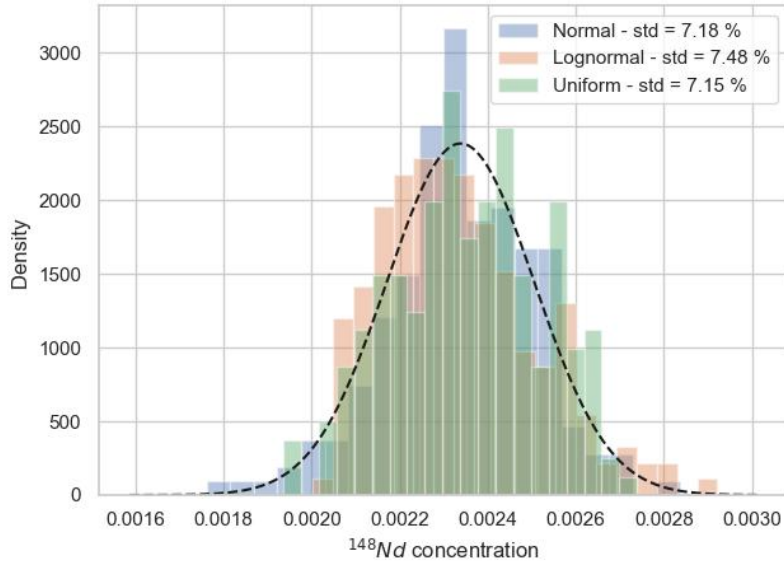


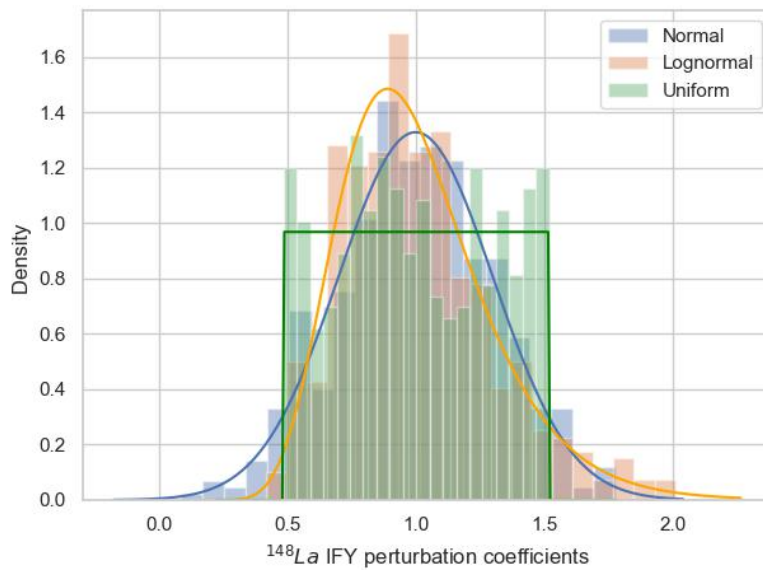
**Figure A.1:** Nuclide vector uncertainty evaluated with different input distributions

results one of the nuclide with the highest uncertainty in its concentration. It is widely used as burnup indicator. It originates from a fast decay chain involving  $^{148}\text{La}$  as relevant contributor, given its large  $^{235}\text{U}$  thermal independent fission yield. The uncertainty results of the discharge concentration of  $^{148}\text{Nd}$  propagated from JEFF-3.3 data through the PWR pin-cell model are reported in Figure A.2a, as computed with the three input parameter distributions. 200 samples were taken for each distribution, resulting in the histograms in Figure A.2b for the  $^{235}\text{U}$  thermal independent fission yield of  $^{148}\text{La}$ .

The distribution difference looks to be much attenuated by the uncertainty propagation procedure, being the concentration distributions more resembling the normal one. This seems to predict a marginal impact of sampling PDF. The standard deviations of the considered concentration distributions are consistent with each other, proving the handling procedure of the negative samples to be reliable.



(a) Distribution of final  $^{148}\text{Nd}$  concentration



(b) Distribution of  $^{148}\text{La}$  IFY perturbation coefficients

**Figure A.2:** Input and output sample distributions

# Appendix B

## Generalized Least Squares formulas

Consider a set of parameters  $\theta$ , observables  $y$  for which a relation is known  $y=f(\theta)$  and a prior knowledge of  $\theta$ , namely a collection of values  $\theta_{prior}$ , and its associated covariance matrix  $V_{prior}$ . Suppose that it is possible to have a collection of new measured data set  $\eta$ , with covariance matrix  $V$ , of the observables  $y$ . With the Generalized Least Squares method it is possible to state that the best estimate  $\theta_{post}$ , which merges the new and prior information, is obtained by satisfying the condition [56]

$$\theta_{post} = \min_{\theta} \chi^2 = \min_{\theta} \begin{bmatrix} \theta - \theta_{prior} \\ \eta - y_{prior} \end{bmatrix}^T \begin{bmatrix} V_{prior} & H \\ H^T & V \end{bmatrix} \begin{bmatrix} \theta - \theta_{prior} \\ \eta - y_{prior} \end{bmatrix} \quad (\text{B.1})$$

To find the value of  $\theta_{post}$  which minimizes the equation B.1, it is possible to linearize the relation  $y=f(\theta)$ :

$$y - y_{prior} = S(\theta - \theta_{prior}) \quad (\text{B.2})$$

with  $S$  that denotes the design matrix of sensitivity coefficients that approximates  $f$  [54].  $y_{prior}$  represents the values of the observables that are calculated using prior parameters  $\theta_{prior}$  —i.e.  $y_{prior} = S\theta_{prior}$ . Matrix  $H$  in B.1 represents the correlations that exist between the prior and new information. For the derivation of the GLS formulas, it is possible to assume that no such correlation is present and so  $H = 0$ . For convenience, a substitution of variables can be done:

$$t = \eta - y_{prior}; \quad p = \theta - \theta_{prior} \quad (\text{B.3})$$

Exploiting these substitutions, the equation B.1 can be written as follow

$$\chi^2 = p^T V_{prior}^{-1} p + (t - Sp)^T V^{-1} (t - Sp) \quad (\text{B.4})$$

$\chi(p)$  results a function of  $p$  or  $\theta$ , because the other quantities are constants. The solution of equation B.1 can be found setting  $d\chi^2(p) = 0$  and assuming that the considered analysis is confined to a region where only a minimum exists. The requirement that  $\chi^2$  be a minimum, that is  $d\chi^2(p) = 0$ , leads to the expression

$$p^T V_{prior}^{-1} - z^T V^{-1} S = 0 \quad (\text{B.5})$$

with  $z = t - Sp$ .

Applying the rules of matrix algebra,  $p$  can be explicitly defined

$$p = (V_{prior}^{-1} + S^T V^{-1} S)^{-1} S^T V^{-1} t = V_{prior} S^T (S V_{prior} S^T + V)^{-1} t \quad (\text{B.6})$$

where  $(V_{prior}^{-1} + S^T V^{-1} S)$  and  $(S V_{prior} S^T + V)$  are square, non-singular matrix, thus invertible. Then, by reapplying the change of variables, the GLS update equation is obtained.

$$\theta_{post} = \theta_{prior} + V_{prior} S^T (S V_{prior} S^T + V)^{-1} (\eta - y_{prior}) \quad (\text{B.7})$$

The covariance matrix for  $\theta_{post}$  can be derived from the law of error propagation as

$$V_{post} = V_{prior} - V_{prior} S^T (S V_{prior} S^T + V)^{-1} S V_{prior} \quad (\text{B.8})$$

# Appendix C

## Q matrix formula

The cumulative fission yields can be calculated using the independent yields and the Q-matrix equation, which involves the use of radioactive branching ratios [70]. In matrix form this sentence can be written as follow:

$$CFY = Q \cdot IFY \quad (C.1)$$

Each term of the above equation can be expressed as:

$$CFY_i = IFY_i + \sum_{j \neq i} b_{j \rightarrow i} CFY_j \quad (C.2)$$

where  $b_{j \rightarrow i}$  is the branching ratio of isotope j which decays to isotope i.

To prove the expression C.2, it is possible to consider the fission product A, which is an end of chain, and its precursor B, which decays with decay constant  $\lambda_B$  and branching ratio  $br(B \rightarrow A) = 1$  to the nuclide A. To follow the evolution in time of the concentration of this two isotopes, the following system of equations can be written:

$$\begin{cases} \frac{dA(t)}{dt} = \lambda_B B(t) \\ \frac{dB(t)}{dt} = -\lambda_B B(t) \end{cases} \quad (C.3)$$

At time  $t=0$  the concentration of the fission product A can be expressed with its independent fission fission yield  $A(t=0) = A_0 = IFY(A)$ . In opposite, after a long time (infinite time), it can be denoted with its cumulative fission yield  $A(t=\infty) = A_\infty = CFY(A)$ .

The system C.3 can be solved by substitution and integration:

$$\int_{t_0}^{t_\infty} \frac{dA(t)}{dt} = \int_{t_0}^{t_\infty} \lambda_B B(t) = \int_{t_0}^{t_\infty} -\frac{dB(t)}{dt} \quad (C.4)$$

Simplifying  $\frac{1}{dt}$  in both terms of C.4 and changing the extremes of integration, the equation C.4 becomes:

$$\int_{A_0}^{A_\infty} dA(t) = \int_{B_0}^{B_\infty} -dB(t) \quad (\text{C.5})$$

The integration of equation C.5 leads to the expression for the evaluation of  $A_\infty$  —i.e. CFY(A):

$$A_\infty = A_0 + \int_{B_0}^{B_\infty} -dB \quad (\text{C.6})$$

If the branching ratio of the nuclide B ( $br(B \rightarrow A)$ ) is not equal to 1, the C.6 becomes:

$$A_\infty = A_0 + \int_{B_0}^{B_\infty} -br(B \rightarrow A)dB \quad (\text{C.7})$$

Considering N isotopes that decay producing the isotope A with its own branching ratio, the equation C.7 can be written as follow:

$$A_\infty = A_0 + \sum_i \int_{I_{0i}}^{I_{\infty i}} -br(I_i \rightarrow A)dI_i \quad (\text{C.8})$$

Finally, the solution of the integral  $\int_{I_{0i}}^{I_{\infty i}} -dI_i$  is:

$$\int_{I_{0i}}^{I_{\infty i}} -dI_i = I_0 + \sum_j \int_{J_{0j}}^{J_{\infty j}} -br(J_j \rightarrow I) dJ_j \quad (\text{C.9})$$

which corresponds, for the equation C.7, to the cumulative fission yield of the nuclide I —i.e. CFY(I). Solving the integrals for all the isotopes, the sum of the integrals in equation C.8 results in the sum of the cumulative fission yields of all the precursors of A, multiplied for its own branching ratio. This means that the cumulative fission yield of the i-th isotope can be expressed with the equation C.2.

# Appendix D

## Sandwich rule

In an indirect measurement, the true but unknown value of the measured quantity or response, denoted by  $R$ , is related to the true but unknown values of arguments, denoted as  $(\alpha_1, \dots, \alpha_k)$ , by a known relationship (i.e., function)  $f$  [95]. This relationship is called *the measurement equation*, and can be generally represented in the form:

$$R = f(\alpha_1, \dots, \alpha_k) \quad (\text{D.1})$$

which can be expressed in terms of *Taylor expansion* as follow:

$$\begin{aligned} R(\alpha_1, \dots, \alpha_k) &\equiv \\ &R(\alpha_1^0 + \delta\alpha_1, \dots, \alpha_k^0 + \delta\alpha_k) = \\ &R(\alpha^0) + \sum_{i_1=1}^k \left( \frac{\delta R}{\delta \alpha_{i_1}} \right)_{\alpha^0} \delta\alpha_{i_1} + \\ &\frac{1}{2} \sum_{i_1, i_2=1}^k \left( \frac{\delta^2 R}{\delta \alpha_{i_1} \delta \alpha_{i_2}} \right)_{\alpha^0} \delta\alpha_{i_1} \delta\alpha_{i_2} + \\ &\frac{1}{3!} \sum_{i_1, i_2, i_3=1}^k \left( \frac{\delta^3 R}{\delta \alpha_{i_1} \delta \alpha_{i_2} \delta \alpha_{i_3}} \right)_{\alpha^0} \delta\alpha_{i_1} \delta\alpha_{i_2} \delta\alpha_{i_3} + \dots + \\ &\frac{1}{n!} \sum_{i_1, i_2, \dots, i_n=1}^k \left( \frac{\delta^n R}{\delta \alpha_{i_1} \delta \alpha_{i_2} \dots \delta \alpha_{i_n}} \right)_{\alpha^0} \delta\alpha_{i_1} \dots \delta\alpha_{i_n} + \dots \end{aligned} \quad (\text{D.2})$$

Using the Taylor-series expansion, the various moments of the random variable  $R(\alpha_1, \dots, \alpha_k)$  (like its mean, variance, etc.) can be calculated considering that the system parameters  $(\alpha_1, \dots, \alpha_k)$  are random variables, distributed according to a joint probability density function  $p(\alpha_1, \dots, \alpha_k)$  [95]. For large complex systems, with many parameters, it is often impractical to consider the nonlinear terms in the

Taylor expansion of the response. In such cases, response  $R(\alpha_1, \dots, \alpha_k)$  is taken to be a linear function of the parameters  $(\alpha_1, \dots, \alpha_k)$ , that is,

$$R(\alpha_1, \dots, \alpha_k) = R(\alpha^0) + \sum_{i=1}^k \left( \frac{\delta R}{\delta \alpha_i} \right)_{\alpha^0} \delta \alpha_i = R^0 + \sum_{i=1}^k S_i \delta \alpha_i \quad (\text{D.3})$$

where  $R^0 = R(\alpha^0)$ , while  $S_i = \left( \frac{\delta R}{\delta \alpha_i} \right)_{\alpha^0}$  denotes the sensitivity of the response  $R(\alpha_1, \dots, \alpha_k)$  to the parameter  $\alpha_i$ .

The mean value of  $R(\alpha_1, \dots, \alpha_k)$  is obtained from D.3:

$$\begin{aligned} E(R) &= \int_{S_\alpha} \left( \sum_{i=1}^k S_i \delta \alpha_i \right) p(\alpha_1, \dots, \alpha_k) d\alpha_1 d\alpha_2 \dots d\alpha_k + R^0 = \\ &= \sum_{i=1}^k S_i \int_{S_\alpha} (\alpha_i - \alpha_i^0) p(\alpha_1, \dots, \alpha_k) d\alpha_1 d\alpha_2 \dots d\alpha_k + R^0 = R^0 \end{aligned} \quad (\text{D.4})$$

The various moments of  $R(\alpha_1, \dots, \alpha_k)$  can be calculated by using D.3 and D.4. This means that the  $l$ -th central moment  $\mu_l(R)$  of  $R(\alpha_1, \dots, \alpha_k)$  is obtained as the following  $k$ -fold integral over the domain  $S_\alpha$  of the parameters  $\alpha$ :

$$\mu_l(R) = E((R - E(R))^l) = \int_{S_\alpha} \left( \sum_{i=1}^k S_i \delta \alpha_i \right)^l p(\alpha_1, \dots, \alpha_k) d\alpha_1 d\alpha_2 \dots d\alpha_k \quad (\text{D.5})$$

The variance of  $R(\alpha_1, \dots, \alpha_k)$  is calculated by setting  $l = 2$  in D.5 and by using the result obtained in D.4, as follows:

$$\begin{aligned} \mu_2(R) &= \text{var}(R) = E((R - R^0)^2) = \\ &= \sum_{i=1}^k S_i^2 \text{var}(\alpha_i) + 2 \sum_{i \neq j=1}^k S_i S_j \text{cov}(\alpha_i, \alpha_j) = S V_\alpha S^T \end{aligned} \quad (\text{D.6})$$

where the superscript ‘‘T’’ denotes the matrix transposition. The column vector  $S = (S_1, \dots, S_k)$ , with component  $S_i = \left( \frac{\delta R}{\delta \alpha_i} \right)_{\alpha^0}$ , denotes the sensitivity vector, and  $V_\alpha$  denotes the covariance matrix for the parameters  $(\alpha_1, \dots, \alpha_k)$ . Each term in this matrix is defined as

$$(V_\alpha)_{ij} = \begin{cases} \text{cov}(\alpha_i, \alpha_j) = \rho_{ij} \sigma_i \sigma_j, & i \neq j \\ \text{var}(\alpha_i) = \sigma_i^2 & \end{cases} \quad (\text{D.7})$$

where  $\rho_{ij}$  is the correlation coefficient.

The result of the relation D.6 is colloquially known as the *sandwich rule* [74].

# Bibliography

- [1] *Program 41.03.01: Used Fuel and High-Level Waste Management Program / Product Abstract*. URL: <https://www.epri.com/research/programs/061149/results/3002018440> (cit. on p. 1).
- [2] European Commission et al. *Observables of interest for the characterisation of Spent Nuclear Fuel*. Publications Office, 2018. DOI: [doi/10.2760/418524](https://doi.org/10.2760/418524) (cit. on p. 2).
- [3] P. Talou. «Making sense of uncertain nuclear data». In: *Annals of Nuclear Energy* 164 (2021), p. 108568. DOI: <https://doi.org/10.1016/j.anucene.2021.108568> (cit. on p. 2).
- [4] R. Capote et al. «Nuclear data evaluation methodology including estimates of covariances». In: *EPJ Web of Conferences* 8 (2010), p. 4001. DOI: [10.1051/epjconf/20100804001](https://doi.org/10.1051/epjconf/20100804001) (cit. on pp. 2, 3, 8).
- [5] Y. Wu. «Neutronics of Advanced Nuclear Systems». In: *Springer Singapore* (2019), pp. 181–212. DOI: [10.1007/978-981-13-6520-1\\_7](https://doi.org/10.1007/978-981-13-6520-1_7) (cit. on p. 6).
- [6] *Nuclear Energy Agency (NEA) - Home*. URL: <https://www.oecd-nea.org/> (cit. on p. 6).
- [7] T. Ware et al. «Validation of JEFF-3.3 and ENDF/B-VIII.0 nuclear data libraries in ANSWERS codes». In: *EPJ Web of Conferences* 239 (2020), p. 19001. DOI: [10.1051/EPJCONF/202023919001](https://doi.org/10.1051/EPJCONF/202023919001) (cit. on p. 6).
- [8] A. Koning et al. «The JEFF-3.1 Nuclear Data Library». In: *JEFF Report 21* (2006) (cit. on p. 7).
- [9] D.A. Brown et al. «ENDF/B-VIII.0: The 8th Major Release of the Nuclear Reaction Data Library with CIELO-project Cross Sections, New Standards and Thermal Scattering Data». In: *Nuclear Data Sheets* 148 (2018), pp. 1–142. DOI: <https://doi.org/10.1016/j.nds.2018.02.001> (cit. on p. 8).
- [10] *International Atomic Energy Agency | Atoms for Peace and Development*. URL: <https://www.iaea.org/> (cit. on p. 8).
- [11] *NNDC | National Nuclear Data Center*. URL: <https://www.nndc.bnl.gov/> (cit. on p. 8).

- [12] D. Rochman et al. «Nuclear Data Uncertainties for Typical LWR Fuel Assemblies and a Simple Reactor Core». In: *Nuclear Data Sheets* 139 (2017), pp. 1–76. DOI: 10.1016/j.nds.2017.01.001 (cit. on p. 8).
- [13] M. Herman et al. «ENDF-6 Formats Manual». In: (2010). URL: [www.nndc.bnl.gov](http://www.nndc.bnl.gov) (cit. on pp. 8–11).
- [14] C. J. Díez et al. «Comparison of nuclear data uncertainty propagation methodologies for PWR burn-up simulations». In: *Annals of Nuclear Energy* 77 (2015), pp. 101–114. DOI: 10.1016/J.ANUCENE.2014.10.022 (cit. on p. 8).
- [15] W. M. Stacey. *Nuclear reactor physics*. Wiley, 2001, p. 707. ISBN: 0471391271 (cit. on p. 13).
- [16] N. M. Schaeffer, U.S. Atomic Energy Commission. Division of Reactor Development, and Technology. *Reactor shielding for nuclear engineers*. 1973, p. 788. ISBN: 0870790048 (cit. on pp. 13, 14).
- [17] J. R. Lamarsh et al. *Introduction to nuclear engineering*, p. 736. ISBN: 9781292025810 (cit. on p. 13).
- [18] J. J. Duderstadt et al. *Nuclear Reactor Analysis*. 1976, p. 672. ISBN: 0471223638|9780471223634 (cit. on p. 15).
- [19] L. Cao et al. «Deterministic Numerical Methods for Unstructured-Mesh Neutron Transport Calculation». In: *Woodhead Publishing Series in Energy* (2021), pp. 1–34. DOI: <https://doi.org/10.1016/B978-0-12-818221-5.00003-9> (cit. on p. 16).
- [20] P. Saracco et al. «The adjoint neutron transport equation and the statistical approach for its solution». In: *The European Physical Journal Plus* 131 (Sept. 2016). DOI: 10.1140/epjp/i2016-16412-0 (cit. on pp. 16–18).
- [21] *Adjoint equation* - Wikipedia. URL: [https://en.wikipedia.org/wiki/Adjoint\\_equation](https://en.wikipedia.org/wiki/Adjoint_equation) (cit. on p. 18).
- [22] M. L. Boas. *Mathematical methods in the physical sciences - Third Edition*. 2005. ISBN: 978-0-471-19826-0 (cit. on p. 18).
- [23] *Divergence Theorem – from Wolfram MathWorld*. URL: <https://mathworld.wolfram.com/DivergenceTheorem.html> (cit. on p. 19).
- [24] G. E. Brown et al. «Commissariat a perturbation theory in nuclear reactions - L'Énergie Atomique». In: () (cit. on pp. 20, 22).
- [25] A. Gandini. «On the Standard Perturbation Theory». In: 79 (4 Dec. 2017), pp. 426–430. ISSN: 0029-5639. DOI: 10.13182/NSE81-A21393. URL: <https://www.tandfonline.com/doi/abs/10.13182/NSE81-A21393> (cit. on pp. 21, 22).

- [26] I. Trivedi et al. «Nuclear Data Uncertainty Quantification and Propagation for Safety Analysis of Lead-Cooled Fast Reactors». In: *Science and Technology of Nuclear Installations 2020* (2020). ISSN: 16876083. DOI: 10.1155/2020/3961095 (cit. on p. 22).
- [27] J. Ma et al. «Generalized Perturbation Theory Based Total Sensitivity and Uncertainty Analysis for High-Fidelity Neutronics Calculation». In: *Frontiers in Energy Research* 9 (Oct. 2021), p. 560. ISSN: 2296598X. DOI: 10.3389/FENRG.2021.743642/BIBTEX (cit. on pp. 23, 24).
- [28] C. J. Díez et al. «Nuclear Data Uncertainty Propagation in Depletion Calculations Using Cross Section Uncertainties in One-group or Multi-group». In: *Nuclear Data Sheets* 123 (2015). Special Issue on International Workshop on Nuclear Data Covariances April 28 - May 1, 2014, Santa Fe, New Mexico, USA <http://t2.lanl.gov/cw2014>, pp. 79–83. DOI: <https://doi.org/10.1016/j.nds.2014.12.014> (cit. on p. 24).
- [29] D. Rochman et al. «Nuclear data uncertainty propagation: Perturbation vs. Monte Carlo». In: *Annals of Nuclear Energy* 38 (5 May 2011), pp. 942–952. DOI: 10.1016/J.ANUCENE.2011.01.026 (cit. on pp. 24, 25).
- [30] A. Bidaud et al. «Understanding Total Monte Carlo uncertainty propagation in burn up calculations with Generalized Perturbation Theory». In: *The European Physical Journal Conferences* (Sept. 2016) (cit. on p. 24).
- [31] A. Koning. *Total Monte Carlo and related applications of the TALYS code system*. 2011. URL: [https://inis.iaea.org/search/search.aspx?orig\\_q=RN:43021154](https://inis.iaea.org/search/search.aspx?orig_q=RN:43021154) (cit. on p. 24).
- [32] *TALYS 1.2*. URL: <https://rsicc.ornl.gov/codes/psr/psr5/psr-548.html> (cit. on p. 24).
- [33] *MCNP® Website*. URL: <https://mcnp.lanl.gov/> (cit. on p. 25).
- [34] *NJOY—Nuclear Data Processing Code*. URL: <http://www.njoy21.io/> (cit. on p. 25).
- [35] Luca Fiorito. «The SANDY tool, power point presentation». In: (2022) (cit. on pp. 26, 31).
- [36] A. Saltelli et al. «Sensitivity Analysis». In: *International Encyclopedia of Statistical Science*. Ed. by Miodrag Lovric. Berlin, Heidelberg: Springer Berlin Heidelberg, 2011, pp. 1298–1301. ISBN: 978-3-642-04898-2. DOI: 10.1007/978-3-642-04898-2\_509 (cit. on pp. 27, 29).
- [37] V. Abedi et al. «Chapter 5 - Ordinary Differential Equations (ODEs) Based Modeling». In: *Computational Immunology*. Ed. by Josep Bassaganya-Riera. Academic Press, 2016, pp. 63–78. ISBN: 978-0-12-803697-6. DOI: <https://doi.org/10.1016/B978-0-12-803697-6.00005-9> (cit. on p. 28).

- [38] S. Hoops et al. «Chapter 8 - Multiscale Modeling: Concepts, Technologies, and Use Cases in Immunology». In: *Computational Immunology*. Ed. by Josep Bassaganya-Riera. Academic Press, 2016, pp. 145–173. ISBN: 978-0-12-803697-6. DOI: <https://doi.org/10.1016/B978-0-12-803697-6.00008-4> (cit. on p. 28).
- [39] T. O'Connor et al. «2 - Quality risk management for pharmaceutical manufacturing: The role of process modeling and simulations». In: *Predictive Modeling of Pharmaceutical Unit Operations*. Ed. by Preetanshu Pandey and Rahul Bharadwaj. Woodhead Publishing, 2017, pp. 15–37. ISBN: 978-0-08-100154-7. DOI: <https://doi.org/10.1016/B978-0-08-100154-7.00002-8> (cit. on p. 28).
- [40] L. Fiorito et al. «Nuclear data uncertainty propagation to integral responses using SANDY». In: *Annals of Nuclear Energy* 101 (Mar. 2017), pp. 359–366. ISSN: 18732100. DOI: 10.1016/J.ANUCENE.2016.11.026 (cit. on p. 30).
- [41] L. Fiorito et al. «JEFF-3.3 covariance application to ICSBEP using SANDY and NDAST». In: *EPJ Web of Conferences* 211 (2019), p. 07003. DOI: 10.1051/EPJCONF/201921107003 (cit. on p. 30).
- [42] M. Dello Buono. «Sviluppo web - GitHub». In: (Mar. 2022). ISSN: 2020/2021. DOI: 10.6084/M9.FIGSHARE.14470464.V4. URL: [/articles/presentation/Sviluppo\\_web\\_-\\_GitHub/14470464/4](/articles/presentation/Sviluppo_web_-_GitHub/14470464/4) (cit. on p. 31).
- [43] *Welcome to SANDY's documentation! — SANDY documentation*. URL: <https://luca-fiorito-11.github.io/sandy-docs/index.html> (cit. on p. 32).
- [44] J. T. Mordkoff. «The Assumption(s) of Normality». In: (2000) (cit. on p. 33).
- [45] Gašper Žerovnik, Andrej Trkov, and Ivan A. Kodeli. «Correlated random sampling for multivariate normal and log-normal distributions». In: *Nuclear Instruments and Methods in Physics Research Section A: Accelerators, Spectrometers, Detectors and Associated Equipment* 690 (Oct. 2012), pp. 75–78. ISSN: 01689002. DOI: 10.1016/j.nima.2012.06.036. URL: <https://linkinghub.elsevier.com/retrieve/pii/S0168900212007024> (cit. on p. 33).
- [46] H. J. Chang et al. «On Sample Size in Using Central Limit Theorem for Gamma Distribution». In: *Information and Management Sciences* (2008). URL: [https://www.researchgate.net/publication/255643904\\_On\\_Sample\\_Size\\_in\\_Using\\_Central\\_Limit\\_Theorem\\_for\\_Gamma\\_Distribution](https://www.researchgate.net/publication/255643904_On_Sample_Size_in_Using_Central_Limit_Theorem_for_Gamma_Distribution) (cit. on p. 34).
- [47] B. Keng. *Maximum Entropy Distributions / Bounded Rationality*. URL: <https://bjlkeng.github.io/posts/maximum-entropy-distributions/> (cit. on p. 35).

- [48] J. Burkardt. «The Truncated Normal Distribution». In: (2014). URL: <http://people.sc.fsu.edu/~E2%88%BCjburkardt/presentations/truncatednormal.pdf> (cit. on p. 35).
- [49] L. Fiorito et al. «Variance decomposition and sensitivity analysis, jefdoc-2120». In: *JEFF Nuclear Data Week of April* (2022). DOI: [https://www.oecd-neo.org/dbdata/nds\\_jefdoc/jefdoc-2120.pdf](https://www.oecd-neo.org/dbdata/nds_jefdoc/jefdoc-2120.pdf) (cit. on p. 37).
- [50] G. Žerovnik et al. «Correlated random sampling for multivariate normal and log-normal distributions». In: *Nuclear Instruments and Methods in Physics Research Section A: Accelerators, Spectrometers, Detectors and Associated Equipment* 690 (Oct. 2012), pp. 75–78. ISSN: 01689002. DOI: 10.1016/j.nima.2012.06.036 (cit. on p. 37).
- [51] *Distribuzione lognormale - Wikipedia*. URL: [https://it.wikipedia.org/wiki/Distribuzione\\_lognormale](https://it.wikipedia.org/wiki/Distribuzione_lognormale) (cit. on p. 37).
- [52] J. E. Marengo et al. «A Geometric Derivation of the Irwin-Hall Distribution». In: *International Journal of Mathematics and Mathematical Sciences* 2017 (2017), pp. 1–6. ISSN: 0161-1712. DOI: 10.1155/2017/3571419 (cit. on p. 38).
- [53] *Irwin–Hall distribution - Wikipedia*. URL: [https://en.wikipedia.org/wiki/Irwin%E2%80%93Hall\\_distribution](https://en.wikipedia.org/wiki/Irwin%E2%80%93Hall_distribution) (cit. on p. 39).
- [54] G. Schnabel et al. «A modified Generalized Least Squares method for large scale nuclear data evaluation». In: *Nuclear Instruments and Methods in Physics Research Section A: Accelerators, Spectrometers, Detectors and Associated Equipment* 841 (2017), pp. 87–96. ISSN: 0168-9002. DOI: <https://doi.org/10.1016/j.nima.2016.10.006> (cit. on pp. 39, 92).
- [55] L. Fiorito et al. «Fission yield covariance generation and uncertainty propagation through fission pulse decay heat calculation». In: *Annals of Nuclear Energy* 69 (2014), pp. 331–343. ISSN: 18732100. DOI: 10.1016/j.anucene.2014.01.038 (cit. on p. 39).
- [56] M. Taboga. *Generalized least squares, Lectures on probability theory and mathematical statistics*. Kindle Direct Publishing. URL: <https://www.statlect.com/fundamentals-of-statistics/generalized-least-squares> (cit. on pp. 40, 92).
- [57] D. L. Smith. «Probability, statistics, and data uncertainties in nuclear science and technology». In: 1991 (cit. on p. 40).
- [58] L. Fiorito et al. «GENERAL INTEREST-PART 3 Application of a Bayesian/generalised least-squares method to generate correlations between independent neutron fission yield data». In: (2014) (cit. on p. 40).

- [59] L. Fiorito et al. «Generation of fission yield covariances to correct discrepancies in the nuclear data libraries». In: *Annals of Nuclear Energy* 88 (Feb. 2016), pp. 12–23. ISSN: 18732100. DOI: 10.1016/J.ANUCENE.2015.10.027. URL: <http://dx.doi.org/10.1016/j.anucene.2015.10.027> (cit. on p. 41).
- [60] L. Fiorito et al. «Fission yield covariance generation and uncertainty propagation through fission pulse decay heat calculation». In: *Annals of Nuclear Energy* 69 (July 2014), pp. 331–343. ISSN: 03064549. DOI: 10.1016/j.anucene.2014.01.038. URL: <https://linkinghub.elsevier.com/retrieve/pii/S0306454914000565> (cit. on pp. 41, 51, 55, 73, 86).
- [61] A. L. Nichols. «Decay data: Review of measurements, evaluations and compilations». In: *Applied Radiation and Isotopes* 55 (1 2001), pp. 23–70. ISSN: 09698043. DOI: 10.1016/S0969-8043(00)00382-1 (cit. on pp. 42, 49).
- [62] M. Pfü et al. «Radioactive decays at limits of nuclear stability». In: (2012). DOI: 10.1103/RevModPhys.84.567 (cit. on p. 42).
- [63] C. J. Díez. «Development of a methodology for nuclear data uncertainty propagation on isotopic evaluation calculations for advanced nuclear systems». In: *Doctoral dissertation* (2014) (cit. on pp. 42, 43).
- [64] A. Sergey et al. «A self-consistent evaluation of  $^{242}\text{Cm}$  alpha and gamma emission intensities». In: *Applied Radiation and Isotopes* 87 (2014). Proceedings of the 19th International Conference on Radionuclide Metrology and its Applications 17–21 June 2013, Antwerp, Belgium, pp. 137–141. ISSN: 0969-8043. DOI: <https://doi.org/10.1016/j.apradiso.2013.11.086> (cit. on p. 43).
- [65] F. Albarede. «Decay Constant». In: *Encyclopedia of Astrobiology*. Ed. by Muriel Gargaud, Ricardo Amils, José Cernicharo Quintanilla, Henderson James (Jim) Cleaves, William M. Irvine, Daniele L. Pinti, and Michel Viso. Berlin, Heidelberg: Springer Berlin Heidelberg, 2011, pp. 413–414. ISBN: 978-3-642-11274-4. DOI: 10.1007/978-3-642-11274-4\_398 (cit. on p. 46).
- [66] S. Lahaye et al. «Comparison of deterministic and stochastic approaches for iso-topic concentration and decay heat uncertainty quantification on elementary fission pulse». In: *Environmental Science* (2016). DOI: 10.1051/C. URL: <http://dx.doi.org/10.1051/epjconf/201611109002> (cit. on pp. 46, 62).
- [67] S. M. Qaim et al. «Positron emission intensities in the decay of  $^{64}\text{Cu}$ ,  $^{76}\text{Br}$  and  $^{124}\text{I}$ ». In: (2006). DOI: 10.1524/ract.2007.95.2.67 (cit. on p. 46).
- [68] *Nuclear Energy Agency (NEA) - JANIS*. URL: [https://www.oecd-nea.org/jcms/pl\\_39910/janis](https://www.oecd-nea.org/jcms/pl_39910/janis) (cit. on pp. 52, 53).

- [69] E. F. Matthews et al. «Stochastically estimated covariance matrices for independent and cumulative fission yields in the ENDF/B-VIII.0 and JEFF-3.3 evaluations». In: *Atomic Data and Nuclear Data Tables* 140 (July 2021). ISSN: 10902090. DOI: 10.1016/j.adt.2021.101441 (cit. on p. 52).
- [70] M. F. James et al. «A new evaluation of fission product yields and the production of a new library (UKFY2) of independent and cumulative yields». In: *Progress in Nuclear Energy* 26.1 (1991), pp. 1–29. ISSN: 0149-1970. DOI: [https://doi.org/10.1016/0149-1970\(91\)90030-S](https://doi.org/10.1016/0149-1970(91)90030-S) (cit. on pp. 52, 53, 94).
- [71] K. Tsubakihara et al. «Evaluation of fission product yields and associated covariance matrices». In: (2020). DOI: 10.1080/00223131.2020.1813643. URL: <https://www.tandfonline.com/action/journalInformation?journalCode=tnst20> (cit. on pp. 53, 55, 56).
- [72] T. R. England et al. «Evaluation and Compilation of Fission Product Yields». In: *Los Alamos - NIS publications* (1993) (cit. on p. 56).
- [73] Ş. Sümer et al. «3.14 Fission Energy Production». In: *Comprehensive Energy Systems* 3-5 (Jan. 2018), pp. 590–637. DOI: 10.1016/B978-0-12-809597-3.00331-X (cit. on p. 58).
- [74] Q. Wu et al. «Nuclear data sensitivity analysis and uncertainty propagation in the KYADJ whole-core transport code». In: *EPJ Web of Conferences* 239 (2020), p. 22012. DOI: 10.1051/epjconf/202023922012 (cit. on pp. 59, 97).
- [75] M. A. Kellett et al. «The JEFF-3.1/-3.1.1 radioactive decay data and fission yields sub-libraries JEFF Report 20 NUCLEAR ENERGY AGENCY Organisation for Economic Co-operation and Development». In: (2009). URL: [www.oecd.org/publishing/corrigenda](http://www.oecd.org/publishing/corrigenda). (cit. on pp. 60, 65).
- [76] «The JEF-2.2 Nuclear Data Library». In: *OECD Publishing* (2000) (cit. on p. 61).
- [77] H. Smith. «The Relative Significance of Actinide Decay Heat for Nuclear Fuel Characterization». In: *Transactions of the American Nuclear Society - Winter Meeting, Reno, Nevada* 85 (Dec. 2001) (cit. on p. 63).
- [78] A. Tobias. *DECAY HEAT*. 1980 (cit. on pp. 63–66).
- [79] K. Takanori et al. «Uncertainty Quantification of Nuclear Reactor Decay Heat». In: *Proceedings of the Reactor Physics* (2015) (cit. on p. 64).
- [80] J. Katakura. «JENDL FP Decay Data File 2011 and Fission Yields Data File 2011». In: (2012). URL: <https://doi.org/10.11484/jaea-data-code-2011-025> (cit. on pp. 64, 73).
- [81] *Validation of SCALE 5 Decay Heat predictions for LWR Spent Nuclear Fuel Office of Nuclear Regulatory Research*. URL: [www.ntis.gov](http://www.ntis.gov) (cit. on p. 64).

- [82] C. Moler et al. «Nineteen Dubious Ways to Compute the Exponential of a Matrix, Twenty-Five Years Later». In: *SIAM Review* 45.1 (2003), pp. 3–49. DOI: 10.1137/S00361445024180 (cit. on p. 65).
- [83] P. Baeten et al. *ALEPH2-A general purpose Monte Carlo depletion code*. URL: <https://www.researchgate.net/publication/286740932> (cit. on p. 65).
- [84] Y. Kawamoto et al. «Feasibility study of decay heat uncertainty reduction using nuclear data adjustment method with experimental data». In: (2016). ISSN: 1881-1248. DOI: 10.1080/00223131.2016.1238785 (cit. on p. 65).
- [85] «ANSI-ANS5.1 standard». In: *American National Standards Institute* (2019). URL: <https://webstore.ansi.org/Search/Find?in=1&st=ANS+5.1> (cit. on p. 65).
- [86] «AESJ standard». In: *Standards Committee, Atomic Energy Society of Japan* (2013). URL: <http://www.aesj.or.jp/sc/english/index.html> (cit. on p. 65).
- [87] *NIST TN 1297: Appendix A. Law of Propagation of Uncertainty / NIST*. Physical measurement laboratory (cit. on p. 71).
- [88] K. Ivanov et al. «Benchmarks for Uncertainty Analysis in Modelling (UAM) for the Design, Operation and Safety Analysis of LWRs». In: I: Specification and Support Data for the Neutronics Cases (Phase I), Version 2.1 (Final Specifications) (2013) (cit. on p. 78).
- [89] G. Radulescu et al. «SCALE 5.1 Predictions of PWR Spent Nuclear Fuel Isotopic Compositions». In: (2010) (cit. on p. 79).
- [90] F. Michel-Sendis et al. «SFCOMPO-2.0: An OECD NEA database of spent nuclear fuel isotopic assays, reactor design specifications, and operating data». In: *Annals of Nuclear Energy* 110, pp. 779-788 (2017) (cit. on p. 79).
- [91] J. Leppänen et al. «The Serpent Monte Carlo code: Status, development and applications in 2013». In: *Annals of Nuclear Energy* 82, pp. 142–150 (2015) (cit. on p. 79).
- [92] I.C. Gauld et al. «Nuclide Importance to Criticality Safety, Decay Heating, and Source Terms Related to Transport and Interim Storage of High-Burnup LWR Fuel (NUREG/CR-6700)». In: *Division of Systems Analysis and Regulatory Effectiveness* (2001) (cit. on pp. 79, 89).
- [93] N. Terranova et al. «A Covariance Generation Methodology for Fission Product Yield». In: *EPJ Web of Conferences* 101 (2016) (cit. on p. 84).
- [94] E. Belfiore et al. «Assessment of FY covariances for JEFF-4.0, jefdoc-2197». In: *JEFF Nuclear Data Week of November* (2022). DOI: [https://www.oecd-neo.org/dbdata/nds\\_jefdoc/jefdoc-2197.pdf](https://www.oecd-neo.org/dbdata/nds_jefdoc/jefdoc-2197.pdf) (cit. on p. 85).

BIBLIOGRAPHY

---

- [95] D. G. Cacuci. *Handbook of Nuclear Engineering*. 2010. DOI: 0387981306 , 9780387981307 (cit. on p. 96).